STATUS OF THESIS

Title of thesis	OPTIMIZATION AND METALLURGICAL STUDY OF RESISTANCE SPOT WELDED HEAT TREATED SUS316L AUSTENITIC STAINLESS STEEL

I MUHAMMED MUSA

hereby allow my thesis to be placed at the Information Resource Center (IRC) of Universiti Teknologi PETRONAS (UTP) with the following conditions:

1. The thesis becomes the property of UTP
2. The IRC of UTP may make copies of the thesis for academic purposes only.
3. This thesis is classified as

☐ Confidential

☑ Non-Confidential

If this thesis is confidential, please state the reason:

____

____

____

The contents of the thesis will remain confidential for ___________ years.

Remarks on disclosure:

____

____

____

	Endorsed by
	Dr. Mazli Mustapha Senior Lecturer Mechanical Engineering Department Universiti Teknologi PETRONAS
Signature of Author	Signature of Supervisor
Permanent address:	Name of Supervisor
2, Nosa Avenue, off Ruben Agho, Off Gapiona, GRA, Benin City, Nigeria.	Dr. Mazli Mustapha
Date: 16/10/2021	Date: 22/10/2021

UNIVERSITI TEKNOLOGI PETRONAS

OPTIMIZATION AND METALLURGICAL STUDY OF RESISTANCE SPOT WELDED HEAT TREATED SUS316L AUSTENITIC STAINLESS STEEL

by

MUHAMMED MUSA

The undersigned certify that they have read and recommend to the Postgraduate Studies Programme for acceptance this thesis for the fulfilment of the requirements for the degree stated.

Dr. Mazli Mustapha
Senior Lecturer
Mechanical Engineering Department
Universiti Teknologi PETRONAS

Signature: ______________________

Main Supervisor: Dr. Mazli Mustapha

Signature: Nabihah

DR. NABIHAH SALLIH
Lecturer
Universiti Teknologi PETRONAS
32610 Seri Iskandar
Perak Darul Ridzuan, Malaysia

Co-Supervisor: Dr. Nabihah Bt Sallih

Signature: ______________________

ASSOC. PROF. DR. MASDI BIN MUHAMMAD
Chair
Mechanical Engineering Department
Universiti Teknologi PETRONAS
32610 Seri Iskandar
Perak Darul Ridzuan, Malaysia

Head of Department: Assoc. Professor Dr. Masdi B Muhammad

Date: 22/10/2021

OPTIMIZATION AND METALLURGICAL STUDY OF RESISTANCE SPOT WELDED HEAT TREATED SUS316L AUSTENITIC STAINLESS STEEL

by

MUHAMMED MUSA

A Thesis

Submitted to the Postgraduate Studies Programme

as a Requirement for the Degree of

MASTER OF SCIENCE

MECHANICAL ENGINEERING

UNIVERSITI TEKNOLOGI PETRONAS

BANDAR SERI ISKANDAR,

PERAK

OCTOBER 2021

DECLARATION OF THESIS

Title of thesis	OPTIMIZATION AND METALLURGICAL STUDY OF RESISTANCE SPOT WELDED HEAT TREATED SUS316L AUSTENITIC STAINLESS STEEL

I MUHAMMED MUSA

hereby declare that the thesis is based on my original work except for quotations and citations which have been duly acknowledged. I also declare that it has not been previously or concurrently submitted for any other degree at UTP or other institutions.

Witnessed by

Dr. Mazli Mustapha
Senior Lecturer
Mechanical Engineering Department
Universiti Teknologi PETRONAS

Signature of Author	Signature of Supervisor
Permanent address:	Name of Supervisor
2, Nosa Avenue, off Ruben Agho, Off Gapiona, GRA, Benin City, Nigeria.	Dr. Mazli Mustapha
Date: 16/10/2021	Date: 22/10/2021

DEDICATION

This research work is dedicated to my family and loved ones for their incessant guidance and support during my studies.

ACKNOWLEDGEMENTS

Firstly, I would like to thank Almighty Allah for granting me good health, strength, and knowledge to execute this project successfully. His favours and mercy in my life are countless, and I consider the successful execution of this project as one of them.

I would also like to express my sincere gratitude to my supervisor, Dr. Mazli Mustapha, for his relentless guidance, support, generosity, selflessness, and encouragement during the project's duration. Words fail me to express my appreciation to him, but his legacies would not be forgotten.

Notwithstanding, I would also like to thank Dr. Turnad Lenggo Ginta for his guidance and motivation during the period he was around. However, he retired and went back to his hometown and could not witness the completion of the project. But his unceasing generosity would not be forgotten in a short while. My sincere appreciation also goes to Dr. Nabihah Sallih, who assisted in the project execution by providing necessary guidance and advice.

Nonetheless, I would like to thank the management of the Universiti Teknologi Petronas for funding this research work through the Yayasan Universiti Teknologi Petronas grant. I would also like to thank the laboratory technologists in the Mechanical Engineering Laboratory, Materials Laboratory and Central Analytical Laboratory for their assistance.

Finally, my utmost gratitude goes to my colleagues, friends, and relatives. Their kind words of encouragement and support made my study here at UTP worthwhile.

ABSTRACT

Resistance Spot Welding (RSW) is a well-known joining technique in the automobile industry. In producing stainless steel RSW joints, one of the problems encountered is poor weld quality indicated by a reduction in weld nugget resulting from inappropriate RSW parameters. Furthermore, the hardness of the Fusion Zone (FZ) influences the mechanical performance of the weld joints as it affects the failure mode. The optimization of the RSW parameters and the application of post-weld treatment has the potential of improving the quality of RSW joints. The incorporation of design of experiment, such as the central composite design of the response surface methodology, facilitates the optimization process. In this research work, the welding current, welding time and electrode pressure, which optimizes the nugget diameter and FZ hardness of RSW 2 mm SUS 316L austenitic stainless steel, were determined. Subsequently, the effect of preheating and post-weld tempering on the FZ hardness was also investigated. A total of twenty experimental runs each were generated for RSW parameters and post-weld treatment parameters using CCD. The domains for the RSW parameters are 6 – 11 KA welding current, 10 – 30 cycles welding time and 4 – 6 bar electrode pressure, while the domains for the post-weld treatment parameters are 100 – 200 ^{o}C preheating temperature, 400 – 600 ^{o}C tempering temperature and 2 – 4 hours holding time. Mechanical characterization of weld joints was achieved using Vickers microhardness tester, while microstructural characterization was conducted using optical microscopy, energy dispersive x-ray analysis and field emission scanning electron microscopy. The optimum RSW parameters that maximized the nugget diameter and minimized FZ hardness were 10.884 KA welding current, 30 cycles welding time, and 5.822 bar electrode pressure, producing a nugget diameter of 9.837 mm and FZ hardness of 196.07 HV. A lower FZ hardness of 149.2 HV was obtained after the application of post-weld treatment at 150 ^{o}C preheating temperature, 500 ^{o}C tempering temperature and 4.7 hours holding time. The reduction in hardness was due to deferritization, growth of austenite and delta ferrite grains and release of residual stresses. RSW parameters optimization and application of appropriate post-weld treatment has a significant potential of improving weld quality.

ABSTRAK

Resistance Spot Welding (RSW) adalah teknik bergabung yang terkenal dalam industri automobil. Dengan menghasilkan sambungan RSW keluli yang tahan karat, salah satu masalah yang dihadapi adalah kualiti kimpalan yang buruk ditunjukkan oleh pengurangan nugget kimpalan. Berikut disebabkan oleh parameter RSW yang tidak sesuai. Selanjutnya, kekerasan Fusion Zone (FZ) mempengaruhi prestasi mekanikal sendi kimpalan kerana mempengaruhi mod kegagalan. Pengoptimuman parameter RSW dan penerapan rawatan pasca kimpalan berpotensi meningkatkan kualiti sendi RSW. Penggabungan reka bentuk eksperimen seperti reka bentuk komposit pusat memudahkan proses pengoptimuman tersebut. Dalam kerja penyelidikan ini, arus kimpalan, masa kimpalan dan tekanan elektrod yang menjadi factor diameter nugget dan kekerasan FZ keluli tahan karat austenite. Selanjutnya, RSW 2 mm SUS 316L telah ditentukan. Selepas itu, kesan pemanasan dan pemanasan pasca kimpalan pada kekerasan FZ juga dikaji. Sebanyak 20 eksperimen dijalankan mengikut parameter RSW dan parameter rawatan pasca kimpalan menggunakan CCD. Domain untuk parameter RSW adalah arus kimpalan 6 - 11 KA, masa kimpalan 10 - 30 kitaran dan tekanan elektrod 4 - 6 bar. Sebagai domain untuk parameter rawatan pasca kimpalan adalah suhu pemanasan 100 - 200 ^{o}C, suhu tempering 400 - 600 ^{o}C dan masa tahan 2 - 4 jam. Pencirian mekanikal sambungan kimpalan dicapai dengan menggunakan penguji mikrohardness Vickers. Sebagai prosedur seterusnya, pencirian struktur mikro dilakukan menggunakan mikroskopi optik, analisis sinar-x penyebaran tenaga dan mikroskop elektron pengimbasan pelepasan medan. Parameter RSW optimum yang meningkatkan diameter nugget dan kekerasan FZ yang minimum didapati menerusi arus kimpalan 10.884 KA, masa kimpalan 30 kitaran dan tekanan elektrod 5.822 bar, menghasilkan diameter nugget 9.837 mm dan kekerasan FZ 196.07 HV. Kekerasan FZ yang lebih rendah sebanyak 149.2 HV diperoleh setelah penggunaan rawatan pasca kimpalan pada suhu pemanasan 150 ^{o}C, suhu tempering 500 ^{o}C dan masa tahan 4.7 jam. Pengurangan kekerasan disebabkan oleh deferritisasi, pertumbuhan biji austenit dan delta ferit dan pelepasan tekanan sisa. Pengoptimuman parameter RSW dan penggunaan rawatan pasca kimpalan yang sesuai mempunyai potensi yang bermakna untuk meningkatkan kualiti kimpalan.

CERTIFICATION

TABLE OF CONTENT

LIST OF FIGURES

LIST OF TABLES

LIST OF EQUATIONS

CHAPTER 1

INTRODUCTION

1.1 Background of Study

Steel is essentially an alloy of iron and carbon, with carbon being the principal constituent. It is the most widely used engineering material in service because of its availability, low cost, and, most importantly, the ease of modifying its properties to suit desired applications. It finds application in building construction, automobile industries, machine tools, among others [1]. The American Iron and Steel Institute (AISI) classified steel based on chemical composition into carbon steel, alloy steel, stainless steel, and tool steel, with stainless steel being preferred for corrosion applications [2]. Stainless steel is further classified into ferritic, martensitic, austenitic and duplex stainless steel, with austenitic stainless steel being a preferred option due to its favourable properties such as strength, especially at severe conditions ranging from elevated temperatures to cryogenic ones, thus, finds application in marine and water reactors [3]. The high chromium composition in austenitic stainless steel preserves the integrity of the metal in service by forming a protective thin film that serves as a barrier between the metal and the environment, thus, reducing corrosion rate. In addition to the strength of austenitic stainless steel, grades with low carbon compositions such as 316L and 304L have a wider range of applications as they can easily be fabricated by several manufacturing processes, especially by welding.

Welding is a permanent technique for creating similar and dissimilar metal joints. Several welding techniques are available in literature, including Friction Stir Welding (FSW), Shielded Metal Arc Welding (SMAW), Gas Tungsten Arc Welding (GTAW), Resistance Spot Welding (RSW), among others. However, resistance spot welding seems to be distinct from the others due to the speed and efficiency in creating several spot welds of high quality in a short while. Thus, finds application in the automobile industry, consumer goods, orthodontics, and robotics [4]. Resistance Spot Welding (RSW) involves heating two metals through electric current supplied through electrodes to the metal interface. Heat generation at the metal interface results from the resistance offered by the metal to the flow of electric current and subsequently leads to a rise in temperature, which continues until a fusion point is reached, thus, forming a weld nugget [5]. The quality of weld joints is mainly dependent on the resistance spot welding parameters (welding current, welding time and electrode pressure or force), as several publications are available in literature discussing the effect of these parameters on the properties of stainless steel [6]. Despite the several benefits derived from the use of spot welding, some problems still arise in its use as a joining technique.

Resistance spot welding is not much different from other welding techniques as it suffers a common challenge of general property deterioration like other conventional welding techniques in similar welded joints. In dissimilar spot welded joints, a more severe challenge of producing good quality joints is encountered due to the difference in the thermophysical and mechanical properties of the parent metals. Weld property deterioration results from the non-uniform heating and cooling of the weld metal, which results in the formation of a hard Fusion Zones (FZ) and induces residual stresses, thus, making the weld joints susceptible to cold cracking and ultimate failure in service [7]. Another factor that results in poor quality in resistance spot welded joints is inappropriate welding parameters resulting in expulsions in the weld joint, increased FZ hardness, and reduction in the Tensile Shear Load Bearing Capacity (TSLBC).

In view of improving the quality of weld joints, experimenters have tried to alter the rate of heating and cooling during the welding process by applying several weld treatment processes mainly, pre and post-weld treatment processes ranging from preheating, tempering, annealing to other surface modification processes such as electrolytic plasma processing [8 – 10]. Weld treatment processes are controlled property modification processes applied to weld joints before, during or after the welding operation. Property modification is achieved by changes in microstructural composition and surface features of the weld metals. Microstructural evolution is achieved mainly by heat treatment processes such as tempering and preheating. In contrast, surface modification mechanisms such as shot peening and plasma processing are used for weld surface property improvement [11 – 13].

The most common pre weld treatment process applied to most weld joints is preheating. It involves heating the base metals to a predetermined temperature prior to welding. It makes the metal more receptive to the welding process and reduces the cooling rate, thus reducing residual stresses and weld susceptibility to cold cracking [14]. In addition, preheating has also been reported to improve fracture toughness and formability of weld joints by reducing the hardness of the weld joint [10]. Tempering, on the other hand, is a post-weld treatment process usually applied to hardened joints. It involves heating the weld joint to a temperature below the critical transformation temperature of the base metals. It confers several benefits such as hardness reduction, which connotes an improvement in the weld fracture toughness and also brittle fracture prevention [15]

Recent publications usually incorporate statistical techniques for data analysis, with Response Surface Methodology (RSM) being one of them. It combines mathematical and statistical tools such as Analysis of Variance (ANOVA), correlation, and regression, which can establish relationships between weld performance parameters such as the hardness of the weld joint and RSW parameters. RSM comprises several designs, but Central Composite Design (CCD) is the most used design for variable optimization due to its simplicity. In addition, it can be used to study the effect of individual variables on the output variable, also known as the response.

1.2 Problem Statement

Previous studies revealed that the spot welding parameters (welding current, welding time and electrode pressure) play a significant role in determining the overall weld quality produced, as the selection of inappropriate parameters might result in poor weld quality. In this regard, Al-Mukhtar and Doos [16] observed cracks in resistance spot welded joints due to inappropriate electrode pressure, while Fukumoto et al. [17] detected weld expulsions in 200 μm austenitic weld joint due to excessive heating resulting from high welding current. In order to gain an insight into the effect of these parameters on the overall weld quality, researchers conducted further experiments. The findings of Kianersi et al. [18], who investigated the effect of welding current and welding time on the properties of 1 mm AISI 316L, revealed that increasing the heat input by increasing either of the parameters (welding current and welding time) resulted in a corresponding increase in peak load, TSLBC and failure energy. The improvement in weld quality was attributed to the increase in the nugget diameter. As maintained by Zhang et al. [19], who conducted an extensive study of the resistance spot welded 1.5 mm AISI 304 stainless steel, increment in nugget diameter influences the failure mode transformation from Interfacial, through partial pull out to complete pull out. Pouranvari et al. [20], in another study, following the investigation of the influence of the effect of welding current on the phase transformation of 1.2 mm AISI 304 stainless steel, expressed that the fusion zone hardness is the predominant factor determining the failure mode in resistance spot welded joints. Subsequently, Hayat and Sevim [21] observed reduced fracture toughness in 1.2 mm DP 600 resistance spot welded joints due to increased hardness of the fusion zone (FZ), while Mukhtar and Doos [16] reported weld cavitation in 1.5 mm austenitic stainless steel resulting from cracking, which was also attributed to increased hardness of the weld joint. Furthermore, Essoussi et al. [22] investigated the service performance of 1 mm AISI 304 stainless steel and reported that the maximum hardness of the joint occurs at the FZ. Jaber et al. [23] concluded that the weld joint's overall quality depends primarily on the FZ properties after conducting a study on the weld quality of 1.5 mm DP 600 stainless steel.

Furthermore, researchers have attempted to improve weld joints' quality by applying several weld treatment processes. Given this, Lincoln [24], reported that increasing preheating temperature reduces residual stresses in weld joints and consequently reduces the susceptibility of cold cracking, which implies a general improvement in weld quality. In another study, Nam et al. [25] reported that increasing the post-weld annealing temperature reduced the hardness of the weld joints but observed carbide precipitation at elevated temperatures. The reduction in hardness was attributed to grain growth and the release of residual stresses. The findings of other researchers revealed that increasing post weld tempering temperature and holding time improves the weld quality by reducing the overall hardness of the joint without precipitating carbides [26, 27].

From the foregoing, it is evident that the nugget diameter and the hardness of the weld joint (especially the FZ) are two cardinal indicators of the overall weld quality, as they are the significant determiners of performance parameters like the mode of failure and mechanical performance of spot welded joints. This also implies that spot welded joints with improved quality can be obtained if these properties are optimized. Two common optimization techniques reported in most literature are Response Surface Methodology (RSM) and the Taguchi Method. Unlike the Taguchi method, the RSM delineates a greater sensitivity of the response variables to changes in factors or input variables which implies a greater accuracy. Furthermore, though experimenters have only reported the individual benefits of preheating and tempering on spot welded joints, the combination of both processes has the potential of producing better joint qualities.

1.3 Objectives of Research

As a response to the aforementioned setbacks discussed in the preceding section, the following objectives were derived.

1. To optimize the welding current, welding time and electrode pressure for SUS 316L austenitic stainless steel using Response Surface Methodology (RSM) with Fusion Zone hardness and nugget diameter as response variables.

2. To investigate the effect of preheating temperature, tempering temperature and tempering holding time on the Fusion Zone hardness of resistance spot welded SUS 316L austenitic stainless steel.

1.4 Scope of Research

This research is oriented towards improving the quality of resistance spot welded joint using 2 mm thick SUS 316L austenitic stainless steel as the material for the case study.

Weld quality improvement was achieved by first optimizing resistance spot welding parameters, namely, welding current, welding time and electrode pressure using Response Surface Methodology (RSM), with the criterion for optimization being the hardness of the weld joint.

Subsequently, further improvement in weld quality was achieved by the application of preheating and post-weld tempering. The effect of pre and post-weld parameters, namely, preheating temperature, post-weld tempering temperature and tempering holding time, was also investigated.

In addition to the hardness of the weld joint, the weld geometric parameter (nugget diameter) was also characterized. Aside mechanical characterization, microstructural characterization was also carried out using Field Emission Scanning Electron Microscope (FESEM), Energy Dispersive X-ray (EDX) spectroscopy and Optical Microscopy (OM) techniques.

1.5 Organization of the Thesis

This research work is sectioned into five chapters with the headings; introduction, literature review, methodology, results, discussion, and conclusion and recommendation.

The first chapter presents a framework of the study by bringing to light the importance of resistance spot welding technique and the attempts recorded by previous researchers to improve the quality of weld joints. Subsequently, a persistent challenge was identified from which the objectives of this study were formulated. The chapter was concluded by clearly stating the scope of the research work.

The second chapter presents an overview of steel types and their applications. This was followed by discussions on RSW as a joining technique coupled with the presentation of an extensive review on the effect of RSW parameters on the properties of welded joints. Studies optimizing these parameters were also presented. Subsequently, different weld treatments procedures were provided alongside their effect on the overall joint quality. The chapter was concluded with notes on RSM procedure.

Chapter 3 commenced by presenting a flow chart summarizing the methodology for achieving the research objectives mentioned in the previous chapter. This was succeeded by carrying out a DOE using Design Expert software. Afterwards, samples were prepared for the spot welding process, accompanied by the appropriate weld treatment process. This section was concluded by characterizing the welded samples mechanically and morphologically.

In chapter 4, the results obtained for the nugget diameter and weld hardness were presented. This was followed by a statistical evaluation culminating in the generation of mathematical models for their prediction. The welding parameters were optimized and subsequently followed by experimental validation. A similar procedure was done for the weld treatment parameters, and the chapter was concluded by discussing the morphological features of the weld joints.

The last chapter presented a conclusion of the research work, which summarises the significant findings related to the stipulated objectives. This was then followed by research proposals in the form of recommendations for future experimenters.

CHAPTER 2

LITERATURE REVIEW

2.1 Stainless Steel

Stainless steel contains other additional elements alongside the primary constituents (iron and carbon), such as chromium, molybdenum, titanium, boron, silicon, etc. The principal alloying element is chromium, which occurs in amounts up to 25 % in some alloys. It is essential to point out that incorporating alloying elements into stainless steel depends on the intended application, which accounts for the bulk of several grades of stainless steel available in service [28].

The several stainless steel applications are due to their low price, favourable properties, and ability to tailor them to suit the desired application. These properties are conferred by the alloying elements, which forms an integral component of the chemical composition of the metal. For instance, the presence of chromium has been reported to increase the corrosion resistance and strength while nickel increases its ductility. The metal has been reported to have been used in the fabrication of heat exchangers, robots, parts of automobiles, cutleries and components of International Thermonuclear Experimental Reactors (ITER) [22 – 24].

The production of stainless steel is usually in three forms: cast, wrought, and powder form, and it takes place in two stages. The first stage involves the melting of scraps alongside desired alloying elements in a furnace. This is then followed by a decarburization process in which the carbon content of the steel is controlled and the removal of impurities from the metal using argon [30]. Figure 2.1 shows the linkage between several grades of stainless steel belonging to the family stainless steel alloy.

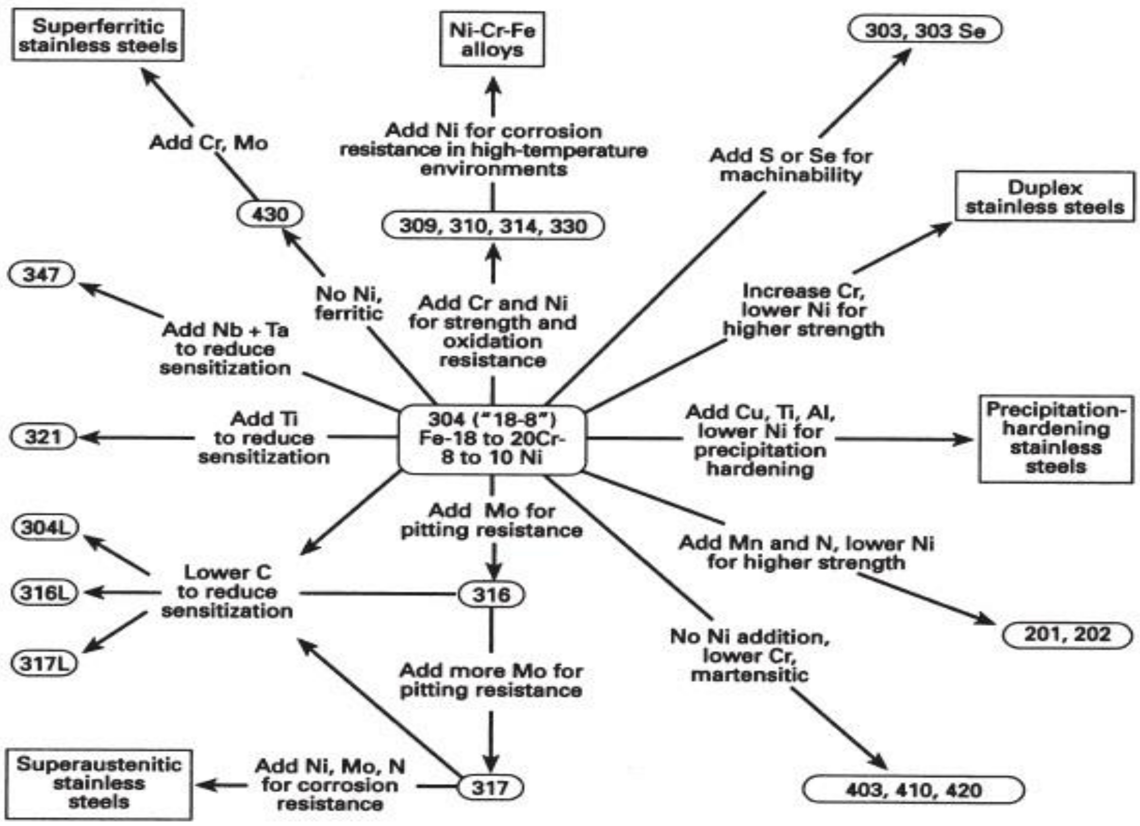

Figure 2.1: Composition and property linkage in the stainless steel family [23].

2.1.1 Types of Stainless Steel

Based on the microstructure, stainless steel can be classified into:

1. Austenitic stainless steel
2. Duplex stainless steel
3. Martensitic stainless steel
4. Ferritic stainless steel

1. **Austenitic Stainless Steel:** The bulk of the stainless steel available in service is austenitic stainless steel (mostly 304L and 316L), as it is preferred to other grades of stainless steel due to its superior properties, strength and corrosion resistance at elevated and cryogenic temperatures. They find application in automobile parts, the food industry, cookware, and thermonuclear components [24, 25].

   With the addition of alloying elements such as molybdenum, the pitting corrosion resistance and creep strength at an elevated temperature is further increased. In addition to the chromium and molybdenum, other alloying elements, such as nickel, manganese, and silicon, are usually added in different proportions, depending on the steel grade. Table 2.1 shows the chemical composition of austenitic stainless steel.

Table 2.1: Chemical composition of 316L austenitic stainless steel (%wt.) [26].

C	Cr	Ni	Mn	Mo	Si	P	S	Fe
0.03	16	10	2	2	1	0.045	0.03	balance

The microstructure of austenitic stainless steel comprises austenite phase (primary phase) and delta ferrite (secondary phase) arranged in a Face Centred Cubic (FCC) orientation with additional inclusions or unwanted phases on rare occasions. Figure 2.2 shows the micrograph of the microstructure of AISI 316L austenitic stainless steel. The alloy composition limits the maximum strength conferred on this grade of stainless steel by coldworking, while the low carbon composition renders it to other fabrication processes such as welding [21, 27].

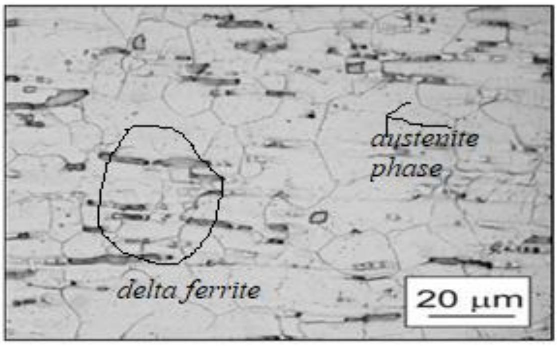

Figure 2.2: Microstructure of AISI 316L austenitic stainless steel [26].

As shown in Figure 2.1, 316L austenitic stainless steel is the lower carbon grade of 316 austenitic stainless steel obtained from the ordinary 316 grade austenitic stainless steel by reducing the carbon composition to minimize sensitization during the fabrication process. The “L” attached to the grade number (316) indicates the low carbon composition, which is approximately 0.03 % or less. It belongs to the family of Chromium – Nickel – Molybdenum austenitic stainless steel containing about 17 % chromium, 10 – 13 % nickel and 2 – 3 % molybdenum [30]. The symbol attached to the grade number depends on the nomenclature and standard adopted in the manufacture of stainless steel. The prevalent nomenclatures used in the manufacturing industry are the American Iron and Steel Institute (AISI) standards, American Society of Testing and Materials (ASTM) and Society of Automotive Engineers (SAE) standard, American Society of Mechanical Engineers (ASME) standard and the Japanese Industrial Standard (JIS). The AISI, ASTM and SAE, and ASTM standards originated in the United States of America, while the JIS standard originated in Japan. All the above-mentioned standards adopt a Unified Numbering System (UNS) developed by the AISI, but there is a slight discrepancy regarding the number of digits and the acronyms that precede the grade number. For instance, all the standards use a three-digit number to indicate the grade number of the stainless steel except for the ASTM/SAE standard, where a five-digit number is adopted. Furthermore, the acronyms preceding the grade number are "AISI", "UNS S", "SA", "SUS" for the AISI standard, ASTM / SAE standard, ASME standard and the JIS standard, respectively. However, there is no significant difference in the composition of the grade of stainless steel across the different standards [34].

2. **Duplex Stainless Steel:** It is also known as dual phase stainless steel and finds application in the automobile industry, petrochemical industry, paper industry, and marine applications as a result of its toughness, yield strength, work hardening rate, formability, corrosion resistance, light weight and crash worthiness [28 – 32]. Special industrial requirements, such as strength and corrosion resistance at elevated temperatures, led to the development of higher grades of duplex stainless steel used in boilers, pressurized reversed osmosis plants, firefighting systems, and heat exchangers [29, 33]. Table 2.2 shows the chemical composition of duplex stainless steel.

Table 2.2: Chemical composition of DP 980 dual phase stainless steel [35].

C	**Cr**	**Al**	**Mn**	**Si**	**P**	**S**	**Cu**	**Fe**
0.13	0.2	0.036	1.33	0.13	0.004	0.014	0.196	balance

The microstructure of duplex stainless steel comprises dispersed austenite in ferrite phases with other alloying elements. The microstructure of SAF 2205 duplex stainless steel is presented in Figure 2.3. Previous research revealed that optimum properties in duplex stainless steel are obtained when the dual phases are in equilibrium; in other words, when the percentage composition of both phases are approximately equal [33 – 35].

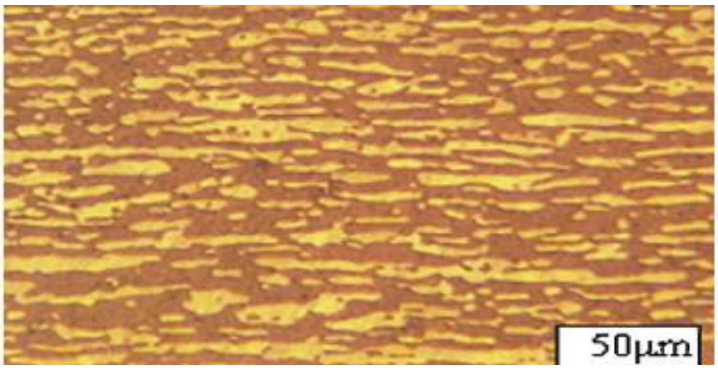

Figure 2.3: Microstructure of SAE 2205 duplex stainless steel [38].

3. **Martensitic Stainless Steel**: It finds application in nuclear power plants, the oil and gas industry, hydraulic turbines, pumps, shafts, surgical tools and bearings due to its favourable mechanical properties, corrosion resistance, ease of heat treatment and weldability [43]. The need to improve the properties of martensitic steels for special industrial applications led to the development of higher grades of martensitic steel such as super martensitic stainless steel (SMSS), lean super martensitic stainless steel (LSMSS), reduced activated ferritic, martensitic (RAFM) stainless steel, China low activation martensitic (CLAM) stainless steel and maraging stainless steel [44]. In these grades of martensitic stainless steel, there is a reduction in the carbon composition to improve weldability, an increase in nickel and molybdenum content to stabilize martensite microstructure and improve the corrosion resistance with other alloying additions such as titanium, vanadium and copper to confer other properties [39 – 40]. Table 2.3 shows the chemical composition (% weight) of AISI 420 martensitic steel.

Table 2.3: Chemical composition (%weight) of AISI 420 martensitic stainless steel [10].

C	**Cr**	**Al**	**Mn**	**Si**	**P**	**S**	**Ni**	**Mo**	**Fe**
0.351	13.71	<0.02	0.548	0.562	0.024	0.009	<0.3	0.084	balance

The microstructure of martensitic stainless steel comprises martensite, austenite and ferrite phases, with the primary phase being martensite [47]. The microstructure of AISI 410S martensitic stainless steel is presented in Figure 2.4.

Figure 2.4: Microstructure of AISI 410S martensitic stainless steel [43].

4. **Ferritic Stainless Steel:** Ferritic stainless steel finds application in the automotive industry, fuel cells, catalytic converters and the oil and gas industries, among others. The wide range of applications of ferritic stainless steel is attributed to their low cost, strength, corrosion resistance, high temperature oxidation resistance, high thermal conductivity, low thermal expansion and weldability compared to their counterpart austenitic stainless steel [42 – 44]. Table 2.4 shows the chemical composition of AISI 4140 ferritic stainless steel.

Table 2.4: Chemical composition of AISI 4140 ferritic stainless steel (% by weight) [47].

C	**Cr**	**Mo**	**Mn**	**P**	**S**	**Si**	**Fe**
0.38-0.43	0.8-1.1	0.15-0.25	0.75-1.0	0.035	0.04	0.15-0.3	balance

The microstructure of ferritic stainless steel comprises ferrite and pearlite [51]. The microstructure of AISI 4140 ferritic stainless steel is shown in Figure 2.5.

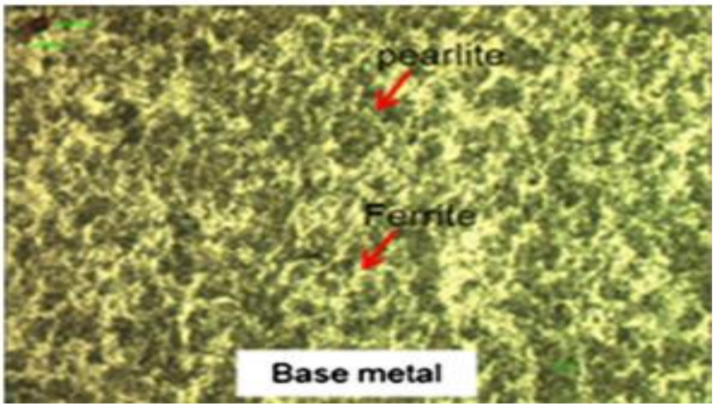

Figure 2.5: Microstructure of AISI 4140 ferritic stainless steel [47].

2.2 Resistance Spot Welding and the Mechanism of Nugget Formation

An English born American Engineer called Elihu Thompson first invented Resistance Spot Welding (RSW) in 1877 as a joining technique for manufacturing processes. Since then, it has been adopted as a major welding technique for most fabrication processes, especially those involving stainless steel [52].

RSW is economical, robust, with a high speed and adaptability for automation, coupled with its suitability for bulk production. These account for its wide adoption by most industries, dominantly, the locomotive industry. In addition, when compared to other welding techniques, the spot is usually formed internally from both sides of the metal as against one side as in Tungsten Inert Gas (TIG) and Metal Inert Gas Welding [49 – 51].

The mechanism of the resistance spot welding process and the formation of the weld nugget is explained as follows. The welding process utilizies the resistance offered by the metals to be welded (base metals) due to the flow of electric current through them. The joining technique involves combining three key elements, namely, heat, force, and time. The heat is supplied by means of electric current, which is usually Alternating Current (AC), the force is applied by means of pressure applied at the electrodes, while the time refers to the duration to complete the entire welding operation. During the welding process, the electric current supplied through the electrodes brings about localized melting of the metals, and when held for sufficient time by the force applied at the electrodes (upper and lower electrodes). The metal's localised melting casts the point that forms the weld nugget that binds the base metals together. Meanwhile, the metals are held in intimate contact by the pressure applied at the electrode till the weld nugget is formed. The RSW parameters (electric current, pressure and time) to be selected for a particular metal depends on a variety of factors with material thickness, type of metal, nature of the joint (similar or dissimilar), cross-sectional area of the electrode being a dearth of them [56]. Figure 2.6 illustrates the RSW process.

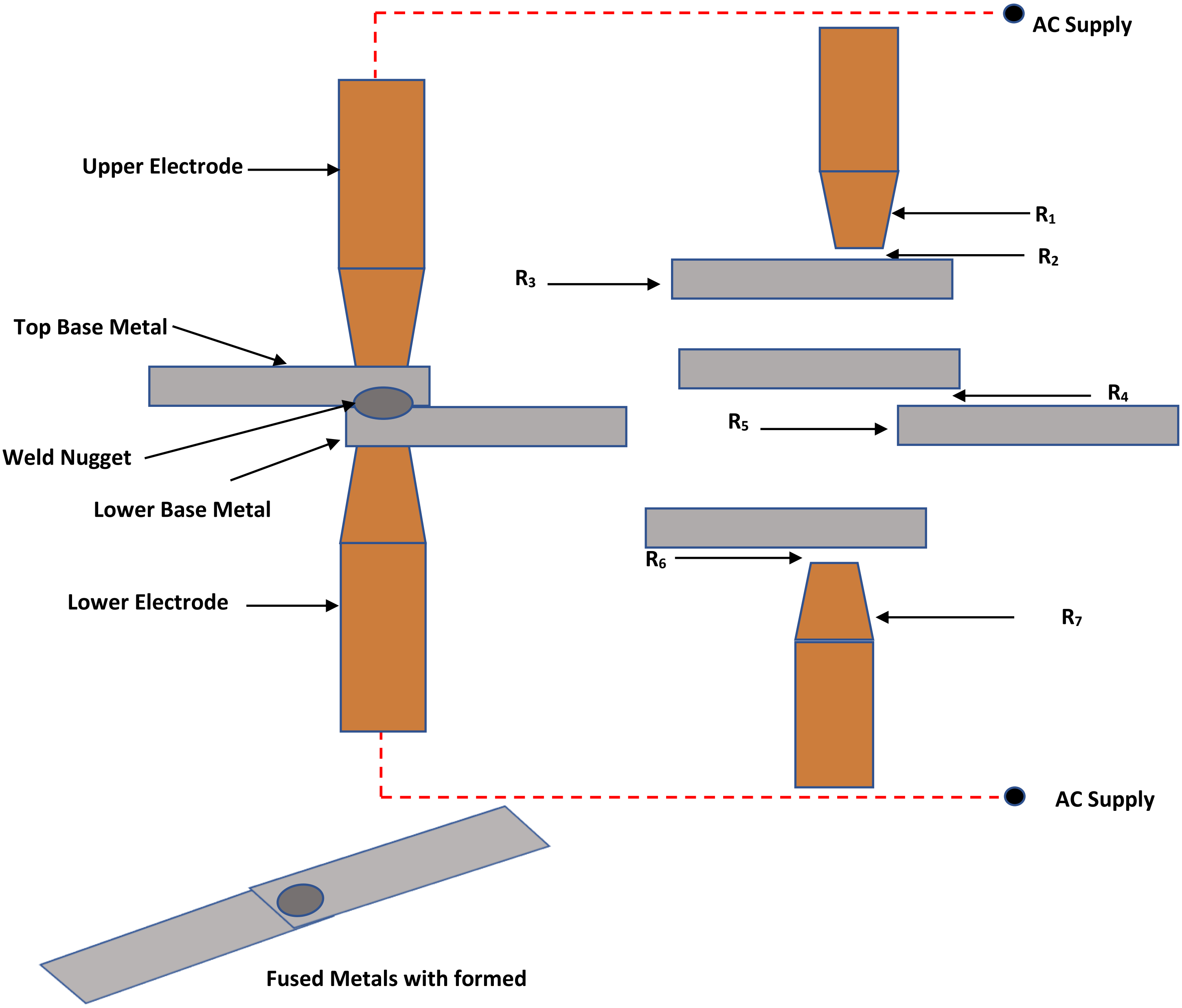

Figure 2.6: Illustration of the resistance spot welding process and mechanism of nugget formation.

2.2.1 Resistance Spot Welding Parameters

As mentioned in the previous section, the three primary parameters required in RSW include electric current, electrode pressure and welding time. The following paragraphs briefly examine each of these parameters.

2.2.1.1 Electric Current

The electric current (mostly alternating current) supplies the heat energy required for the welding process, with the amount of heat generated being a function of the total resistance. It is important to point out that, aside the resistance offered by the metals to be joined, resistance is also offered by the welding circuit. But the design of most RSW equipment is such that this resistance is insignificant compared to the former [56].

The total resistance includes resistance at the interface between the top metal and welding electrode (R_1), the resistance of the top metal (R_2), the resistance at the interface between the top metal and the bottom metal (R_3), the resistance of the bottom metal (R_4), the resistance between the bottom metal and the welding electrode (R_5) and the resistance of the electrode (R_6). These resistances are illustrated in Figure 2.6. This cumulative resistance, offered by the various components, generates the heat energy required for the fusion of the metals. The heat generated is in accordance with joules law, which shows a direct relationship between the square of current and heat energy generated. This accounts for the ginormous heat energy generated during the process [57].

2.2.1.2 Welding Time Cycle

This refers to the total time required to complete the welding operation. At a constant welding current, the heat energy generated in the metals is different due to the discrepancy in the welding time during the various stages of the welding process and the differential in the resistance offered by the various sections. The total welding time cycle comprises the squeeze time, weld time, hold time and off time.

At the inception of the welding process, pressure is first applied to the metals to make them receptive to the electric current. This time interval between the pressure application and the introduction of electric current is called the squeeze time. This is followed by the application of the welding current, which causes the fusion of the metals. The time duration taken to apply the welding current is known as the welding time. Subsequently, the fused metals are held in position for some time to allow for solidification of the weld nugget. This time is known as the holding time or cooling time. Eventually, the electrodes are removed from the fused metals after a duration of time called the off time. The welding time is usually measured in cycles (1 cycle = 0.02 seconds) [58].

2.2.1.3 Electrode Pressure

The electrode pressure provides the force required to hold the metals to be joined in intimate contact to ease the flow of electric current through them. The pressure to be applied to the metals depends on several factors, including the type of metal, the thickness, and the size. In general, the metals to be joined should not be over-pressurized as this might influence the welding process by reducing the total electrical resistance, resulting in higher heat generation and, in some cases, weld distortion [59].

2.2.2 Review of Effect of Spot Weld Parameters on the Properties of Stainless Steel.

Discussions from the previous sections revealed that the properties of stainless steel obtained from resistance spot welding are predominantly dependent on the spot welding parameters. Ample literatures are available addressing the effects of these parameters on the properties of different grades of stainless steel as well as their effects on dissimilar joints; some involving different grades of stainless steel while others involve stainless steel and other metals such as aluminium and low carbon steel. The following sections present the effect of welding time, electrode pressure (force) and holding time on the properties of stainless steel.

2.2.2.1 Effect of Spot Weld Parameters on the Properties of Similar Stainless Steel Weld Joints.

This section presents literatures on the effect of spot welding parameters on the properties of similar stainless steel weld joints comprising austenitic, duplex, martensitic and ferritic stainless steel.

2.2.2.1.1 Similar Austenitic Stainless Steel Weld Joints.

Some of the previous studies addressing the effect of spot welding parameters on the properties of austenitic stainless steel are summarized in Table 2.6.

Table 2.6: Review of effect of resistance spot welding parameters on the properties of austenitic stainless steel

Year	Author	Title	Research Focus
2008	D. Ozyurek [60].	An effect of weld current and weld atmosphere on the resistance spot weldability of 304L austenitic stainless steel.	Effect of nitriding atmosphere and welding current on the properties of austenitic stainless steel.
2008	S. Fukumoto et al. [17].	Small-scale resistance spot welding of austenitic stainless steel.	Effect of small-scale resistance spot welding on the properties and microstructure of austenitic stainless steel.
2009	B. Kocabekir et al. [6].	An effect of heat input, weld atmosphere and weld cooling conditions on the resistance spot weldability of 316L austenitic stainless steel.	Effect of weld time, nitriding, and borax cooling on the properties of austenitic stainless steel.
2011	I. Hwang et al. [61].	Expulsion reduction in resistance spot welding by controlling of welding current waveform.	An alternative method for reducing expulsion in spot welded joints using pulse welding current.
2013	A. Al-Mukhtar and Q. Doos [16].	Cracking phenomenon in spot welded joints of austenitic stainless steel.	Causes of cracking phenomenon observed in spot welded joints.
2014	D. Kianersi et al. [18].	Effect of welding current and time on the microstructure, mechanical characterizations, and fracture studies of resistance spot welding joints of AISI 316L austenitic stainless steel.	Optimum resistance spot welding parameters for 1 mm austenitic stainless steel.
2014	H. Moshayedi and I. Sattari-Far. [62].	Resistance spot welding and effects of welding current and time on residual stresses.	Effect of welding current and time on the nugget diameter and residual stresses of austenitic stainless steel.
2016	Q. Fan et al. [63].	Expulsion characterization of stainless steel resistance spot welding based on dynamic resistance signal.	Weld quality prediction using dynamic resistance with tensile shear strength as criterion.
2019	H. Essoussi et al. [22].	Microstructure and mechanical performance of resistance spot welding of AISI 304 stainless steel and AISI 1000 series steel.	Effect of microstructure on the properties of RSW austenitic stainless steel.

2020	Y. Zhang et al. [19].	A comparative study between the mechanical and microstructural properties of resistance spot welding joints among ferritic AISI 430 and austenitic AISI 304 stainless steel.	Properties of resistance spot welded AISI 304 austenitic stainless steel.

An investigation of the properties of resistance spot welded stainless steel revealed that the most important property of the joints that can be used as a tool for quality prediction is the nugget diameter. This property has been found to significantly affect the tensile shear load bearing capacity and, by extension, the failure energy. The nugget diameter has been reported to increase with increasing energy input, mainly the welding current and welding time [18].

Further investigation was carried out by Kianersi et al. [18] to ascertain the effect of these parameters on the properties of austenitic stainless steel. Their findings revealed that an increase in welding current and time brought about a corresponding increase in weld penetration, width of Heat Affected Zone (HAZ), electrode indentation depth, peak load and failure energy, and a decrease in thickness of the HAZ. They attributed the property improvement to an increase in nugget diameter brought about by increased heat input and metal molten volume at the weld nugget. The reduction in the HAZ thickness was due to the plastic deformation at the interface between the weld metal and electrodes brought about by a high welding current. This was also accompanied by the transformation of the failure mode from interfacial through partial pull out to complete pull out, as also reported by Pouranvari et al. [64].

Furthermore, the findings of Zhang et al. [19] also revealed that increasing nugget size of spot welded austenitic stainless steel leads to a transformation in failure mode from interfacial to complete pull out. This was accompanied by an increase in peak load and energy absorption ability of the welded joints, attributed to the massive plastic deformation. In addition, they also observed the presence of shrinkage cavities at the FZ, which is an indication of dendrites solidification. A related study carried out by Pouranvari et al. [66, 67] revealed that austenitic spot welded are more susceptible to interfacial failure due to the concentration of high strains at the weld nugget whose magnitudes exceeds the critical limits. Another notable finding from the study is that the higher the hardness ratio of the FZ to the BM, the higher the susceptibility of the joints to fail in pull out mode.

As expected, the resulting properties from a resistant spot welding process are primarily dependent on the properties of the base metals, as the properties of the resulting joint are a product of the chemistry between the base metals, the spot welding parameters, and the ambient welding conditions. The findings of Essoussi et al. [22], who studied the effect of base metal properties on the quality of 1 mm spot welded austenitic stainless steel, revealed that the maximum hardness of the joints was observed at the fusion zone due to the presence of alloying elements which tend to form non-metallic inclusions at the region. In addition, they also reported that the mode of failure is also a function of the base metal properties as they observed a plug fracture mode for the welded joints.

A very common phenomenon that occurs during welding, especially with inappropriate welding parameters, is weld expulsion. It has been reported to result in dissipation of energy, unattractive weld appearance, electrode wear and, in some cases, results in high corrosion rate of the welded joints. In an attempt to investigate the relationship between resistance spot welding parameters and expulsion observed in austenitic stainless steel weld joint, Fan et al. [63], predicted the quality of resistance spot welded 301 stainless steel of different thicknesses (2 mm and 3 mm) using dynamic resistance. They discovered that increasing welding current results in a corresponding increase in expulsion tendency, leading to a corresponding decrease in tensile shear strength. Similar findings were also reported by Han et al. [67], who explained that the reason for the increased tensile shear strength observed in most spot welded joints at very high welding current above the limits specified in the welding lobe where expulsion is present, is because the increase in tensile strength brought about by increasing welding current supersedes the reduction brought about by expulsions. They concluded that preheating and the use of low electrode pressures are possible ways of reducing weld expulsions.

Aside the spot welding parameters, other factors such as the environmental conditions where the spot welding is carried out has been found to have considerable effects on the joint quality produced by spot welding. The effect of nitriding environment and welding current on the properties of 1 mm spot welded 304L austenitic stainless steel was investigated by Ozyurek [60]. Their findings revealed that the tensile shear load bearing capacity increased with the welding current and was further increased with nitriding. The former resulted from the increase in nugget diameter while the latter resulted from the solid solution strengthening resulting from the precipitation and diffusion of nitrogen atoms into the microstructure. A similar explanation was provided by Pant et al. [68]. Furthermore, a general increase in hardness was reported at the fusion zone, but changes in welding current had no significant effect on the hardness of the welded joint.

Similar findings were reported by Kocabekir et al. [6], who carried out further studies on the effect of nitriding, borax cooling and welding current on the properties of 1 mm 316L austenitic stainless steel. They found that borax cooling reduced the TSLBC due to the reduction in nugget diameter and weld penetration depth coupled with the increased cooling rate. It was also discovered that nitriding decreased weld penetration depth despite the overall increase in TSLBC. The hardness test revealed that changes in welding time had no significant effect on the hardness, which was attributed to the unhardenable austenite microstructure. At the same time, nitriding increased the hardness due to the high heat dissipation rate caused by the pressurized nitrogen gas jet.

A type of spot welding technique that has received less attention from researchers is small-scale spot welding. It is a term used to refer to a spot welding technique carried out on metals whose thickness is 0.5 mm or less. It finds application in biomedical equipment and electronic appliances [62, 63]. In order to understand the effect of spot welding parameters on the microstructure and properties of austenitic stainless steel performed on a small scale, Fukumoto et al. [17] welded several grades of austenitic stainless steel of 200 µm thickness using spot welding. Their study revealed that increasing welding current brought about weld nugget growth which was accompanied by an increase in tensile shear strength. These results are similar to those obtained for large scale resistance spot welding [63]. In addition, weld expulsion was also observed at high welding current values but did not significantly affect the tensile shear strength. Reduction in weld expulsion was minimal at high electrode pressures. They also reported that the microstructure of the weld joint was fully austenitic with the absence of hot cracking.

An alternative method for reducing expulsion in welded joints was proposed by Hwang et al. [61]. From the results of their findings, they observed that employing a pulse welding current comprising heating and cooling phases not only reduced expulsion in resistant spot welded joints but also increased the acceptable welding current range.

Unlike other properties of spot welded joints, the induced residual stress has received less attention in literature despite its effect on the overall weld quality. It has been reported to be dependent on electrode diameter and material-type, pre and post-weld treatment processes, work piece thickness in addition to the resistance spot welding parameters [71]. During spot welding, a combination of thermal and mechanical stresses is generated by electric current and electrode forces. Moshayedi and Sattari-Far [62] analysed the effect of welding current and welding time on the residual stresses of 1 mm spot welded austenitic stainless steel. Their analysis revealed that residual stresses at the nugget centre were mainly compressive and transformed to tensile stresses as outside the weld nugget. It was also observed that increasing welding current and time brought about a corresponding increase in the maximum radial residual stresses and was also accompanied by a shift of maximum residual stress from the weld nugget to outside the nugget due to the weld nugget growth. The rate of increase in residual stress brought about by increasing current was found to be more significant than the latter because of the heat loss from the weld joint in the form of conduction and radiation at longer welding times. However, increasing residual stresses have detrimental effects on welded joints' fatigue and fracture strength, but Popovskiki and Berezienko [72] have shown that increasing holding time can reduce residual stresses.

Another common weld defect peculiar to spot welded joints is cracking and has been reported to be a function of the welding current, welding time and ultimately, the hardness of the weld joint. Al-Mukhtar and Doos [16] studied cracking occurrence observed in resistance spot welded 1.5 mm austenitic stainless steel. They reported that regions having high microhardness, such as the HAZ and nugget diameter, are more susceptible to cracking, leading to cavitation. They concluded that cracks' initiation and propagation depend on post-weld treatment temperature and electrode pressure. Another possible source of cavities is the electrode sticking to the weld metal. Other factors that could influence cracking in austenitic stainless steel are cooling rate, fuse metal depth, and solidification mode.

From the preceding, it is clear that the nugget diameter is a major quality prediction parameter, and it increases with energy input, which is accompanied by an increase in TSLBC, weld penetration, width of HAZ, electrode depth indentation, peak load, failure/absorption energy, residual stresses, hardness, transformation of failure mode, weld expulsion and cracking tendency. A reverse trend exists for HAZ thickness and fatigue strength. While Cracks and expulsions in weld joints can be minimised by applying appropriate electrode pressures, preheating and use of pulse welding current also minimises expulsions. In addition to appropriate heat input, increasing the holding time can also reduce residual stresses.

2.2.2.1.2 Similar Duplex Stainless Steel Weld Joints.

Table 2.7 presents some of the studies regarding the effect of resistance spot welding parameters on duplex stainless steel properties.

Table 2.7: Review of effect of resistance spot welding parameters on the properties of duplex stainless steel.

Year	Author	Title	Research focus
2012	F. Hayat and I. Sevim [21].	The effect of welding parameters on fracture toughness of resistance spot-welded galvanized DP 600 automotive steel sheets.	Study of the effect of Welding current and time on the fracture toughness of 1.2 mm DP600 stainless steel.
2014	X. Wan et al. [73].	Modelling the effect of welding current on resistance spot welding of DP 600 steel.	Effect of welding current on the properties of resistance spot welded 1.7 mm DP 600 stainless steel.
2015	A. Ramazani et al. [74].	Characterization of microstructure and mechanical properties of resistance spot welded DP 600 steel.	Properties of resistance spot welded DP 600 stainless steel.
2017	H. Jaber et al. [23].	Peak load and energy absorption of DP 600 advanced steel resistance spot welds.	Effect of Welding current on the failure mode, failure energy, peak load, and joint ductility of resistant spot welded DP 600 stainless steel.
2020	F. Badkoobeh [75].	Microstructure and mechanical properties of resistance spot welded dual-phase steels with various silicon contents.	Effect of silicon content on the properties of RSW dual phase stainless steel.

Like in austenitic stainless steel, resistance spot welding parameters also affect duplex stainless steel properties, such as the fracture toughness. Hayat and Sevim [21] investigated the effect of welding current and time on the fracture toughness of spot welded galvanized duplex stainless steel. Their findings revealed that the fracture toughness increases with energy input (increasing current or welding time). However, increasing energy input above critical limits resulted in a reduction of fracture toughness characterised by a decrease in weld nugget diameter and increasing hardness due to excessive metal melting and splashing. In a similar study, Sevim [79 – 80] also reported that reduction in fracture toughness during spot welding is due to the fast cooling rate, which results in shrinkages and cold cracking.

As observed in austenitic stainless steel, increasing welding current did not significantly affect the hardness variation on the weld metal, according to the investigations of Wan et al. [73]. They also observed that increasing energy input brought about a corresponding increase in the TSLBC, fracture energy and absorption energy. This was attributed to the increase in the size of the nugget diameter. This increase was accompanied by a transformation of failure mode from Interfacial to complete pull out. As expected, the weld nugget growth rate was reduced at high welding currents due to the increase in heat dissipation.

Ramazani et al. [74] studied the microstructural evolution of resistance spot welded 1.5 mm duplex stainless steel. They reported a hardness variation from the fusion zone to the base metal, with the maximum hardness occurring at the fusion zone. The observed maximum hardness was attributed to the martensite grains whose formation was due to the high recorded cooling rate reaching 600 ^{o}C/s higher than the 400 ^{o}C/s reported by Zhao et al. [78].

As already established, the findings of Jaber et al. [23] corroborated that the weld nugget diameter is the most significant factor in determining joint quality alongside other criteria such as the weld mechanical performance and the mode of failure. They also reported that increasing energy input by reducing electrode pressure or increasing welding current and time brought about a corresponding increase in indentation depth, energy absorption, peak load, and joint ductility. This increase was accompanied by the transformation of the failure mode from interfacial to complete pull out. They concluded that the overall joint quality depends primarily on the properties of the fusion zone.

A recent study was carried out by Badkoobeh et al. [75] to investigate the effect of silicon content on the properties of resistance spot welded 2 mm duplex stainless steel. They discovered that increasing the silicon content increased the nugget diameter and ductility due to an increase in electrical resistance and a reduction in thermal conductivity. The tensile strength, yield strength, shrinkage cavities, peak load, maximum shear stress and fracture energy followed a reverse trend. The deterioration observed in mechanical properties was ascribed to the severe weld expulsion accompanied by electrode indentation. Meanwhile, the failure mode metamorphosized from interfacial to pull out mode.

In summary, it can be said that the quality of the weld joint is predominantly dependent on the properties of the fusion zone, which are in turn influenced by the RSW parameters. Increasing the energy input increases the TSLBC, peak load, joint ductility, absorption energy, weld nugget diameter, fracture toughness and transforms the failure mode from interfacial to complete pull out. Increasing energy input above certain limits may lead to a drastic reduction in fracture toughness and increase the tendency of cold cracking due to increased hardness and weld expulsion. Increasing the silicon content in duplex stainless steel had an overall detrimental effect on the mechanical properties of duplex stainless steel due to the severe electrode indentation and weld expulsion.

2.2.2.1.3 Similar Martensitic Stainless Steel Weld Joints.

Table 2.8 presents some relevant studies addressing effect of resistant spot welding parameters on the properties of martensitic stainless steel.

Table 2.8: Review of the effect of resistance spot welding parameters on the properties of martensitic stainless steel.

Year	**Author**	**Title**	**Research focus**
2009	V. Badheka et al. [4].	Resistance spot welding of martensitic stainless steel (SS 420) - part 1.	Effect of small scale RSW parameters on the properties of martensitic stainless steel.
2014	M. Alizadeh-Sh et al. [79].	Microstructure–properties relationships in martensitic stainless steel resistance spot welds.	Effect of welding current on the microstructure and fracture toughness of AISI 420 martensitic stainless steel.
2017	M. Tamizi et al. [80].	Welding metallurgy of martensitic advanced high strength steels during resistance spot welding.	Effect of welding current on the microstructure, failure mode and mechanical properties of Advanced high strength martensitic stainless steel.
2018	M. Pouranvari et al. [81].	Resistance spot welding of MS 1200 martensitic advanced high strength steel: Microstructure-properties relationship.	Effect of welding current on the microstructure and properties of MS 1200 martensitic stainless steel.
2020	M. Pouranvari et al. [82].	Enhanced mechanical properties of martensitic stainless steels resistance spot welds enabled by in situ rapid tempering.	Effect of in-process second pulse welding current and tine on the properties of 1.5 mm annealed AISI 420 martensitic stainless steel.

Antithetically, with reference to the welding of austenitic and ferritic stainless steel, martensitic stainless steel is difficult to weld as they generally possess poor weld qualities, especially those containing very high carbon and chromium content. However, they can still be subjected to resistance spot welding in the tempered, annealed, or hardened state. In an attempt to bring to light the weld properties of martensitic stainless steel, Badheka et al. [4] investigated the effect of RSW parameters on the properties of cold-rolled AISI 420 martensitic stainless steel. Their findings revealed that increasing the energy input led to a corresponding increase in weld nugget, TSLBC and hardness. Meanwhile, the ductility ratio and the cross tension breaking load followed a reverse trend. The difficulty in obtaining a good quality weld was further demonstrated in the small size of the welding lobe with the joints characterized by a brittle failure.

Another research was conducted by Alizadeh-Sh et al. [79] to study the effect of welding current on the properties of 1.25 mm cold rolled annealed martensitic stainless steel. Their findings revealed that increasing the welding current increases the nugget diameter, failure energy and peak load. The hardness and the mode of failure were not significantly affected by changes in the welding current as the maximum hardness occurred in the fusion zone while the mode of failure was partial interfacial mode exhibiting cleavage fracture. While the fusion zone hardness was attributed to the high cooling rate, the volume fraction of carbon and chromium in retained austenite, the fracture energy was dependent on the hardness of the weld metal, and the sharpness of the notch at the interface and presence of delta ferrite.

Researchers have also made advancements in modifying the properties of martensitic stainless steel to produce steel grades with higher strength, often referred to as advanced high strength steel. This steel grade has reduced carbon content to lower the hardness of the fusion zone and ultimately improve joint quality. The effect of welding current on the properties of cold-rolled 1.5 mm MS 1400 advanced high strength martensitic steel was investigated by Tamizi et al.[80]. They reported that the hardness of the fusion zone was independent of the welding conditions, while a HAZ softening phenomenon was observed in the Inter-Critical HAZ (ICHAZ) and Sub-Critical HAZ (SCHAZ). The softening observed in the ICHAZ was attributed to the formation of ferrite-martensite dual phases, while martensite tempering was responsible for the SCHAZ softening. Increasing the welding current was also found to increase the size of the HAZ, weld nugget diameter, hardness ratio and transform the failure mode from IF to PF. The increase in the size of the HAZ and its thermal softening was due to the increase in carbide precipitation and coarsening of the precipitates. The HAZ softening was found to reduce the TSLBC of the joints and, by extension, the overall joint quality; hence they recommended its minimization if good quality joints are desired.

Similar results were also reported by Pouranvari et al. [81], who investigated the effect of heat input on the microstructure and properties of 1.5 mm cold rolled MS 1200 martensitic stainless steel. They reported that the transformation observed in the failure mode from Interfacial mode to pull out mode was due to the increase in the size of the fusion zone with energy input, and was largely dependent on the interaction between plastic constraint in the HAZ and its softening. They spelled out that the properties of the weld joint, mainly the fusion zone, is not only dependent on the RSW parameters but rather, it is the result of the interaction between the RSW parameters and the chemistry taking place in the microstructure during the welding process, in other words, the metallurgical characteristics. This was used as the underlying principle to account for why the hardness of the fusion zone was unaffected by the heat input.

From the preceding, it is evident that the primary cause of property deterioration in martensitic weld joints is the high hardness of the fusion zone. In an attempt to reduce the hardness of the fusion zone of resistance spot welded martensitic stainless steel and consequently, improve the fracture toughness, a technique was recently proposed by Pouranvari et al. [82] which employs an in-process second pulse welding current for a period of time on the weld joints. Their findings revealed that the application of a double pulse welding current significantly improved fracture toughness, peak load, and absorption energy. Increasing the second pulse welding time led to a transformation in failure mode from full interfacial failure to partial interfacial mode, but no significant effect was recorded for the nugget diameter. The overall improvement in weld quality was due to the reduction in the hardness of the weld joint as a result of martensite decomposition and the precipitation of carbides.

In conclusion, martensitic stainless steel generally has poor weld properties primarily due to martensite, chromium, and carbon content, resulting in weld joints with high hardness values. Increasing heat input during the welding process increases the size of weld nugget, TSLBC, peak load, fracture energy, while ductility ratio and cross tension breaking load follow a reverse trend. The hardness of the fusion zone is unaffected by changes in the welding current as current changes induced no phase transformation. HAZ softening was observed in high grades of martensitic stainless steel, which had a detrimental effect on the overall joint quality. Martensitic weld joint quality can be improved by employing a double pulse welding current.

2.2.2.1.4 Similar Ferritic Stainless Steel Weld Joints.

Table 2.9 summarises some of the recent studies on the effect of RSW parameters on the properties of ferritic stainless.

Table 2.9: Review of effect of RSW parameters on the properties of ferritic stainless steel**.**

Year	**Author**	**Title**	**Research focus**
2014	M. Alizadeh-Sh et al. [83].	Resistance spot welding of AISI 430 ferritic stainless steel: Phase transformations and mechanical properties.	Effect of welding current on the metallurgical and mechanical properties of resistant spot welded AISI 430 ferritic stainless steel.
2015	M. Alizadeh-Sh et al. [84].	Welding metallurgy of stainless steels during resistance spot welding Part II –heat affected zone and mechanical performance.	Effect of heat input on the phase transformation and solidification on the properties of the fusion zone of AISI 430 ferritic stainless steel.
2015	M. Pouranvari et al. [85].	Welding metallurgy of stainless steels during resistance spot welding Part I: fusion zone.	Effect of welding current on the phase transformation and fusion zone hardness of Ferritic stainless steel.
2018	A. Subrammanian et al. [86].	Multi-objective Optimization of Resistance Spot Welding of AISI 409M Ferritic Stainless Steel.	Optimization of the tensile strength and electrode indentation of Resistant spot welded ferritic stainless steel.
2020	Y. Zhang et al. [19].	A comparative study between the mechanical and microstructural properties of resistance spot welding joints among ferritic AISI 430 and austenitic AISI 304 stainless steel.	Strain distribution, mechanical properties and microstructure of AISI 430 ferritic stainless steel.

Ferritic stainless steel like austenitic and duplex stainless steel can easily be subjected to spot welding process as they also have a low carbon content and consequently a less tendency of producing brittle joints as observed in the case of martensitic stainless steel. The effect of RSW parameters on the properties of 1.2 mm cold rolled annealed ferritic stainless steel was presented by M. Alizadeh-Sh et al. [83]. The results of their findings revealed that hardness increases from the base metal towards the direction of the fusion zone with the HAZ divided into three distinct zones, namely, High Temperature HAZ (HTHAZ), Medium Temperature HAZ (MTHAZ) and Low Temperature HAZ (LTHAZ), each characterized by different microstructure which is a function of the regional temperature. They also reported that all the samples failed in a pull out mode irrespective of the level of energy input. Meanwhile, other weld properties such as the peak load and fracture energy were observed to increase with the welding current mainly due to the increase in bonding area or nugget diameter.

Further study was carried out by Alizadeh-Sh et al. [84] to investigate the phase transformations in the fusion zone due to solidification and post solidification processes that occur during resistant spot welding. Their study used 1.2 mm AISI 430 ferritic stainless steel as the base metal for investigation. As previously observed in other grades of stainless steel, they reported that increasing the heat input by increasing welding input had no significant effect on the hardness of the fusion zone of the welded metal due to reasons explained earlier for other grades of stainless steel. In addition, they also reported that the joints failed in a double pull out mode which is an indication of good quality joints.

In another related study, Pouranvari et al. [85] expressed that the hardness of the fusion zone is the predominant factor that determines the failure mode of the spot welded joint. It has also been established that the weld ductility and transition of failure mode from interfacial to complete pull out as vice versa is also determined by the hardness of the weld joint [87]. This implies that the weld joint's hardness is a critical parameter to be put under control if good quality joints are desired. In the research conducted by Pouranvari et al. [85] to ascertain the phase transformation and subsequently the hardness of 1.2 mm AISI 430 ferritic stainless steel, it was revealed that the hardness of the fusion zone was due to martensite and carbide precipitation and the grain growth of the ferrite phase. They also concluded that changes in heat input by adjusting the current, welding time or electrode pressure had no significant effect on the hardness of the weld joint.

In addition to failure mode transition determination, the hardness of the weld joint has also been reported to be the cause of failure in 1.5 mm AISI 430 ferritic stainless steel in the interfacial mode, which is an indication of low fracture toughness. Zhang et al. [19] explained that the hardness of the weld joint was due to martensite precipitation formed as a result of the fast cooling rate associated with the spot welding process. A soft HAZ was also observed, which was attributed to the coarsening of grains in the presence of martensite. In addition, as observed in other grades of stainless steel, increasing the nugget diameter by increasing heat input brought about a corresponding increase in the peak load and absorption energy.

Following the previously reviewed studies, it is lucid that the nugget diameter is a key determining factor in obtaining good quality weld joints. One predominant factor with a very high positive correlation with this property is the tensile shear load bearing capacity. It has also been established that increasing the heat input during the welding process increases the nugget diameter and consequently the tensile load bearing capacity, while other factors such as the electrode indentation and weld expulsion have detrimental effects on the weld quality. This implies that selecting optimum welding parameters that minimizes weld quality reduction factors, such as the abovementioned ones, and maximizes the nugget diameter should be the manufacturing objective if quality and durable joints are desired. A study on the optimization of the tensile shear load bearing capacity and electrode indentation of 2 mm cold rolled AISI 409M ferritic stainless was conducted by Subrammanian et al. [86]. Their research work optimized the weld quality by minimizing the electrode indentation and maximizing the tensile shear load bearing capacity using the Taguchi model and Response Surface Methodology. They concluded that the optimum resistance spot welding parameters for 2 mm AISI 409M ferritic stainless steel are welding current, welding time and electrode pressure of 11.5 KA, 14 cycles and 3.5 KN, respectively.

In summary, ferritic stainless steel generally has good weld properties due to its low carbon content compared to its martensitic stainless steel counterpart. Like other grades of stainless steel, increasing heat input during the welding process increases the peak load, fracture toughness, nugget diameter and the mode of failure. The hardness of the fusion zone was also documented to significantly affect failure mode transition from interfacial to pull out mode and vice versa. Selecting optimum resistant spot welding parameters is one of the ways of ensuring that good quality joints of desired properties are produced.

2.2.2.2 Dissimilar Stainless Steel Weld Joints.

Table 2.10 summarises some of the relevant literature addressing the effect of RSW parameters on the properties of joints involving dissimilar metals.

Table 2.10: Review of effect of RSW parameters on the properties of dissimilar stainless steel joints.

Year	Author	Title	Research focus
2006	M. Vural et al. [88].	Effect of welding nugget diameter on the fatigue strength of the resistance spot welded joints of different steel sheets.	Effect of welding current on the nugget diameter and fatigue strength of galvanized and bare AISI 304 dissimilar joint.
2012	L. Kolarik et al. [89].	Resistance Spot Welding of dissimilar Steels.	Effect of welding current on the weld properties of AISI 304 stainless steel and DC Low carbon steel dissimilar weld joint.
2017	X. Yuan et al. [90].	Resistance spot welding of dissimilar DP 600 and DC 54D steels.	Effect of RSW parameters on the properties of DC 54D Ultralow carbon steel and galvanised DP 600 stainless steel.
2019	K. Kishore et al. [91].	Resistance spot weldability of galvannealed and bare DP 600 steel.	Determination of optimum welding current and time for galvanized DP 600 and bare DP 600 dissimilar joint using load bearing capacity.
2020	Y. Zhang et al. [19].	A comparative study between the mechanical and microstructural properties of resistance spot welding joints among ferritic AISI 430 and austenitic AISI 304 stainless steel.	Properties and microstructure of resistance spot welded AISI 430 ferritic and AISI 304 austenitic stainless steel dissimilar joint.

The need to achieve a compromise between the quality of weld joints and the cost of the metals led to the evolution of dissimilar weld joints. Unfortunately, the difference in mechanical and thermophysical properties of the participating metals posed another challenge. Despite this challenge, good quality joints have been produced using different welding techniques, and in some cases, interlayer and filler materials are incorporated. The following paragraphs address the effect of resistance spot welding parameters on dissimilar stainless steel joints involving different grades of stainless steel.

In service, automobiles and other structures containing spot welds are subjected to cyclic loading, which might be another possible cause of failure due to crack initiation, propagation, and growth. The findings of Rathbun et al. [92] revealed that the fatigue performance of welded joints is a function of the geometric factors of the weld joints, which implies implicitly that the fatigue life of spot welded joints depends on the heat input during the welding process. The investigations of Vural et al. [88], who conducted a study on the effect of heat input on the fatigue strength of bare and galvannealed AISI 304 austenitic stainless steel, revealed that the dissimilar joint possessed a very low fatigue limit as compared to the similar joint counterpart. They attributed the results of their findings to the antisymmetric nugget formation. They also reported that the hardness of the joint was considerably higher than the similar counterpart as the heat input was increased alongside an increase in the size of the nugget diameter.

Similar results were also reported by Kolarik et al. [89], who studied the weld properties of 2 mm cold rolled AISI 304 austenitic stainless steel and DC low carbon dissimilar weld joint. Like the results obtained by Vural et al. [88], they also reported a very high hardness in the fusion zone considerably higher than those of either base metal. In addition, they also reported an asymmetrical weld nugget shape which was attributed to the differential in chemical and thermomechanical properties of the participating base metals. Further analysis to ascertain the reason for the relatively high hardness of the fusion zone revealed that there was increased diffusion of iron from the austenitic stainless steel towards the fusion zone. This was also accompanied by a reduction in the chromium, nickel, and manganese content at this zone. The results obtained from the weld joint characterisation revealed that the fusion zone's size at the stainless steel side was larger than that of carbon steel. In contrary, the HAZ on the carbon steel side was larger than that of the stainless steel side to the higher thermal conductivity possessed by carbon steel.

The dissimilar joint of ultralow carbon steel and duplex steel finds application in constructing parts of a white body such as the panel. The performance of such joints in service has been reported to be dependent collectively on the mechanical properties of the participating base metals and the properties of the resulting joint [93]. The behaviour of 1 mm ultralow carbon steel and 1.6 mm galvanized stainless steel under the influence of varying RSW parameters was presented by Yuan et al. [90]. As recorded for similar weld joints involving stainless steel, increasing the heat input increased the nugget diameter and TSLBC. High current values above certain critical limits resulted in weld expulsion, which triggered an increase in electrode indentation. They attributed the improved tensile properties to the increased melting and extension of the plastic ring at different electrode pressures. As previously observed, the failure mode was also reported to transform from interfacial mode to plug or complete pull out with increasing energy input which was attributed to the increasing nugget diameter.

Duplex stainless steel in a dissimilar joint with its galvanized form has also been used in the automobile industry due to its desired properties. A common challenge reported to be encountered in its usage is the production of poor quality weld joints characterized by redistribution of zinc in the weld metal. Research to optimize the properties of 1.3 mm bare DP 600 and galvanized DP 600 was presented by Kishore et al. [91]. The result of their findings is similar to those obtained in similar stainless steel joints as the nugget diameter, load bearing capacity, and toughness were found to increase with welding current and time. This was also accompanied by a transformation of failure mode from interfacial to pull-out mode. The joints possessed a greater load bearing capacity in the tensile test than in the coach peel test for any welding parameter [94]. In addition, maximum hardness was observed at the fusion zone, and explanations provided by Nielson et al. [95] attributed the hardness to the formation of a complete martensite structure due to the fast cooling rate. Further analysis revealed that the zinc coating diffused from the fusion zone towards the heat affected zone with a reducing thickness.

Finally, a prominent dissimilar stainless steel joint with vast applications due to its favourable weld properties and cost compared to alternative metal joints serving a similar purpose is the austenitic - ferritic stainless steel joint. A study to reveal the properties of this dissimilar joint was presented by Zhang et al. [19]. The result of their findings revealed that the hardness of the fusion zone is reasonably higher than that of the base metal. Further investigations revealed that the increment resulted from the columnar dendrite solidification at the fusion zone comprising of austenite and ferrite grains while martensite was precipitated at the grain boundaries. This explanation also supported the transformation of the failure mode from interfacial mode to complete pull out with an increase in heat input coupled with the increase in nugget diameter.

In conclusion, the production of dissimilar stainless steel joints comes with a lot of complexities birthed by the difference in chemical and thermophysical properties of the participating base metals. A result of this differential in properties of the participating base metals is the formation of an asymmetrical weld nugget shape. Furthermore, as observed in welding of similar stainless steel base metals, increasing the heat input led to a corresponding increase in the nugget diameter, TSLBC, toughness and tendency of failure mode transition from interfacial to pull out. In the reviewed dissimilar stainless steel joints, a considerable high hardness was recorded in the fusion zone, accounting for the low fatigue strength observed in some dissimilar joints.

2.2.4 Optimization of Resistance Spot Welding Parameters

The previous section highlighted the effects of RSW parameters on the properties of stainless steel similar and dissimilar weld joints. It was discovered that some changes in spot welding parameters in one way or another improve the weld joint's quality while others are detrimental to it. For instance, an increase in the nugget diameter was reported to increase the load bearing capacity, while an increase in hardness, on the other hand, reduces the fracture toughness of the joints. Again, specific weld properties are desired for different applications, such as the fracture toughness desired in white bodies to improve the crash worthiness. In order to obtain weld joints of desired properties, there is a need to select the best spot welding parameters, as the spot welding parameters significantly influence the weld properties. The process described above is termed optimization. The following sections highlight the optimization of spot welding parameters and weld properties in similar and dissimilar joints.

2.2.4.1 Optimization of RSW Parameters for Similar Stainless Steel Weld Joints

This section examines the optimization of RSW parameters for similar stainless steel weld joints, including austenitic, duplex, martensitic and ferritic stainless steel.

2.2.4.1.1 Similar Austenitic Stainless Steel Weld Joints

Table 2.11 summarizes some studies on the optimization of RSW of austenitic stainless steel.

Table 2.11: Review of optimization of RSW parameters and properties of austenitic stainless steel weld joints.

Year	Author	Title	Research focus
2010	A. G. Thakur and V. M. Nandedkar [96].	Application of Taguchi method to determine resistance spot welding conditions of austenitic stainless steel AISI 304.	Optimization of the tensile shear strength of austenitic stainless steel weld joint using Taguchi method.
2012	N. Singh and Y. Vijayakumar [97].	Application of Taguchi method for optimization of resistance spot welding of austenitic stainless steel AISI 301L.	Optimization of electrode indentation of 7.5 mm AISI 301L austenitic stainless steel using L 32 orthogonal array of the Taguchi technique.
2014	D. Kianersi et al. [57].	Resistance spot welding joints of AISI 316L austenitic stainless steel sheets: Phase transformations, mechanical properties, and microstructure characterizations.	Optimization of RSW parameters and properties of austenitic stainless steel joints.
2020	R. Kumar et al. [98].	Impact of process parameters of resistance spot welding on mechanical properties and micro hardness of stainless steel 304 weldments.	Optimization of welding current, welding time, electrode pressure and holding time for 1 mm austenitic stainless steel using Taguchi method.

D. Kianersi et al. [57] investigated the effects of spot welding parameters on the properties of 1 mm 316L austenitic stainless steel and subsequently obtained optimum parameters based on the desired properties. In their study, the welding current and time were varied between 4 - 9 KA and 4 - 7 cycles with a step-wise increase of 1 KA and 1 cycle, respectively, while the squeeze time, holding time and electrode pressure were held constant. The research objective was to optimize the TSLBC, indentation depth, penetration rate, peak load, and failure energy. A study of the interaction effect between these properties and the spot welding parameters was also conducted. The results obtained from their analysis revealed that the optimum parameters for the weld joint are 8 KA and 4 cycles.

In another study, Thakur and Nandedkar [96] attempted to examine the performance characteristics and the effect of RSW parameters on the properties of 1 mm AISI 304 austenitic stainless steel. Their optimization objective was to obtain optimum parameters that would maximize tensile shear strength. The selected domains for the resistant spot welding parameters are 0.38 - 0.54 MPa, 7.5 - 9.5 KA and 6 – 10 cycles for the electrode pressure, electric current and welding time, respectively. Their analysis employed an L 27 orthogonal array of the Taguchi technique for DOE, while ANOVA and the Signal to Noise (S/N) ratio were used as the criteria for selecting the optimum parameters. The results of their examination revealed that welding current and electrode pressure were the most and least significant parameters affecting the tensile shear strength, respectively. The optimum parameters from the analysis are 0.46 MPa, 9.5 KA and 10 cycles for electrode pressure, welding current and time, respectively.

In a similar study, Kumar et al. [98] studied the effect of welding current, welding time, electrode pressure and holding time on the tensile properties of 1 mm austenitic stainless steel. Afterwards, they optimised the tensile shear load bearing capacity and obtained optimum resistance spot welding parameters. Like in the previous study, they also employed the L 16 orthogonal array of the Taguchi technique while ANOVA and Signal to Noise ratio (S/N) ratio were also used as criteria for optimizing performance parameters. The results of their analysis revealed that the optimum performance parameters for the analysed grade of stainless steel are 5 KA, 18 cycles, 5.5 bar and 30 cycles for welding current, welding time, electrode pressure and holding time.

Lastly, Singh and Vijayakumar [97] investigated the effect of spot welding parameters on the electrode indentation, weld penetration, nugget diameter and tensile strength of AISI 301L austenitic stainless steel and subsequently optimized the electrode indentation by obtaining the process parameters that will minimize it. Their study adopted the L 32 orthogonal array of the Taguchi technique while ANOVA, signal to noise ratio (S/N) and T - test were used to obtain the optimum parameters. Their analysis revealed that the welding time had a more significant effect on the electrode indentation compared to the other parameters. In addition, the optimum parameters obtained are 50 cycles, 9.5 KA and 70 cycles for the welding time, welding current and holding time, respectively.

In summary, it can be concluded that the optimum parameters obtained from a given optimization process depend on the optimization objective and the selected domain of the spot welding parameters, which is influenced by the thickness of the material, among other factors. Parameters that optimizes the TSLBC, indentation depth, penetration rate, peak load, and failure energy of 316L austenitic stainless steel are 8 KA welding current and 4 cycles welding time. For 1 mm 304 grade, the weld current is the most significant weld parameter affecting the TSLBC with the optimum parameters being 4.6 bar, 9.5 KA or 10 cycles electrode pressure, welding current and welding time respectively or 5.5 bar, 5 KA, 18 cycles and 30 cycles electrode pressure, welding current, welding time, and holding time respectively. Furthermore, the welding time has a more significant effect on the electrode indentation of 301L austenitic stainless steel. The parameters that minimise it are 50 cycles, 9.5 KA and 70 cycles welding time, electric current and holding time, respectively.

2.2.4.2 Other Grades of Steel and Metals

This section examines literature dealing with the optimization of process parameters and properties for other grades of stainless steel and other metals. Table 2.12 summarizes some studies on the optimization of RSW of other metals such as low carbon steel, ferritic stainless steel, and titanium.

Table 2.12: Review of optimization of RSW parameters and properties of low carbon steel, ferritic stainless steel, and titanium weld joints.

Year	**Author**	**Title**	**Research focus**
2007	H. Sun et al. [99].	Effect of variable electrode force on weld quality in resistance spot welding.	Optimization of variable electrode force for 1.5 mm resistance spot welded Hot Dip Galvanized Low Carbon steel.
2014	D. Zhao et al. [100].	Multi-objective optimal design of small scale resistance spot welding process with principal. component analysis and response surface methodology	Determination of the optimum parameters for small scale resistance spot welding of titanium alloys using RSM.
2015	S. Shafee et al. [101].	Resistance Spot Weld Quality Characteristics Improvement by Taguchi Method.	Optimization of direct tensile strength and tensile shear strength of 0.8 & 1 mm resistance spot welded low carbon steel.
2020	P. Ravichandran et al. [102].	Process parameter optimization and performance comparison of AISI 430 and AISI 1018 in resistance spot welding process.	Optimization of the tensile strength and microhardness of ferritic stainless steel weld joint using RSM.
2020	D. Zhao et al. [103].	Multi-objective optimization of the resistance spot welding process using a hybrid approach.	Heat input and weld quality optimization for a resistance spot welded titanium alloy using a combination of regression and entropy weight method

Ravichandran et al. [102] studied the effect of weld time, holding time, squeeze time and electric current on the tensile strength and hardness of 1.2 mm AISI 430 ferritic stainless steel and subsequently optimized them by obtaining the process parameters that would maximize them (i.e. hardness and tensile strength). The Design of experiment was achieved using RSM with the domain for the control parameters being 6 - 8 KA for welding current, 10 – 14 cycles for squeeze time and 7 - 9 cycles for welding time while the holding time and off time were kept constant. The parameters which maximized the hardness and tensile strength with the highest desirability are 8 KA, 14.75 cycles and 6.3 cycles for the welding current, squeeze time and welding time, respectively.

Like the stainless steel family, low carbon steel can also be subjected to RSW due to its low carbon content and ease of welding. The effect of RSW parameters on low carbon steel weld quality was investigated by Shafee et al. [101]. They eventually optimized the TSLBC and the direct tensile strength by obtaining the process parameters which would maximize them. The design of experiment was achieved using the L 9 orthogonal array of the Taguchi technique with S/N ratio and ANOVA adopted as the criteria for optimization. The domains of the parameters are 1.8 - 2.2 KN for electrode force, 3.5 - 4.5 KA for welding current and 1 - 2 seconds for welding time, while the squeeze time and holding time were held constant at 5 cycles. The results of their analysis revealed that the welding current was the most significant factor for the TSLBC, but for the direct tensile strength, it was the welding time.

All the previous studies considered before now directed their research light towards the effect of RSW parameters, mainly welding current, welding time and constant electrode pressure on the properties of various steel types. A few researchers have investigated the effect of variable electrode pressure on the weld properties, and fewer experimenters have conducted the optimization of variable electrode force on the weld quality. Few years back, a study was conducted by Sun et al. [99] to investigate the effect of variable electrode pressure on weld quality and subsequently obtain the optimum electrode force parameters that would maximize weld quality parameters, mainly tensile strength and the nugget diameter. The results of their findings revealed that the use of variable electrode pressure comprising the squeezing pressure, welding pressure and forging pressure improved the weld quality generally by yielding about 35 % and 45 % increase in the Tensile strength and nugget diameter, respectively. They also explained that for best weld quality properties, the forging force should be greater than the squeezing force, which must be higher than the welding force. It was also discovered that employing the use of the variable electrode force did not significantly increase the wear of the electrode.

Other metals aside, steel can also be subjected to large and small scale resistance spot welding, especially those with desirable properties such as light weight, corrosion resistance and good service performance, particularly in severe conditions. A good candidate that suites the abovementioned characteristics is titanium which finds several industrial applications. Zhao et al. [100] presented a study of optimising spot welding parameters of 0.4 mm Titanium alloy using Box-Behnken design of the Response Surface Methodology. They attempted to maximize the tensile shear strength, failure energy and penetration rate with the following domains: 8 – 12 ms, 1.6 - 2.4 KA and 76.2 – 127 N for welding time welding current and electrode force, respectively. The results of their evaluation revealed that the parameters with the maximum desirability are 9.39 ms, 2.4 KA and 127 N for the welding time, welding current and electrode force, respectively.

Recently, another study on the optimization of weld quality and heat input for a resistance spot welded titanium alloy was authored by D. Zhao et al. [103]. The experimental design was achieved using central composite design, while process parameter optimization was achieved using a combination of regression and entropy weight methods. The selected domains for the welding parameters are 6 – 10 ms, 1.2 - 2.0 KA and 3 – 7 MPa for the welding time, welding current and electrode pressure, respectively. The multi-response optimization comprises improving the maximum displacement, failure energy, peak load, and weld nugget diameter. The results of their analysis produced the following parameters: 10 ms, 1.83 KA and 7 MPa with desirability of 0.736 as the optimum parameters.

Summarily, optimum parameters can also be obtained for other steel grades, as in stainless steel. It was established that while the welding current is the most significant parameter affecting the TSLBC, it is the welding time in the case of direct tensile strength. It was discovered that employing variable electrode force with the forging force > squeezing force > welding force improves the TSLBC by 35 % and the nugget diameter by 45 %. Optimum parameters which maximize the hardness and TSLBC of 1.2 mm ferritic stainless steel are 8 KA, 14.75 cycles and 6.3 cycles electric current, squeezing time and welding time. Parameters that optimizes the TSLBC for small scale resistance spot welding of 0.4 mm titanium are 9.39 ms, 2.4 KA and 127 N welding time, electric current, and electrode pressure.

2.2.4.3 Dissimilar Stainless Steel Weld Joints

A summary of some of the recent literatures on the optimization of RSW parameters and properties of stainless steel dissimilar weld joints is presented in Table 2.13.

Table 2.13: Review of optimization of RSW parameters and properties of stainless steel dissimilar weld joints.

Year	Author	Title	Research focus
2017	K. Vignesh et al. [104].	Optimization of resistance spot welding process parameters and microstructural examination for dissimilar welding of AISI 316L austenitic stainless steel and 2205 duplex stainless steel.	Optimization of electrode diameter, welding current and heating time for AISI 316L and 2205 DP stainless steel dissimilar weld joint using Taguchi method.
2019	A. Biradar and B. Dabade [105].	Optimization of resistance spot welding process parameters in dissimilar joint of MS and ASS 304 sheets.	Optimization of the weld strength of a resistance spot welded dissimilar mild steel and austenitic stainless steel using factorial regression.
2020	A. Hernández et al. [106].	Optimization of resistance spot welding process parameters of dissimilar DP 600 / AISI 304 joints using the infrared thermal image processing.	Weld quality optimization of a dissimilar joint of DP 600 and AISI 304 using Infrared (IR) characterization and RSM.

The dissimilar joint of austenitic stainless steel and duplex stainless steel is a recommended substitute for similar spot welded austenitic stainless steel joints. This accounts for their application in biomedical equipment, ovens, and pharmaceutical devices. A study to optimize the tensile shear strength of a dissimilar weld joint of 2 mm AISI 316L and 2205 DP stainless steel was presented by Vignesh et al. [104]. In their research, the electrode diameter was included as one of the process parameters to be optimized, which is quite unconventional. Design of experiment and property optimization was achieved using Taguchi L 27 orthogonal array and ANOVA. The domains of the process parameters were 6 - 8 mm, 7-9 KA and 7 - 9 cycles for the electrode tip diameter, welding current and heating cycle, respectively. Their evaluation revealed that the optimum parameters that produced the best joint quality were 6 mm, 9 KA, and 9 cycles.

In another related study, Hernández et al. [106] applied an unorthodox approach to characterize the geometric properties of the weld joint, which involved the application of non-invasive infrared rays (IR) to produce isotherms which served as a significant parameter to control the quality of the weld joints produced during the welding process. The non-destructive nature of this technique puts it in a position to be a possible tool for future prediction of the quality of weld joints. In their experiment, 1.2 mm dissimilar weld joint comprising duplex and austenitic stainless steel were joined while optimization of process parameters and mechanical properties was achieved using RSM. Like the previous studies, the process parameters of interest were the welding current and time with domains of 3 – 5 KA and 300 – 500 ms, respectively, while the response variable was the peak load and the diameter obtained from the infrared measurement known as the isotherm diameter. The results of their study revealed that the optimum process parameters with the highest desirability were 4.85 KA and 300 ms welding current and time, respectively.

Finally, Biradar and Dabade [105] investigated the effect of spot welding process parameters on mild steel and austenitic stainless steel dissimilar weld joint properties. Their experiments considered varying thickness (0.8 - 1.5 mm) of the participating base metals and optimized the weld strength (TSLBC) using Factorial regression and ANOVA. The results of their study revealed that a negative correlation exists between the metal thickness and hardness of the fusion zone. Optimum parameters were selected based on maximum weld strength criteria. Mathematical models were also developed for the weld strength in terms of the welding parameters for the different base metal thicknesses.

In summary, optimum weld parameters can also be obtained for dissimilar weld joints involving stainless steel, as was observed in similar stainless steel weld joints in the previous sections. The obtained parameters are functions of the desired designed objectives such as 6 mm electrode diameter, 9 KA welding current and 9 cycles welding time for 1.2 mm austenitic-duplex weld joint. It was also discovered that the quality of weld joints could be effectively controlled using a non-destructive technique involving IR radiations to measure isotherms. In addition, another study revealed a negative correlation between the base metal thickness and the hardness of the fusion zone of an austenitic-mild steel weld joint.

2.3 Weld Treatment Processes

The plethora of literature reviewed in the previous sections revealed that the welding process generally comes with weld property deterioration and is even more severe when inadequate weld parameters are used. This necessitates the introduction of weld treatment processes to improve the properties of the produced joints and, consequently, improve their service performance.

2.3.1 Pre and Post – weld Treatment Processes

Weld treatment processes applied to weld joints are mostly carried out before the welding process or after it has been concluded. Weld treatment processes such as preheating are usually carried out before commencing the welding process, while other heat treatment processes such as annealing and tempering are done after the welding procedure has been concluded. The former is generally termed pre-weld treatment processes, while the latter is known as post-weld treatment processes.

Preheating involves heating the metals to be joined to a specific temperature, either as a whole or just the section to be joined before commencing the welding process. The decision for preheating and the preheating temperature are governed by factors like the metal thickness, rigidity of the metals, chemistry of the base metals, heat input and carbon equivalence [110 – 111]. As a rule of thumb, the need for preheating and the preheating temperature increases with material thickness and carbon equivalence. Some recorded benefits of preheating include reduction in heat input during actual welding, residual stresses, hydrogen cracking tendency, while other properties such as ductility and toughness are improved. Depending on the nature and size of the components to be preheated, furnaces, ovens, electrical strip heaters, banks of heating torches, and radiant or induction heaters can be employed [24].

Most of the post-weld treatment processes comprise mainly the conventional heat treatment processes. Heat treatment is a series of operations or processes which involves subjecting a metal to a definite time-dependent cycle comprising heating to a particular temperature, holding, or soaking at the temperature, followed by cooling at a desired rate. This process is depicted in Figure 2.7.

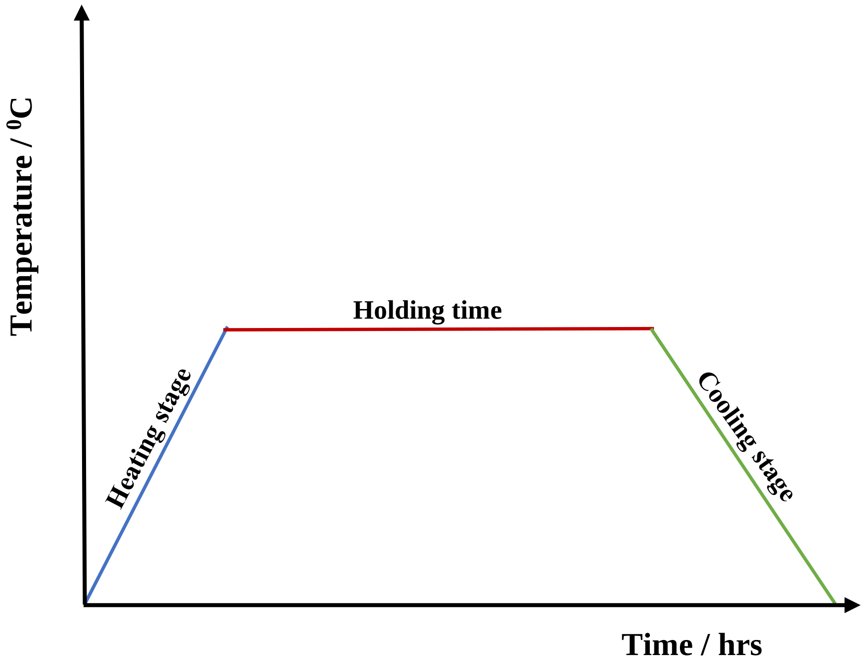

Figure 2.7: Stages involved in a heat treatment cycle

Manipulation of these processes, particularly the heating temperature, holding time and cooling rate, have been reported to confer desired properties in metals especially stainless steel. Though the rate of heating is not considered significant relative to the other phases in unstressed steel, it is of great importance when the steel is stressed. Meanwhile, the holding time and cooling rate are highly dependent on the thickness of the metal. As a rule of thumb, it is required to soak every inch of steel thickness for 30 minutes while thicker sections are allowed a slower cooling rate for desirable properties [109].

2.3.1.1 Types of Post – weld Treatment Processes

Several post-weld treatment processes have been reported in literature. The choice of heat treatment process depends on the desired properties, as different heat treatment processes confer different properties in steel. Generally, they are categorized into hardening and softening processes based on the overall effect on the hardness of the microstructure of the metal to which they were applied. Some reported heat treatment processes include annealing, normalizing, tempering, surface hardening, case hardening and tempering.

Annealing is a softening process carried out either in the form of full annealing, process annealing and spheriodizing depending on the purpose. In full annealing, the metal is heated to a temperature above recrystallization temperature followed by holding at that temperature and then a slow cooling process is achieved either in a furnace, lime, mica, or ashes. On the other hand, process annealing is a stress relieving process applied to low carbon steel, which has been subjected to cold working where steel is heated to a temperature close to the A_1 critical line. Meanwhile, spheriodizing is a special form of annealing process where steel is heated to form a pearlite microstructure containing globular carbides [110].

Normalizing involves heating a metal above recrystallization temperature (usually A_3 critical line), holding at the temperature, and then followed by air-cooling. Normalizing aims to eradicate the effect of any previous heat treatment or cold working on the metal and, consequently, homogenize the microstructure. Meanwhile, hardening involves heating a metal above the A1 critical line temperature, then holding it at the temperature for sufficient time, followed by rapid cooling either by quenching in oil, water or any other medium. Case hardening processes such as carburizing, nitriding, cyaniding and carbonitriding alongside other surface hardening processes like induction and flame hardening are common hardening processes reported by experimenters [111].

Tempering, also known as drawing, involves reheating a hardened steel to some temperatures below the A1 critical line and usually followed air-cooling to reduce hardness and subsequently increase the toughness, ductility, malleability, and impact resistance. The selected tempering temperature is a function of the desired properties as high tempering temperatures increases toughness while low tempering temperatures permits the metal to retain a certain level of hardness. In addition, the tempering time should be sufficient to allow for a complete transformation in the microstructure and is also subject to the thickness of the metal to be tempered [109].

2.3.2 Iron-Carbon Equilibrium Diagram

The iron-carbon equilibrium diagram (Figure 2.8) plots the constitutional phases of an iron-carbon alloy such as steel at different temperatures as a function of percentage carbon composition under the condition of equilibrium, i.e., very slow cooling.

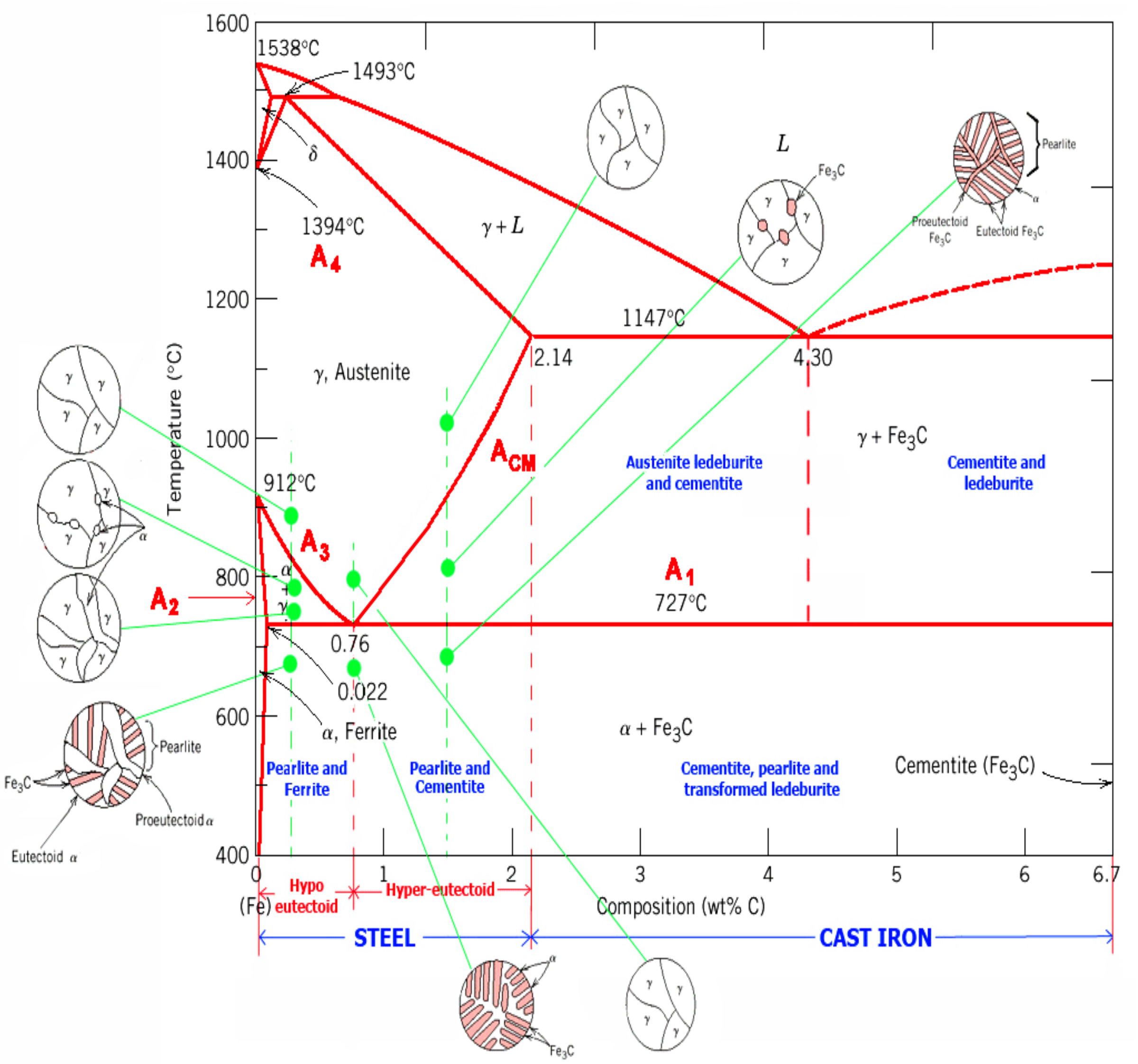

Figure 2.8: Iron-Carbon equilibrium diagram [245].

The iron-carbon equilibrium diagram above shows various phases present in an iron-carbon alloy at a given carbon composition and temperature. Conventionally, most iron-carbon alloys phase transformations are in line with those predicted by the equilibrium phase diagram. However, the phase transformation process may be altered by the presence of phase stabilizers in sufficient amounts, such as those of austenite and ferrite. For instance, the presence of austenite phase stabilizers such as Nickel and Manganese allows the austenite phase to persist below the critical line A_1 even up till room temperature with increasing content of Nickel or Manganese. In the same light, sufficient amount of the ferrite phase stabilizers such as chromium and molybdenum can also delay the transformation of the ferrite phase to the austenite phase at temperatures above the A_1 critical line beyond which ferrite phase ordinarily does not exist. The effect of phase stabilizers on phase transformation on the equilibrium diagram is illustrated in Figure 2.9.

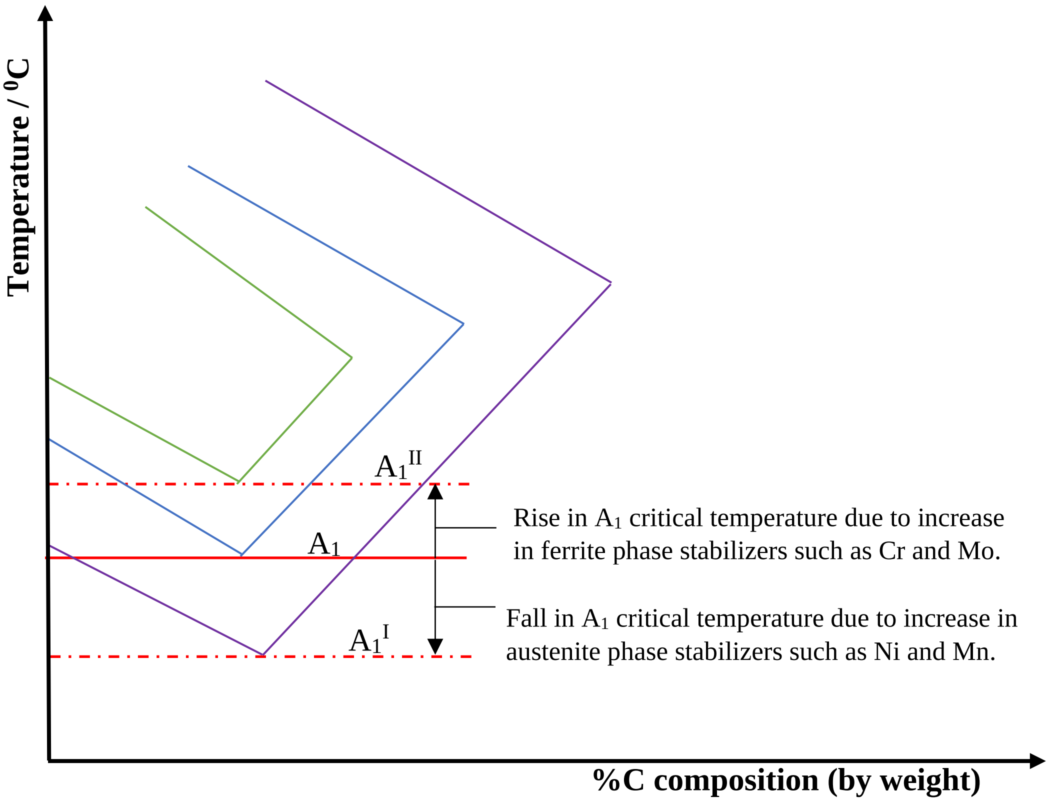

Figure 2.9: Effect of phase stabilizers on the A_1 critical transformation temperature.

2.3.3 Review of Effect of Weld Treatment Processes on the Properties of Similar Stainless Steel Weld Joints.

It was explained in the preceding sections that application of heat treatment to stainless steel is an apposite technique for modifying their properties to suit the desired application, and more so, the choice of the weld treatment process is dependent on the desired properties as different weld treatment process have been reported to confer different weld properties. Like the sub-division categories used in the previous sections, this section carefully examined the effects of weld treatment processes on the properties of stainless steel similar weld joints under the headings of austenitic, duplex, martensitic and ferritic stainless steel.

2.3.3.1 Similar Austenitic Stainless Steel Weld Joints

This refers to weld joints comprising of austenitic stainless steel as the parent metals. Despite the versatility of austenitic - austenitic weld joints, a common setback reported by experimenters in producing these joints is the presence of delta ferrite in amounts up to 5 %, which produces an overall deleterious effect on the properties of the weld joints. Though the delta ferrite phase reduces grain boundary weakness and the tendency of hot cracking at high temperatures, it causes embrittlement due to the formation of the sigma phase [112]. The precipitation of unwanted phases can be prevented using phase stabilizers of the austenite phase, such as nickel, manganese, nitrogen, or those of the ferrite phase, such as chromium, molybdenum, and silicon. Phase precipitation can also be prevented by controlling the cooling rate during welding through preheating or quenching [113]. The application of proper pre and post-weld treatment have also been reported to eliminate unwanted phases and homogenize the microstructure of austenitic stainless steel.

Nam et al. [25] investigated the effects of annealing temperature and holding time on the properties of austenitic stainless steel. They reported that the hardness and tensile strength of the weld metal decreased with increasing annealing temperature as a result of the formation of coarse austenite grains and the release of residual stresses. The precipitation of carbides at the temperature range of 650 – 850 ^{o}C was also observed but dissolved at high annealing temperatures. Hamada et al. [114] and Tseng et al. [115] also reported carbide precipitation in austenitic stainless steel with post-weld heat treatment in that temperature range. The precipitation of intermetallic carbides is attributed to the instability of ferrite phase stabilizers in that temperature range, as reported by Sahlaoui and Sidhom [116] and Sahlaoui et al. [117]. The fluctuation observed in the elongation is due to the fluctuation in carbide precipitation with the annealing temperature. Meanwhile, fracture toughness was found to decrease between the temperature range of 650 – 850 ◦C, as also reported by Kozuh et al. [112], who opined that the reason for the reduction in the precipitation of the sigma phase.

A common phenomenon during welding thin-walled structures, especially with electron beam welding, is the buckling effect. This occurrence is due to the thermal tensioning of the weld metal as a result of temperature differences between the weld metal and the adjacent metal [122, 123]. Though most experimenters do not generally consider the application of the heat treatment in preventing buckling due to its time-consuming nature and the inability to control the precipitation of unwanted phases, it has been reported to be an effective tool for minimizing the phenomenon [124, 125]. The report of Zhang et al. [122], who investigated the effect of multi-beam preheating in buckling effect reduction in austenitic stainless steel, revealed that multi-beam preheating reduces buckling distortion by 80 %. The buckling effect reduction is a result of the thermal stress-relieving process induced by the preheating.

In addition to the hardness reduction and improvement of mechanical properties, post-weld heat treatments are used as stress-relieving mechanisms. Post-weld cool treatment is a form of post-weld treatment based on the principle of reverting the tensile stresses set up during the welding process to compressive stress by making the temperature of the weld metal lower than that of the adjacent metal. This is achieved by using a cooling fluid, such as water supplied at a constant velocity for a given period. Jia et al. [123] investigated the effect of preheating and post-weld cool treatment on residual stress reduction. Their research applied post-weld cool treatment to austenitic stainless steel over a cooling range of 1.5 – 2 times the weld width. They concluded that post-weld cool treatment reduces longitudinal residual stresses while preheating reduces longitudinal and transverse residual stresses. The residual stresses also decreased with increasing cooling range while cooling time had no significant effect.

An enhanced form of low carbon 316 austenitic stainless steel finds application in the fabrication of International Thermonuclear Experimental Reactor (ITER) components. Xin et al. [124] studied the effect of different post-weld age treatment on the properties of this grade of steel. The results of their findings revealed that increasing the ageing temperature coarsened the cells and dendrites with the occurrence of sub-grain boundaries at high temperatures. They also reported no significant changes in the tensile strength and yield strength due to microstructural stabilization by nitrogen and manganese, which are austenite phase stabilizers. The increment observed in elongation and impact energy is due to the release of residual stresses and precipitation of the sigma phase, respectively [125].

In addition to residual stress relief, applying a brief post-weld treatment to austenitic stainless steel improves corrosion resistance. In view of this, Rajani et al. [126] investigated the effect of controlled preheating on the corrosion properties of austenitic stainless steel. They observed an improved corrosion resistance for samples with controlled preheating. The increase in corrosion resistance was attributed to the reduction in the amount of delta ferrite due to the reduction in cooling rate, giving room for transformation. This is accompanied by a reduction in austenite-delta ferrite interfaces, which are pitting corrosion sites.

Recently, Muhammed et al. [28], attempted to establish a relationship between the microstructure of austenitic stainless steel and their mechanical properties. The result of their findings revealed that the properties of austenitic stainless steel are highly dependent on the delta ferrite composition and carbide precipitation. It was further observed that the preheating, post-weld treatment temperature and holding time were negatively perfectly negatively correlated with the delta ferrite composition indicating delta ferrite phase transformation to sigma phase, while the tensile strength, hardness and corrosion density showed a positive correlation with the delta ferrite composition. Moreover, the hardness of the weld joint was found to be moderately positively correlated with the tensile strength.

Consequently, despite the deleterious effects of delta ferrite and carbide precipitates in the austenitic stainless steel microstructure, they also confer certain desired properties. For instance, delta ferrite transforms to the sigma phase at elevated temperatures, which improves grain boundary strengthening and reduces cracking at elevated temperatures. The prevention of carbide precipitation and the elimination of delta ferrite can be achieved by introducing alloying additions or controlling the cooling rate by applying weld treatment processes. Aside carbide precipitation prevention, controlling the cooling rate of austenitic stainless steel reduces residual stresses, improves corrosion resistance, and reduces buckling distortion. Furthermore, a negative correlation exists between the delta ferrite composition and post-weld treatment parameters while exhibiting a negative correlation with tensile strength, hardness, and corrosion density.

2.3.3.2 Similar Duplex Stainless Steel Weld Joints

The ease of fabricating similar duplex stainless steel weld joints using several welding techniques is attributed to their low carbon content [131 – 133]. Despite the versatility of these weld joints, some challenges associated with these joints have been documented by some researchers. The hardness of the fusion zone, formation of shrinkage voids, Interfacial failure mode and general property deterioration across the weld joint are some of the problems reported in literature [134 – 135].

In the preceding sections, it was mentioned that optimum properties in duplex stainless steel are obtained when there is equilibrium between the hard ferrite and soft austenite. This automatically implies that weld property deterioration in duplex stainless steel is attributed to the upset in equilibrium between the austenite and ferrite phases. Another contributing factor is the formation of unwanted secondary phases such as sigma, intermetallics and chi phases during the welding process. During welding, there is a tendency of the joints undergoing ferritization (increase in ferrite content), leading to the formation of intermetallics and martensite upon solidification [136 – 138].

The solidification transformation of ferrite to austenite in duplex stainless steel is usually in three forms: grain boundary austenite (GBA), Widmanstätten austenite (WA) and intergranular austenite (IGA). The frequently occurring ones are the GBA and WA, as their formation at high temperatures requires a very low driving force [139 – 142]. The need to improve the properties of welded duplex stainless steel led researchers to apply several pre and post-weld treatment processes ranging from in-process and post-weld tempering to brief annealing post-weld treatment, shot peening, plasma ion nitriding, to laser continuous heat treatment.

Nikoosohbat et al. [139] investigated the effect of an in-process tempering on duplex stainless steel properties. An in-process tempering is the application of a post-weld tempering current pulse to the weld metal, and the magnitude is dependent on the metal thickness, weld composition and desired properties. Their findings revealed that the hardness of the weld metal reduced with increasing tempering current cycle due to the tempering of the hard martensite. The tensile shear strength and a peak load of the samples that failed in an interfacial failure mode were found to function the hardness as samples without in-process tempering possessed the highest tensile shear strength. In other words, there is a correlation between the hardness and strength of the weld metal.

The effect of post-weld tempering on duplex stainless steel properties was studied by Luo et al. [130]. The result of their experiment revealed that the ferritization of the weld metal alongside the precipitation of secondary austenite phase and sigma phases occurred during the welding process. Upon post-weld tempering, all the phases increased in intensity, exhibiting a segregational phenomenon, leading to an overall reduction in hardness. This led to the conclusion that, despite hardness reduction by post-weld tempering, it poses detrimental effects on the mechanical properties of duplex steel as it precipitates deleterious secondary phases.

Brief annealing post-weld treatment is one of the processes adopted to prevent the precipitation of deleterious secondary phases and unwanted transformation in the microstructure of duplex stainless steel. In this regard, Zhang et al. [38] presented a study on the effect of brief annealing post-weld treatment on the properties of duplex stainless steel. They reported that the hardness of the weld metal increased at temperatures above the equilibrium temperature as a result of excessive ferritization coupled with the precipitation of solid solutions of chromium and molybdenum, which was accompanied by a reduction in impact energy. The improvement in impact energy observed at low annealing temperatures results from the reduction in residual stress coupled with the balanced phase composition.

Some researchers have also reported that brief annealing post-weld treatment affects the corrosion properties of duplex stainless steel [140]. In view of this, Yang et al. [141] investigated the effect of annealing temperature and brief holding time on the properties of duplex stainless steel. They observed an overall reduction in the weld metal's corrosion resistance, which was attributed to the excessive ferritization of the weld joint. Consequently, it resulted in the precipitation of nitrides and the disruption of the ferrite-austenite equilibrium.

Nitride precipitation in duplex stainless steel reduces corrosion resistance by enhancing the critical current density and passivation potential, as reported by Parren et al. [142]. The reduction in corrosion resistance was characterized by a selective attack of the ferrite phase, as revealed by the critical pitting test (CPT) analysis. Subsequently, upon applying the brief annealing post-weld treatment, the corrosion resistance improved with increasing holding time and temperature. This was characterized by deferritization of the weld joint and an increase in stabilizers of the austenite phase to obtain a microstructure almost similar to that of the base metal. They concluded that the pitting resistance equivalent number (PREN) of duplex stainless steel is a function of the PREN of the weaker phase.

As reported by researchers, heat input variation during the welding process is a form of weld treatment process applied to duplex stainless steel. It can be achieved by altering the welding speed, voltage, current or welding time depending on the welding technique adopted. Slow welding speed, high welding current and long welding time is an indication of high energy input as vice versa [143]. The effect of welding speed on briefly annealed duplex stainless steel was investigated by Saravanan et al. [144]. The results of their study revealed that the application of post-weld annealing treatment increases the austenite phase composition, as also reported by Pramanik et al. [145]. The increase in hardness observed with low welding speed is attributed to the ferritization of the weld joint due to high energy input and an increase in residual stresses. On the other hand, it may also result from the formation of finer grains or the precipitation of phase stabilizers such as nitrogen, chromium, silicon and manganese in the weld zone, as reported by Saravanan et al. [146]. They concluded that the improvement in corrosion resistance and the reduction in hardness of duplex stainless steel is a result of the reduction in weld zone ferritization and reduction in residual stresses.

Liu et al. [147] studied the effect of continuous laser heating on the properties of duplex stainless steel. The result of their findings revealed that laser heating improved the mechanical properties of duplex stainless steel by reducing the ferritization of the weld zone and increasing the formation of secondary austenite of the Widmanstätten type. The corrosion tests revealed that the reduction in the selective attack of the ferrite phase and improved corrosion resistance was achieved by increasing laser heating energy. This is due to the elimination of nitrides from the ferrite zone coupled with the ferrite transformation to Widmanstätten austenite.

Shot peening and nitriding are surface modification processing technologies that can be applied to welded joints to reduce crack propagation, residual stresses, surface hardness and increase wear resistance. It is a non-destructive coldworking surface treatment process that leads to the generation of compressive stresses, which deforms the material plastically, resulting in high impact strength [152, 153]. The effect of shot peening and nitriding on the properties of duplex stainless steel was investigated by Selvabharathi et al. [150]. They observed that shot peening created defects on the metal surface occupied by nitrogen upon nitriding and reformed the grain boundaries to produce micro twins. The formation of micro twins in duplex stainless steel has been reported to provide strain energy that transforms austenite to martensite [13].

Despite the precipitation of the S phase during the welding process, the increased hardness of the nitrided weld metal is attributed to the micro twin grain boundaries and the precipitated martensite. Though the precipitation of the S phase has a detrimental effect on the hardness of duplex stainless steel, it has also been found to prevent the formation of chromium nitride, which implies an increase in corrosion resistance [151]. They concluded that overall improvement in the tensile strength of the shot-peened nitrided duplex stainless steel was attributed to the fine martensite grains, reduction in residual stresses and increased twin grain boundaries.

A current investigation was conducted by Muhammed et al. [28] to establish a relationship between the ferrite phase content, phase stabilizers composition, post-weld treatment parameters and the properties of duplex stainless steel weld joints. The results of their findings revealed that the ratio of the ferrite phase to austenite phase must be approximately unity if optimum weld properties are desired. The ferrite-austenite ratio was positively correlated with the hardness and negatively correlated with the ultimate tensile strength and corrosion density. Further investigations revealed that ferrite phase stabilizers were positively correlated with the ultimate tensile strength of the weld joint.

Summarily, it can be said that optimum properties in duplex stainless steel are obtained when the austenite and ferrite phases are in equilibrium, and their quotient is approximately one. Welding upsets this equilibrium and leads to property deterioration by setting up residual stresses and precipitating unwanted secondary phases through ferritization. Despite the deleterious effect of the S phase and delta ferrite on the properties of duplex stainless steel, they have been found to improve corrosion resistance. The improvement in properties of welded duplex stainless steel joints through weld treatment processes is achieved by deferritization, release of residual stresses and martensite tempering. In addition, the ferrite-austenite ratio was found to be positively correlated with hardness and negatively correlated with the ultimate tensile strength and corrosion density, while the ferrite phase stabilizers were also positively correlated with the ultimate tensile strength.

2.3.3.3 Similar Martensitic Stainless Steel Weld Joints

Like austenitic and martensitic stainless steel similar weld joints, martensitic stainless steel is easily subjected to several welding processes due to its low carbon content. However, they face a major setback of poor weld properties due to brittle martensite and delta ferrite at the weld joint. The presence of martensite can lead to cold cracking and eventually material failure, while delta ferrite deteriorates its mechanical properties [156 – 160]. Weld property improvement in martensitic stainless steel can be achieved by refining the martensite grains and the precipitation of secondary phases along grain boundaries, which resist dislocation movement, thus improving strength. This can be achieved by applying weld heat treatment processes, mainly the preheating, tempering, normalizing, ageing and solution treatment [161 – 162].

The effect of preheating and post-weld tempering on the properties of martensitic stainless steel was investigated by Köse and Kaçar [10]. The result of their research revealed that the weld joint had high martensite content and a small amount of delta ferrite. A similar result was reported by Baghjari and Akbari Mousavi [154] and Berretta et al. [159]. The hardness of the weld metal was found to be improved by preheating and post-weld tempering due to the reduction in cooling rate by preheating, which activated the martensite-ferrite transformation and coupled with the precipitation of fine carbides. Other researchers have also reported hardness reduction in martensitic weld joints due to fine carbide precipitation [164 – 165]. Reduction in hardness implies an increase in toughness and formability, which is usually accompanied by a reduction in chromium content, which implies poor corrosion properties.

Post-weld tempering temperature has also been reported to affect the tensile strength of martensitic stainless steel. Muthusamy et al. [47] investigated the effect of post-weld tempering temperature and heat input on the properties of martensitic stainless steel. They reported that increasing heat input increases the toughness and hardness of the weld metal. Meanwhile, the tensile strength was found to decrease with both increasing heat input and tempering temperature. The increase in toughness and hardness of the weld metal and the reduction in tensile strength was attributed to the increase in delta ferrite composition with increasing tempering temperature and heat input.

The effect of tempering holding time on the properties of martensitic stainless steel was studied by Tavares et al. [26]. In their experiment, a post-weld tempering temperature of 650 ^{o}C was applied while varying the holding time between 15 – 60 minutes. They found out that the hardness, toughness, and elongation of the weld metal reduced with holding time as a result of martensite tempering and coupled with the precipitation of intermetallic phases containing molybdenum, while no significant effect was observed on the tensile properties.

The level of retained austenite phase in martensitic stainless steel determines its mechanical and corrosion properties. With the objective of improving the mechanical properties of martensitic stainless steel by increasing the level of retained austenite, Zappa et al. [162] investigated the combined effect of double tempering and solution treatment on preheated martensitic stainless steel. They discovered that retained austenite increased from 14 % to 42 % after the second tempering. The application of first tempering reduced the hardness and tensile properties while toughness and elongation were improved. The application of the double tempering was found not to have a significant improvement in mechanical properties despite the increase in retained austenite content.

Kumar et al. [8] investigated the effect of normalizing post-weld treatment on the properties of martensitic steel. They found that the hardness and ultimate tensile strength of martensitic steel reduced with increasing preheat temperature and increased with the normalizing temperature. A reverse trend was reported for the impact energy and ductility. The reduction in hardness and ultimate tensile strength, accompanied by an increase in ductility and impact energy with increasing preheat temperature, resulted from the cooling rate reduction, which coarsened the microstructure. Meanwhile, increasing normalizing temperature, on the other hand, increased the cooling rate and refined the microstructure.

RAFM and CLAM stainless steel are two grades of martensitic stainless steel that have applications in ITER components due to their high creep strength. Manugula et al. [163] investigated the effect of Post-Weld Direct Tempering (PWDT) and Post-Weld Normalization Tempering (PWNT) on the properties of RAFM stainless steel. The results of their experiments revealed that both PWDT and PWNT reduce the hardness of the weld metal, with PWNT providing a greater reduction. Hardness reduction by PWDT resulted from martensite tempering, loss of solid solution strengthening, and the elimination of dislocation associated with the transformation of martensite. Meanwhile, a reduction in hardness by PWNT was solely a result of martensite tempering. As for the impact energy, PWNT increased the impact energy, while PWDT brought about its reduction. The poor impact energy offered by PWDT was a result of high carbon martensite and the presence of delta ferrite, while the presence of tempered martensite coupled with delta ferrite elimination improved the impact energy during PWNT. The ultimate tensile strength followed the same trend, while the elongation was found to be higher for the sample with PWDT.

A similar study on the effect of PWNT time on the properties of CLAM stainless steel was investigated by Li et al. [164]. The hardness of the weld metal was found to decrease with increasing tempering time due to the sufficient time available for martensite transformation. They also reported a decrease in heat shock resistance and ultimate tensile strength with increasing tempering time while the elongation and impact energy followed a reverse trend. The presence of lath martensite in the weld metal accounted for its superior thermal shock resistance. The authors recommended PWNT of 30 minutes for a better property combination for applications involving thermal shock resistance.

Maraging stainless steel is a low carbon martensitic steel produced by age hardening. It possesses ultra-high strength, fracture toughness, excellent machining properties and weldability. Its favourable properties are the reasons for its adoption as a structural element in the aviation and space industry and defence and power applications. Fe - Ni and Fe -Cr - Ni is two major types of maraging steel available. However, in recent times, many alloying modifications have been made for improved performance [169 – 170]. Microstructural changes or property modification in maraging steel are achieved by solution annealing and precipitation hardening.

An et al. [167] investigated the effect of ageing heat treatment on the properties of Fe - Cr -Ni type maraging stainless steel. The result of their findings revealed that ageing produces a homogeneous microstructure with less alloying elements. In addition, the microstructural homogeneity was found to have a positive correlation with ageing temperature. Hardness variation observed across the weld metal was attributed to the microstructural evolution mechanisms resulting from the different alloying elements present in martensite.

A new study presented by Muhammed et al. [28] revealed that martensitic stainless steel weld joint properties are a function of the microstructure, which contains martensite, ferrite and austenite phases. They also attempted to establish a connection between the microstructural composition and the mechanical properties. The results of their findings revealed that the ferrite phase was positively correlated with the hardness and impact toughness, while a negative correlation was established between the tensile strength and ferrite composition. A negative correlation was also observed between the hardness and ultimate tensile strength.

To sum up, the presence of martensite and delta ferrite in the weld joints of martensitic stainless steels has detrimental effects on their properties, predominantly hardness and ultimate tensile strength. However, for applications where resistance to thermal shock is desired, the martensite phase is desired. The application of weld treatment processes such as preheating, normalizing, tempering, and ageing improves the mechanical properties. Preheating and increasing post-weld treatment time reduces hardness and tensile strength by reducing the cooling rate, martensite tempering and precipitation of intermetallic phases. A reduction in hardness is also achieved by normalizing and tempering but, normalizing confers greater strength than the latter. On the other hand, increasing the ageing temperature homogenizes the microstructure, and homogeneity is strongly correlated with the temperature. In addition, hardness and impact toughness are positively correlated with the ferrite phase content, while a reverse trend was observed for the tensile strength.

2.3.3.4 Similar Ferritic Stainless Steel Weld Joints

As observed in other grades of stainless steel, ferritic stainless steel is not different, as the weld joints also suffer challenges, including a reduction in fracture toughness and the overall reduction in strength as a result of the thermal stress field, which creates residual stresses in the weld metal [168]. The weld property obtained after welding is dependent on several factors, predominantly, the microstructure and chemical composition of the metal. The application of appropriate microstructural modification processes such as post-weld heat treatment and plasma processing have been reported by researchers to improve the properties of welded ferritic stainless steel joints [173 – 175].

Grade 91 ferritic stainless steel, also known as chromium-molybdenum ferritic stainless steel, is specifically used for high temperature applications such as in boilers and heat exchangers in petrochemical and power plants owing to its high temperature creep resistance and stress corrosion cracking, especially in corrosive environments [168]. Ahmed et al. [172] investigated the effect of annealing holding time on the properties of chromium-molybdenum boiler ferritic stainless steel. The results revealed that the ultimate tensile strength, yield strength, elongation and reduction in the area increases with holding time. The reduction observed in strength and ductility after a long holding time was as a result of the spheroidization of pearlite grains. They also reported that the increase in impact energy with temperature and holding time was as a result of grain refinements coupled with the formation of dendrites.

The effect of single and multiple tempering time on the properties of modified chromium-molybdenum ferritic stainless steel was reported by Dey et al. [173]. They found out that the yield strength and ultimate tensile strength decreases with single tempering holding time as a result of martensite tempering coupled with the precipitation of fine precipitates while multiple tempering time did not show any significant effect. This was also accompanied by a corresponding increase in toughness and ductility. They also reported that the impact toughness increased with both single and multiple tempering time and concluded that the tempering of welded ferritic stainless steel for a sufficient time can restore the properties and that there was no need for multiple tempering times, as it had no significant improvement on the properties of the weld metal.

Taniguchi and Yamashita [174] studied the effect of manganese and nickel alloying additions on the properties of annealed grade 91 ferritic stainless steel. A reversal in mechanical properties, primarily; tensile strength, absorbed energy and rupture time with annealing temperature, was observed in the samples with high content of manganese and nickel. This was attributed to the precipitation of fresh martensite at temperatures above the critical transformation temperature. A different trend was observed in samples with low alloy additions, as the tensile strength increased with temperature while the absorbed energy decreased with temperature. This observation was attributed to the small amount of precipitated fresh martensite due to the low alloying additions. They concluded that the upper limit post-weld heat treatment temperature for chromium-molybdenum ferritic stainless steel is a function of the mechanical properties, not the critical transformation temperature.

The application of post-weld heat treatments can sometimes be cost-effective and time-consuming. This led to the introduction of other property modification mechanisms, such as electrolytic plasma processing (EPP). Property modification by EPP is due to the chemical, mechanical, electrical and thermal effect of the plasma introduced to the surface of the material [152, 153]. Dewan et al. [51] investigated the effect of annealing, hardening and EPP on the properties of ferritic stainless steel. Their findings revealed that, while annealing and hardening reduced and increased the hardness of the weld metal, respectively, EPP had no significant effect, as it is a surface mechanism and does not involve grain refinement. It has also been reported that EPP treatment reduces residual stresses induced during welding but increases the compressive stresses due to the thermal shock during the EPP process [9]. Maximum tensile strength was observed in the EPP treated samples, while hardening did not affect tensile strength and ductility. The high tensile strength derived from the EPP treatment was due to the formation of surface martensite. From their findings, it was also discovered that the application of EPP treatment after annealing had no significant benefit in terms of property improvement, as it leads to increased compressive stresses and a reduction in toughness.

Recently, a study was published by Muhammed et al. [28] to establish a relationship between the properties of ferritic stainless steel weld joints and weld treatment parameters. Their research work established a relationship between post weld treatment temperature, residual stress, and hardness. The results of their findings revealed that the residual stress is perfectly negatively correlated with temperature, while the ultimate tensile strength was positively correlated with the hardness of the weld joint. This suggests that residual stresses induced by the welding process are eliminated at high temperatures of post-weld treatment.

Conclusively, while increasing annealing temperature reduces the hardness of ferritic stainless steel, adequate annealing holding time increases ultimate tensile strength and impact energy. On the other hand, Tempering reduces the ultimate tensile strength due to martensite tempering but increases toughness and ductility. Multiple tempering times did not show any significant difference in properties; therefore, it is not recommended. EPP, a surface modification mechanism, reduces residual stresses and increases tensile strength due to fresh martensite precipitation. For high Cr heat resistant ferritic stainless steel, the upper critical limit for post-weld treatment is a function of the mechanical properties, not the upper critical temperature. Furthermore, the residual stress is perfectly negatively correlated with the post-weld treatment temperature, while the ultimate tensile strength is positively correlated with the hardness of the weld joint.

2.3.4 Review of Effect of Weld Treatment Processes on the Properties of Dissimilar Stainless Steel Weld Joints.

A dissimilar stainless steel weld joint, as the name implies, is a weld joint comprising stainless steel and other metals as the participating base metals. It also includes weld joints comprising different grades of stainless steel, such as a joint comprising of austenitic and duplex stainless steel as the base metals.

A review of the literature of the dissimilar welding of stainless steel revealed that most of the dissimilar joints involve austenitic stainless steel. Generally, this form of welding is carried out to optimize the properties conferred by each base metal, with the objective of minimizing cost and obtaining excellent service performance [155]. It finds application in petroleum industries, chemical plants, ITER components, nuclear plants, and aerospace industries [156 – 158]. The major challenge faced during the dissimilar welding of stainless steel with other metals is the difference in the thermophysical and chemical composition of the base metals, which results in intermetallic phase precipitation, residual stress generation and overall property deterioration; hence, the need for pre and post-weld treatment [159 – 164]. The following subsections present the effect of weld treatment processes on the properties of different dissimilar weld joints involving stainless steel.

2.3.4.1 Dissimilar Austenitic Stainless Steel Weld Joint with Carbon Steel and Cast Iron

Carbon steel possesses good strength and wear resistance, and it is quite cheap. Cast iron, on the other hand, has a good combination of strength and toughness. These metals' dissimilar joint with stainless steel is desired because it combines strength and corrosion resistance. Austenitic stainless steel-carbon steel joints find applications in boilers, oil and gas industries and thermal power plants, while the latter is used in the automobile industry and general machinery [179, 180]. The microstructure of carbon steel comprises pearlite dispersed in a ferrite matrix, while ductile cast iron consists of graphite embedded in a ferritic and pearlitic matrix [181, 182].

The joint quality obtained from the dissimilar weld joint is a function of the chemical composition and microstructure of the base metals, among other factors. The major difficulty encountered in the welding of stainless steel-carbon steel is the formation of chromium carbide, which is accompanied by the decarburization of the carbon steel, leading to the deterioration in mechanical properties and the reduction in corrosion resistance [183, 184]. Stainless steel–

cast iron joints, on the other hand, face the challenge of poor weldability coupled with the precipitation of ledeburite, which increases the hardness of the weld joints and eventually leads to failure [182, 185]. The application of adequate weld treatment processes can improve the property of these welded joints.

The effect of annealing temperature on the properties of the dissimilar joint of 1045 carbon steel and 304 austenitic stainless steel was investigated by Ma et al. [177]. The result of their experiment revealed that increasing annealing temperature increases carbide precipitation due to an increase in the diffusion rate of carbon atoms. This was also accompanied by an increase in the hardness of the fusion zone and a corresponding decrease in corrosion resistance owing to the depletion in chromium content. However, at low annealing temperatures, the reduction in fusion zone hardness was reported due to the increase in ferrite content, reduced dislocation density and coarse austenite grains. Though the tensile strength fluctuated with increasing annealing temperatures, the maximum strength of the joint obtained was approximately equivalent to that of the stainless steel base metal. They also reported no significant changes in the microstructure of the stainless steel base metal, as the post-weld treatment temperatures were below the transformation temperature.

Similar results were also reported by Sadeghi et al. [176], who studied the effect of annealing temperature on the properties of the A537CL1 carbon steel pressure vessel and A321 austenitic stainless steel dissimilar joint. They reported that increasing annealing temperatures decreased the ultimate tensile strength, yield strength, ductility, toughness, and impact energy. This reduction in mechanical properties at high annealing temperatures was due to the carbide precipitation. However, the residual stresses reduced at low annealing temperatures; at high annealing temperatures, it was found to increase. This was attributed to the difference in thermal expansion of the base metals. It can be deduced from their findings that optimum mechanical properties are obtained at low annealing temperatures

Sawada and Nakamura investigated the effect of preheating temperature on the properties of austenitic stainless steel and ductile cast iron dissimilar joint [175]. The results of their findings revealed that the hardness of the fusion zone increased with increasing preheating temperature due to martensite precipitation and chilling. Chilling is a term used to refer to the appearance of cementite in cast iron, and it has been reported to cause embrittlement [186, 187]. The tensile strength was also reported to increase with increasing preheating temperature and welding speed. This resulted from an increase in Deformed Layer of Spheroidal Graphite (DLSG), chill reduction and reduction in martensite precipitation.

From the preceding, it is evident that aside the difference in thermophysical and chemical properties of dissimilar weld joints, stainless steel - carbon steel joints are posed with decarburization, formation of carbides and reduction in corrosion resistance while stainless steel-cast iron joints face precipitation of ledeburite and consequently increased hardness. Increasing the post-weld temperature further deteriorates the weld quality in the former, but improved properties are obtained when heat treatment is conducted at low temperatures. In the latter case, increasing preheating temperature was found to further increase the fusion zone hardness while the tensile strength was considerably improved.

2.3.4.2 Dissimilar Austenitic Stainless Steel Weld Joint with Ferritic and Martensitic Stainless Steel

Ferritic stainless steel is flexible, cheap and possesses good corrosion resistance. Their dissimilar joints with austenitic stainless steel have applications in the power industry, petrochemical industry and oil and gas industry. On the other hand, martensitic stainless steel possesses void swelling resistance and good thermophysical and thermomechanical properties. Their dissimilar joints with austenitic stainless steel are major structural elements used in the Test Blanket System (TBS) [188 – 191]. The dissimilar welding of austenitic stainless steel to martensitic stainless steel suffers the challenge of martensite transformation on the martensitic stainless steel side, which results in hardening, hence, the need for post-weld treatment. Austenitic-ferritic stainless steel joints, on the other hand, face the challenge of carbide precipitation, which leads to weld property deterioration, including corrosion resistance**.**

Researchers have reported several methods of reducing carbide precipitation in these joints. Some of these techniques include using a low energy input welding technique, adding alloying elements with a high affinity for carbon, such as vanadium, titanium and niobium, and the use of adequate post-weld heat treatment. It has also been reported that adequate post-weld treatment is less cost-intensive when compared to its counterparts [192 – 194].

Ghorbani et al. [191] investigated the effect of annealing temperature and filler electrode on the properties of AISI 304L austenitic stainless steel and AISI 430 ferritic stainless steel dissimilar joints. Their findings revealed that the tensile strength and ductility increase with annealing temperature due to carbide precipitation at elevated temperatures and a reduction in the delta ferrite composition of the weld metal. The corrosion resistance was found to diminish with annealing temperature and the use of the ferritic or austenitic filler electrode. A reduction in corrosion resistance was attributed to the martensite formation due to the fast cooling rate, while the formation of secondary phases such as the sigma phase and sulphides with the use of ferritic and austenitic filler electrodes led to a reduction in corrosion resistance.

The effect of tempering temperature on the properties of CLAM / 316L dissimilar joints was studied by Zhang et al. [192]. They reported that the hardness of the dissimilar joints reduced with tempering temperature due to martensite tempering, while the tensile strength fluctuated with tempering temperature as a result of the precipitation, dissolution, and re-precipitation of carbides. They also reported low impact energy for the dissimilar joints, lower than both base metals.

Conclusively, austenitic-ferritic stainless steel joint faces the challenge of carbide precipitation and consequently reduction in corrosion resistance. The quality of such joint can be improved by employing a low heat input welding technique, post-weld treatment or introducing alloying elements. On the other hand, the dissimilar joint of austenitic and martensitic stainless steel is characterized by increased hardness due to martensite precipitation. Tempering of martensite through post-weld treatment is an adequate method of improving the joint quality.

2.3.4.3 Dissimilar Austenitic Stainless Steel Weld Joint with Titanium and Nickel Alloy

Titanium and nickel alloys belong to the family of shape memory alloys and find application in the aerospace industry and biomedical instruments due to their ability to recover their original shape after mechanical deformation (pseudo-elasticity) and also retain the deformed shape up to their recovery temperature (shape memory effect) [197 – 201]. The limited use of titanium and its alloys is due to its expensive nature; consequently, it is welded with stainless steel to reduce the cost and extend its range of applications [198].

The microstructure of titanium-nickel alloys contains about 45 % titanium and 55 % nickel, while pure titanium metal contains about 99 % titanium with other alloying additions [203], [204]. The major challenge encountered in their dissimilar welding with stainless steel, aside the general difficulty encountered in producing good quality joints, is the precipitation of deleterious intermetallic phases [199]. Secondary phase precipitation can be minimized by incorporating an interlayer of aluminium, copper, silver or nickel-based filler metal [205, 206]. General property modification of the weld joints is achieved by applying appropriate post-weld treatment.

Chen et al. [203] investigated the effect of high annealing temperature (650 – 850 ^{o}C) on the properties of NiTi / 304 SS dissimilar joints. Their findings revealed that the tensile strength, elongation, and microhardness increases with annealing temperature. The improvement in mechanical properties was attributed to the precipitation of intermetallic phases. The effect of low annealing temperature (200 – 400 ^{o}C) was investigated by Mirshekari et al. [204]. They reported an improved tensile strength and hardness due to the release of residual stresses and less precipitation of intermetallic phases. They also reported that better corrosion resistance is exhibited at low annealing temperatures due to the disruption of the sessile dislocation networks, which are pitting corrosion sites in addition to less precipitation of intermetallics and residual stress release [209, 210].

The effect of preheating, friction welding parameters and surface condition on the properties of cp-titanium/316L dissimilar weld was studied by Akbarimousavi and Goharikia [207]. The results of their experiments revealed that samples with surface smoothening followed by cleaning with acetone had the best tensile properties. This indicates that these joints are very sensitive to the surface conditions of the base metals before welding. Surface cleaning eliminates intermetallics, which have been reported to cause a reduction in the strength of welded joints due to their brittle nature [212, 213]. They also discovered that increasing forging pressure eliminates intermetallics from the weld interface to the flash region.

It can be deduced from the foregoing that the dissimilar joint of stainless steel with titanium and nickel alloy is usually prone to precipitation of intermetallic phases. The precipitation of these phases can be minimized by cleaning up the metal surface prior to the welding process and subsequently employing the use of an interlayer during the welding process and eventually applying post-weld treatment.

2.3.4.4 Dissimilar Austenitic Stainless Steel Weld Joint with Copper and Aluminium Alloy

Copper is malleable, corrosion-resistant and has a high thermal and electrical conductivity. These properties are combined with stainless steel's strength and corrosion resistance in a dissimilar weld joint, which finds application in nuclear power plants [214, 215]. On the other hand, aluminium is light, and its dissimilar joint with stainless steel is desired when weight reduction is the design priority, like in the automobile and aerospace industries.

The microstructure of copper and aluminium contains about 98 % of the pure metal with about 2 % alloying additions [216, 217]. Creating dissimilar copper/stainless steel joints and aluminium/stainless steel has posed a great challenge for some decades now. Though some researchers have fabricated joints with good strength using some low heat input welding techniques, the properties obtained from such joints do not meet the minimum mechanical requirements; hence, they have limited applications [218 – 224]. In order to obtain joints with improved mechanical properties, a combination of two or more welding techniques known as hybrid welding has been attempted by several researchers with several post-weld treatment processes [221].

The hybrid welding of copper/stainless steel dissimilar joints with gas tungsten arc welding assisted heating, and external cooling was investigated by Joshi and Badheka [222]. They observed that deformation (in the form of flash) and oxidation (in the form of a black stirred surface) increased with preheating temperature. A similar result was reported by Mofid et al. [223]. The low oxidation rate observed at low temperatures is due to the formation of a water blanket on the surface of the stirred metal, as reported by Zhang et al. [224]. The tensile strength was also observed to deteriorate with assisted heating or cooling due to the high deformation rate at elevated temperatures and the low copper/stainless steel bond strength at low temperatures. They concluded that, though assisted heating and cooling reduced the hardness of the stir zone, optimum weld properties for copper/stainless steel joints are obtained in the as weld condition, without assisted heating or cooling.

The effect of hybrid welding and tool rotation speed on the properties of aluminium alloy/stainless steel dissimilar joints was studied by Bang et al. [225]. From their findings, it was discovered that joints with good strength almost equal to that of the aluminium base metal were obtained at an intermediate tool rotation speed using hybrid welding. They also found out that the maximum reduction in hardness of the stir zone was obtained with hybrid welding, which was attributed to the refinement of grain size by preheating coupled with the reduction in dislocation density.

Dong et al. [226] studied the effect of post-weld heat treatment and holding time on the properties of aluminium alloy/stainless steel dissimilar joint welded using the zinc-based filler electrode. The result of their findings revealed that the interfacial layer thickness increases with post-weld treatment temperature due to the increase in precipitation of zinc-rich phases coupled with the increase in the diffusion rate of aluminium and iron to the interfacial layer. They also reported a fluctuation in the tensile strength with temperature and holding time due to a fluctuation in the precipitation of fine zinc-rich phases at the interfacial layer. They concluded that optimum joint properties are obtained at intermediate holding times and post-weld temperatures.

To conclude, stainless steel-copper and stainless steel-aluminium dissimilar joints are generally difficult to fabricate, and when one is eventually able to create such joints, they tend to possess poor mechanical properties. This challenge can be conquered by employing hybrid welding techniques and incorporating adequate weld treatment processes.

2.4 Response Surface Methodology (RSM)

Response Surface Methodology (RSM) is a statistical tool first introduced by Box and Wilson in 1951 [227]. It combines statistical and mathematical techniques to develop, analyse and optimize processes in which the output (called response) is a function of other variables. The response is the dependent variable while the input variable is the independent variable [232, 233]. RSM finds application in fields where several input variables determine a product's performance measures, quality characteristics, or process. These include industries, biological and clinical sciences, social sciences, food science, and even physical science and engineering [233, 234]. The objective of RSM is to determine the optimum response given certain input variables and also to understand the change in response in a given direction following adjustment in the input variable [231].

The major statistical tools used in RSM are regression analysis, bivariate correlation, ANOVA, among others. The regression analysis is used to establish a relationship between the response and control or independent variables. The result of the regression analysis is the generation of a regression model, which can be used to predict the response variables in terms of the control variables, with the accuracy of the model being dependent on the R^2 value. Generally, R^2 values close to 1 are desired. On the other hand, the bivariate correlation analysis is used to establish a relationship between the independent variables and the response variable as regards the nature of changes that will occur in the response variable when the control or independent variables are increased or decreased. Two common correlation coefficients adopted are the Pearson and the Spearman correlation coefficients. But for linear relationships, the Pearson correlation coefficient is preferred [28]. The strength of the correlation is indicated by the coefficient of correlation, as values close to 1 indicate perfect correlations. The ANOVA is used to investigate the effect of the control variables on the response variables by identifying the most significant parameters.

For instance, if the tensile strength (Y) of spot welded austenitic stainless steel is dependent on the preheat temperature(X_1), soaking time (X_2) and tempering temperature (X_3), we could write the expression as:

$$\boldsymbol{Y = f(X_1) + fX_2) + f(X_3) + e} \tag{2.1}$$

Where e is a statistical error or variability not accounted for by *f*.

The variables in the equation are called natural variables since they are in their natural unit, but they are transformed to coded variables with zero mean and the same standard deviation.

2.4.1 Response Surface Methodology (RSM) Optimization Procedure

All applications of RSM either fall into the category of mapping a response surface over a particular region of interest, optimization of a response or selecting operating conditions to achieve specific customer requirements [229]. The application of RSM in solving a problem is usually sequential. It involves identifying variables, screening experiments, choice of experimental design, analysis of data, evaluation of the fitted model and determination of optimum conditions [232]. These stages are briefly discussed as follows.

Identification of Variables

This is the first stage of the application process. At this stage, the experimenter generates ideas to ascertain which factors or independent variables are important to the response study.

Screening Experiment

After identifying the variables that will affect the desired response, a screening experiment is carried out. The variables that have a more significant effect on the response are selected in the experiment, while the ones with minor effects are eliminated. This phase is sometimes called phase zero of the RSM study. A full or factorial two-level design may be implemented [233, 236].

Choice of experimental design

The choice of experiment design is a key decision as it goes a long way in determining the accuracy of approximation and cost of constructing response surfaces. The key objective of the design of experiments is to select points where the response should be evaluated [230]. In this stage, the first-order model is the first point of call, but the second-order model should be employed if there is a need to evaluate curvature.

A two-level factorial design can be used to estimate defects in the first order model, but it fails for higher levels. Other symmetrical designs include three-level functional design, box behnken design, central composite design and doehlert design. Codification of variables is also done at this stage. It involves the transformation of real value variables into coordinates inside a scale with a dimensionless value. The transformation is done using the expression below.

$$\boldsymbol{x_i} = \left(\frac{z_i - z_i^0}{\Delta z_i}\right)\boldsymbol{\beta_d} \tag{2.2}$$

Where Δz_i is the difference between the real value in the central point and the real value in the superior or inferior level, β_d is the major coded limit value in the matrix for each variable and $z_i^0$is the real value in the central point.

Analysis of Data

After obtaining the required data and choosing the design of the experiment, the next phase is to carry out statistical analysis of the data by fitting a mathematical equation to describe the behaviour of the response [232]. This equation is then written in a matrix notation and solved using multiple regression techniques, i.e., the least squares method. After the transformation, an equation that describes the response surface in the experimental domain is constructed using a vector containing the parameters given below.

$$\boldsymbol{b} = (\boldsymbol{X}_{n.m}^{T}\boldsymbol{X}_{m.n})^{-1}(\boldsymbol{X}_{n.m}^{T}\boldsymbol{Y}_{m.i}) \tag{2.3}$$

Where b is the vector constituted by the parameters of the model, m is the number of lines from the matrix, n is the number of columns from the matrix, y is the response, and X is the matrix of the chosen experimental design.

In using this multiple regression techniques, it is assumed that there are independent errors with a profile of zero mean and common unknown variance; as a result, authentic repetition of the central point can be used to estimate the variance of each component using the following equation.

$$\breve{\boldsymbol{V}}(\boldsymbol{b})_{\boldsymbol{n.n}} = (\boldsymbol{X}_{\boldsymbol{n.m}}^{\boldsymbol{T}}\boldsymbol{X}_{\boldsymbol{m.n}})^{-\mathbf{1}}\boldsymbol{s}^{\mathbf{2}} \tag{2.4}$$

Taking the square root of the above equation gives the standard error for the coefficient of b, which compose the response equation.

Evaluation of fitted model

After fitting a model to describe the surface response, the fitted model needs to be evaluated as it may not completely describe the experimental domain. This evaluation is achieved using analysis of variance (ANOVA). The idea behind the use of ANOVA is to compare the variance between the result of the analysis carried out and the response generated as there are some random errors inherent in the response [233]. The results can then be used in forecasting. ANOVA uses dispersion as the main tool in data set evaluation. The relationship between the deviation d_i, observation (y_i) or its replica (y_{ij}) and the media ($\bar{y}$) is given as;

$$\boldsymbol{d}_{\boldsymbol{i}}^{\mathbf{2}} = \left(\boldsymbol{y}_{\boldsymbol{ij}} - \overline{\boldsymbol{y}}\right)^{\mathbf{2}} \tag{2.5}$$

When all the deviations are summed, we obtain a parameter known as the sum of the square of total variation denoted as $SS_{tot,}$ which is also equivalent to the sum of the square of variation resulting from regression and residuals. Mathematically we write:

$$\boldsymbol{SS}_{\boldsymbol{tot}} = \boldsymbol{SS}_{\boldsymbol{reg}} + \boldsymbol{SS}_{\boldsymbol{res}} \tag{2.6}$$

The SS_{res} is a combination of two other deviations: the sum of the square due to pure error (SSPe) and the sum of squares due to lack of fit (SS_{LOF}). Mathematically we write:

$$\boldsymbol{SS}_{\boldsymbol{res}} = \boldsymbol{SS}_{\boldsymbol{pe}} + \boldsymbol{SS}_{\boldsymbol{LOF}} \tag{2.7}$$

When the sum of the square is divided by the degree of freedom, we obtain the media for the sum of the square. Table 2.14 shows the degree of freedom for each of the variances and the corresponding media.

Table 2.14: Degree of freedom and media for different variances.

Variation	Sum of the Square	Degree of Freedom	Media
Regression	$\sum_{i}^{m}\sum_{j}^{n_1}(\check{y}_i - \bar{y})^2$	p-1	$MS_{reg} = \frac{SS_{reg}}{p-1}$
Residual	$\sum_{i}^{m}\sum_{j}^{n_1}\left(y_{ij} - \check{y}_i\right)^2$	n-p	$MS_{res} = \frac{SS_{res}}{n-p}$
Lack of Fit	$\sum_{i}^{m}\sum_{j}^{n_1}(\check{y}_i - \bar{y}_i)^2$	m-p	$MS_{LOF} = \frac{SS_{LOF}}{m-p}$
Pure Error	$\sum_{i}^{m}\sum_{j}^{n_1}\left(y_{ij} - \bar{y}_i\right)^2$	n-m	$MS_{pe} = \frac{SS_{pe}}{n-m}$
Total	$\sum_{i}^{m}\sum_{j}^{n_1}\left(y_{ij} - \bar{y}\right)^2$	n-1	

Note that n is the number of observations, m number of levels in the design, p is the number of parameters of the model, $\check{y}_i$ is the estimated value by the model for each level, $\bar{y}$ is the overall media, y_{ij} is the replicate performed in each level, $\bar{y}_i$ is the media of the replicate performed in the same experimental conditions.

The model can be evaluated either using regression or lack of fit. A model is said to be well fitted if it has significant regression and a non-significant lack of fit. In other words, in using the regression test, the value of the ratio should be higher than the tabulated value of fisher distribution (F test), but for the lack of fit test, the value of the ratio should be lower than the tabulated value [232]. The two ratios are given below.

For regression test,

$$\frac{MS_{reg}}{MS_{res}} \approx \boldsymbol{F_{Vreg}, V_{res}} \tag{2.8}$$

For the lack of fit test,

$$\frac{MS_{LOF}}{MS_{pe}} \approx \boldsymbol{F_{VLOF}, V_{pe}} \tag{2.9}$$

Where F_{Vreg}, V_{res} ,F_{VLOF}, V_{pe} are the degrees of freedom associated with each variation.

Determination of Optimum Conditions

This involves determining the values of the independent variables that would result in optimization (i.e. minimum/maximum values) over a certain region of interest [230]. Optimization is dependent on obtaining a good, fitted model that represents the mean response. For first degree models, the method of steepest ascent or descent can be used for optimization.

After experimentation, a second-degree model should be employed to ascertain the region of optimum parameters [234]. Visual inspection can be used if the linear model does not indicate the direction of the optimum condition [232]. For cases where the model is a quadratic equation, optimum points (minimum, maximum and saddle points) can be determined by solving the resulting equation from the derivative of the equation and equating it to zero. In order to visualize the predicted model, a surface plot should be used.

2.4.2 Building Empirical Models

Two important models used in RSM are the first degree and the second-degree model. The expression for the first degree is given as;

$$\boldsymbol{y = \beta_0 + \sum_{i=1}^{k} \beta_i x_i + e} \tag{2.10}$$

Alternatively as,

$$\boldsymbol{y = \beta_0 + \beta_1 x_1 + \beta_2 x_2 \ldots + \beta_k x_k + e} \tag{2.11}$$

The second model is more flexible, represents curvature, easy to estimate parameters and works better in real response surface problems [227]. The expression for this model is given as;

$$\boldsymbol{y = \beta_0 + \sum_{i=1}^{k} \beta_i x_i + \sum_{i<j} \sum \beta_{ij} x_i x_j + \sum_{i=1}^{k} \beta_{ii} x_i^2 + e} \tag{2.12}$$

Alternatively as,

$$\boldsymbol{y = \beta_0 + \beta_1 x_1 + \beta_2 x_2 + \beta_{11} {x_1}^2 + \beta_{22} {x_2}^2 + \beta_{12} x_1 x_2 + e} \tag{2.13}$$

Where y is the response or output, k is the number of variables, β_0 is a constant term, β_i is a coefficient of a linear parameter, x_i is the independent variable, and e is the statistical error.

The values of β_i can be evaluated using linear regression analysis.

In order to determine the optimum variable and response and establish a relationship between the dependent and independent variables, a series of experiments are carried out. The result or the response from these experiments can be represented by an n × k matrix denoted as D called Design Matrix.

$$\boldsymbol{D} = \begin{bmatrix} x_{11} x_{12} \dots x_{1k} \\ x_{21} x_{22} \vdots x_{2k} \\ \vdots \quad \vdots \quad \vdots \quad \vdots \\ x_{n1} x_{n2} \dots x_{nk} \end{bmatrix} \tag{2.14}$$

x_{ij} denotes the i_{th} design of x_j (i=1, 2…k and u = 1, 2…n), and y_i is the response value obtained by applying an i_{th} value of x, i.e., x_i (x_{i1}, x_{i2}, x_{i3}, …x_k) and each row is a design point in a k Euclidean dimensional space. If we write the response as a function of the input parameter x_i we have,

$$\boldsymbol{y_i = f^1(x_i)\beta + e_i} \tag{2.15}$$

Where e_i is the error term associated with the u_i experimental run.

The above equation can be expressed in a matrix form as $y = X\beta + e\ where\ y = y_1,\ y_2, \dots\ y_n, X\ is\ a\ matrix\ of\ order\ n \times$ m whose ith row is f(x_i) $and\ e = e_1, e_2, \dots e_n$.

Note that the first column of X is the column of ones denoted 1n.

The least square estimator $\hat{\beta}$ can be obtained by assuming that e has a mean of zero and a variance-covariance matrix given by $\varphi^2$1n. The estimator is given as;

$$\boldsymbol{\hat{\beta} = (X^1X)^{-1}X^1y} \tag{2.16}$$

The variance-covariance of $\hat{\beta}$ is of the form:

$$\boldsymbol{var(\hat{\beta}) = (X^1X)^{-1}X^1(\varphi^2 1n)X(X^1X)^{-1} = \varphi^2(X^1X)^{-1}} \tag{2.17}$$

Using the estimator obtained, an estimate of $\hat{\imath}(x_i)$ of the mean square response at x_i is obtained by simply substituting $\hat{\beta}$ for β in the equation we have;

$$\boldsymbol{\hat{\imath}(x_i) = f^1(x_i)\hat{\beta}} \tag{2.18}$$

The term $f^1(x_i)\hat{\beta}$ is called the predicted response.

At any point in the experimental domain denoted as Q, the predicted response is given as:

$$\boldsymbol{y}(\boldsymbol{x}) = \boldsymbol{f}^{\mathbf{1}}(\boldsymbol{x})\boldsymbol{\beta} \tag{2.19}$$

where x∈Q. the variance of $\hat{y}(x)$ will be of the form of:

$$\boldsymbol{var}[\widehat{\boldsymbol{y}}(\boldsymbol{x})] = {}^{\varphi\mathbf{2}}\boldsymbol{f}^{\mathbf{1}}(\boldsymbol{x})(\boldsymbol{X}^{\mathbf{1}}\boldsymbol{X})^{-\mathbf{1}}\boldsymbol{f}(\boldsymbol{x}) \tag{2.20}$$

2.4.3 Central Composite Design (CCD)

Central Composite design is one of the most popular second-order designs, and it was first used by Box and Wilson in 1951 [235]. A typical central composite design consists of three parts. They are the full factorial or fractional factorial design, the additional design, and the central point. In the full factorial or fractional factorial design, the factor's level is coded as -1,1. It is calculated using the expression $2^{k,}$ where k is the number of control variables. The additional design, also known as the axial design, is denoted by 2k as 2k points are usually selected in the axis of the independent variable and usually at a distance of α from the design centre. The last part is the design centre, denoted as c_p [231, 236].

The distance of the chosen axial design from the design centre denoted as α is obtained using the expression: $\alpha = (2k)^{\frac{1}{4}}$. Note that 2k represents the number of factorial runs.

For 2, 3 and 4 variables, respectively, $\alpha = 1.41, 1.68$ and 2.0.

These three parts are combined to give the total number of design points in a central composite design. Mathematically, we write:

$$\boldsymbol{N_d} = \mathbf{2}^{\boldsymbol{k}} + \mathbf{2}\boldsymbol{k} + \boldsymbol{c_p} \tag{2.21}$$

Where N_d indicates the total number of design points, k is the number of independent variables or control variables and c_p is the centre point. Figure 2.10 shows the central composite design optimization diagrams while Table 2.15 and 2.16 show the experimental matrix for two and three variables composite design, respectively.

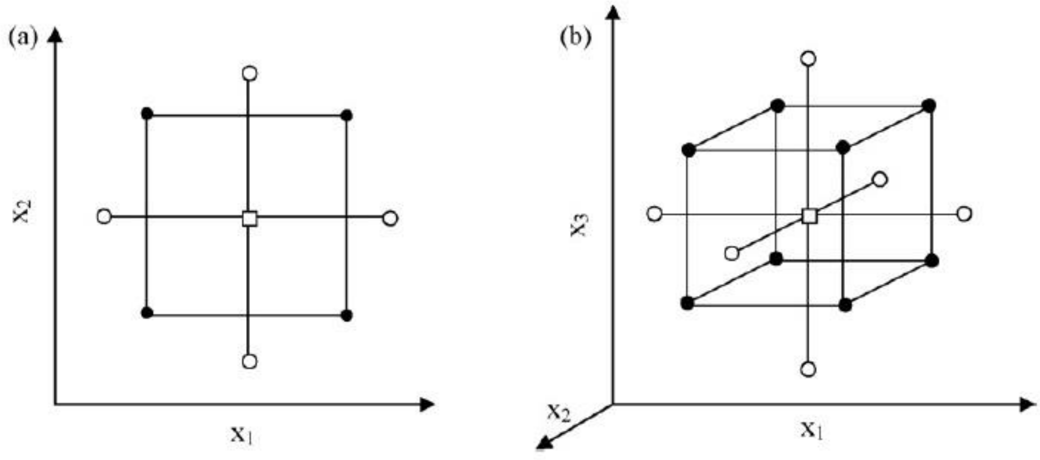

Figure 2.10: Central composite design for the optimization of; (a) Two variables (b) Three variables.

Table 2.15: Experimental matrix for two-variable composite design.

	X_1	X_2
Factorial design	-1	-1
	1	-1
	-1	1
Axial Points	-α	0
	α	0
	0	-α
	0	α
Centre Points	0	0

Table 2.16: Experimental matrix for three-variable composite design.

	X_1	X_2	X_3
Factorial Design	-1	-1	-1
	1	-1	-1
	-1	1	-1
	1	1	-1
	-1	-1	1
	1	-1	1
	-1	1	1
	1	1	1
Axial Points	-α	0	0
	α	0	0
	0	-α	0
	0	α	0
	0	0	-α
	0	0	α
Centre points	0	0	0

2.6 Chapter Summary

This chapter comprehensively highlighted the effect of resistance spot welding parameters on the properties of stainless steel weld joints and the progress made by experimenters in improving the weld quality by applying several weld treatment processes. Following the literature review, it was discovered that the majority of the experimenters paid attention to the resistance spot welding of stainless steel with a thickness of 1.5 mm or less. This is because complexity and difficulty in creating stainless steel RSW joints positively correlate with the metal thickness. The optimum parameters for stainless steel weld joint are largely dependent on the metal thickness, which influences other weld quality parameters. In addition, most experimenters that have attempted to optimize weld quality of stainless steel in general focused mainly on the TSLBC while a few others who adopted a multi-objective approach included other parameters like failure energy, electrode indentation and peak load, neglecting the hardness of the weld joint despite its significant influence on the overall joint quality.

Furthermore, if the spectrum is further narrowed to austenitic stainless steel, no literature was found. Meanwhile, the findings of researchers who have attempted to improve the quality of resistance spot welded joints revealed that preheating and tempering could reduce the hardness of the FZ. However, no studies have been reported to have combined both weld treatment processes on stainless steel spot welded joints. In this research, the optimum parameters that simultaneously maximize the TSLBC and minimize the FZ hardness were first determined. Subsequently, a combination of preheating and tempering was further applied to the joints to improve the weld quality through FZ hardness reduction.

CHAPTER 3

METHODOLOGY

3.1 Methodology

Figure 3.1 presents the overall flow chart of the activities, including the experimental procedures that were put together to achieve the research objectives. Figures 3.2 and 3.3 show a detailed flow of activities for the first and second experiment stage, respectively.

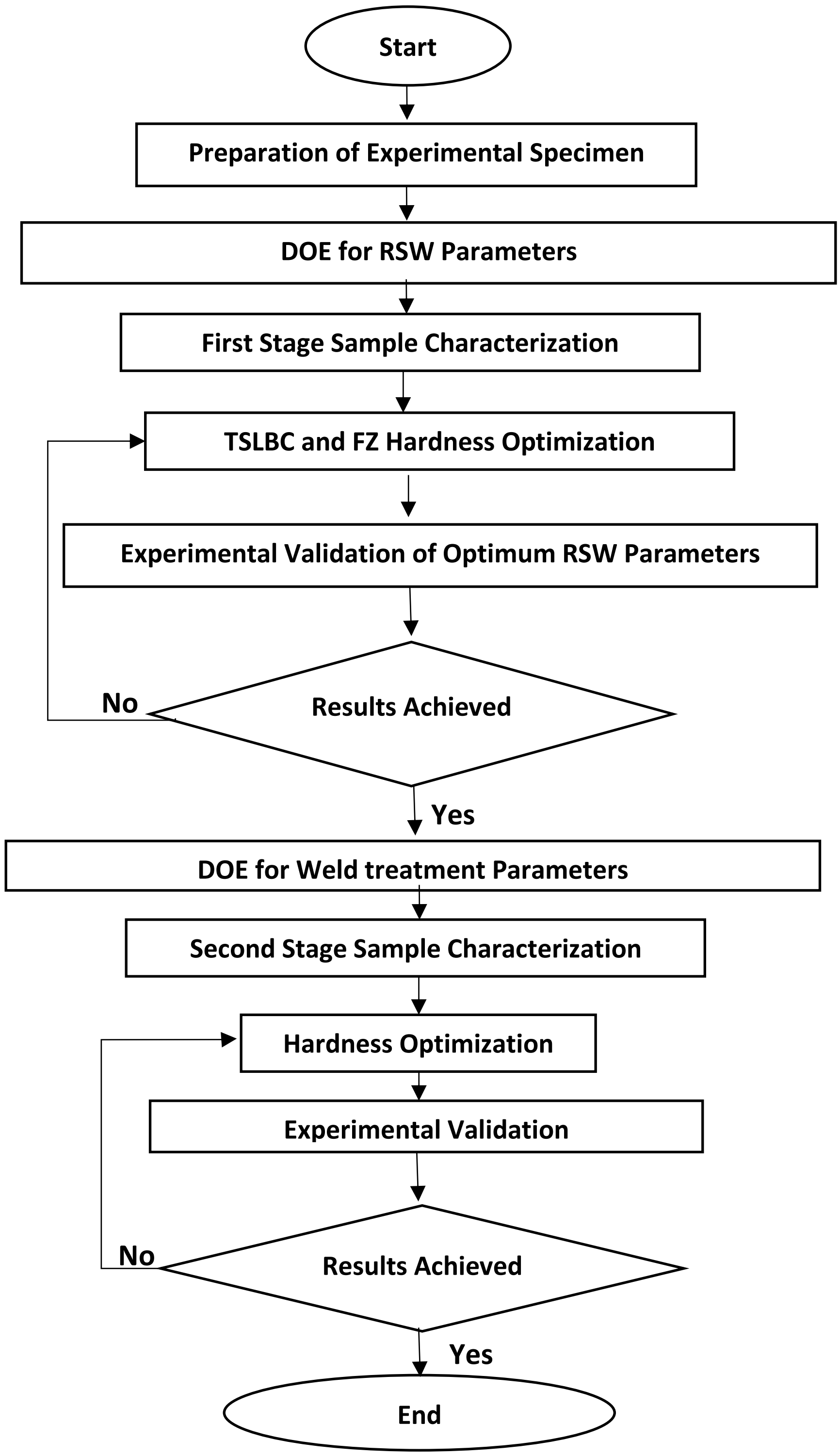

Figure 3.1: Flow chart of the entire experimental procedure.

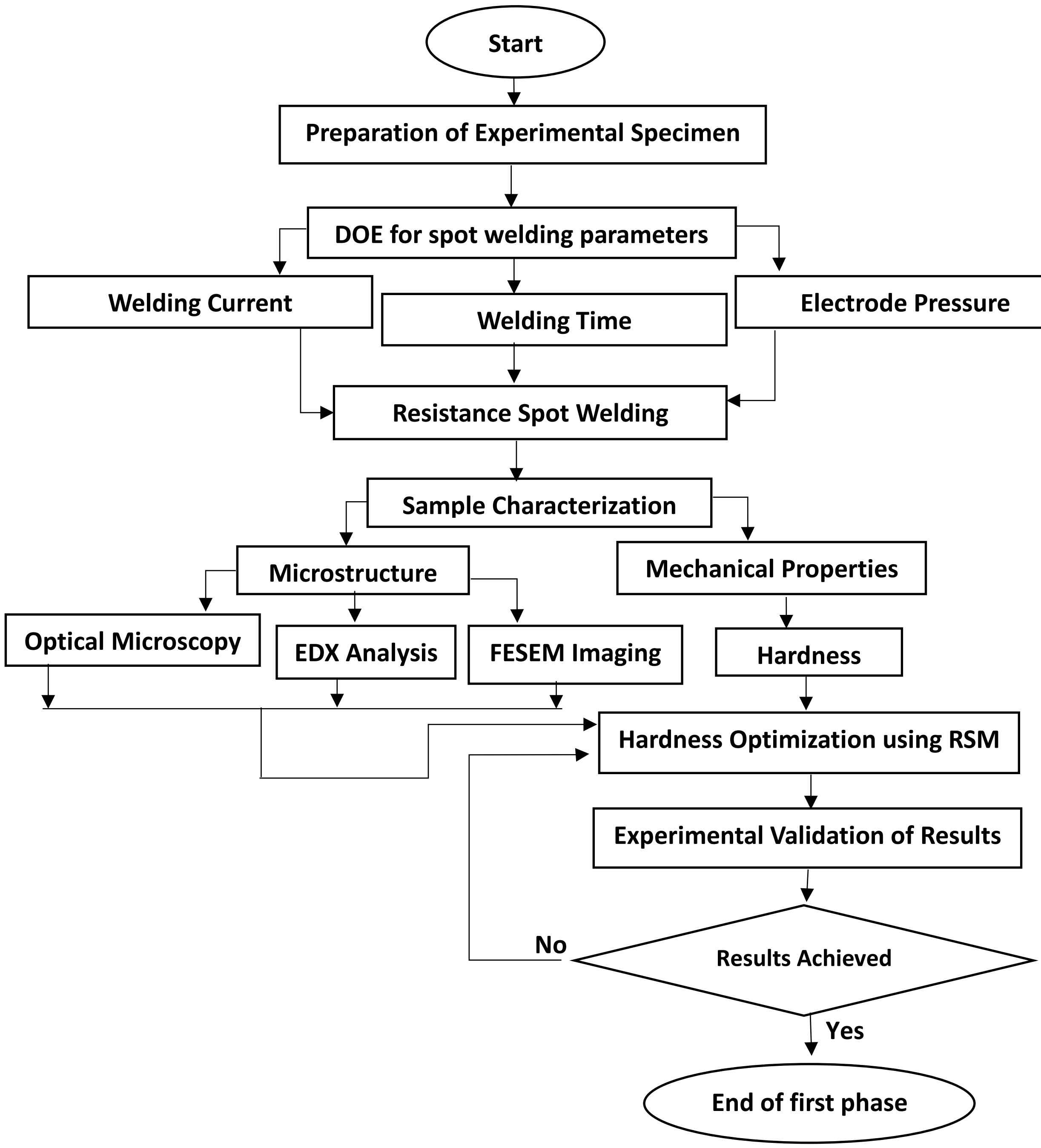

Figure 3.2: Process flow of the first stage showing experimental procedure.

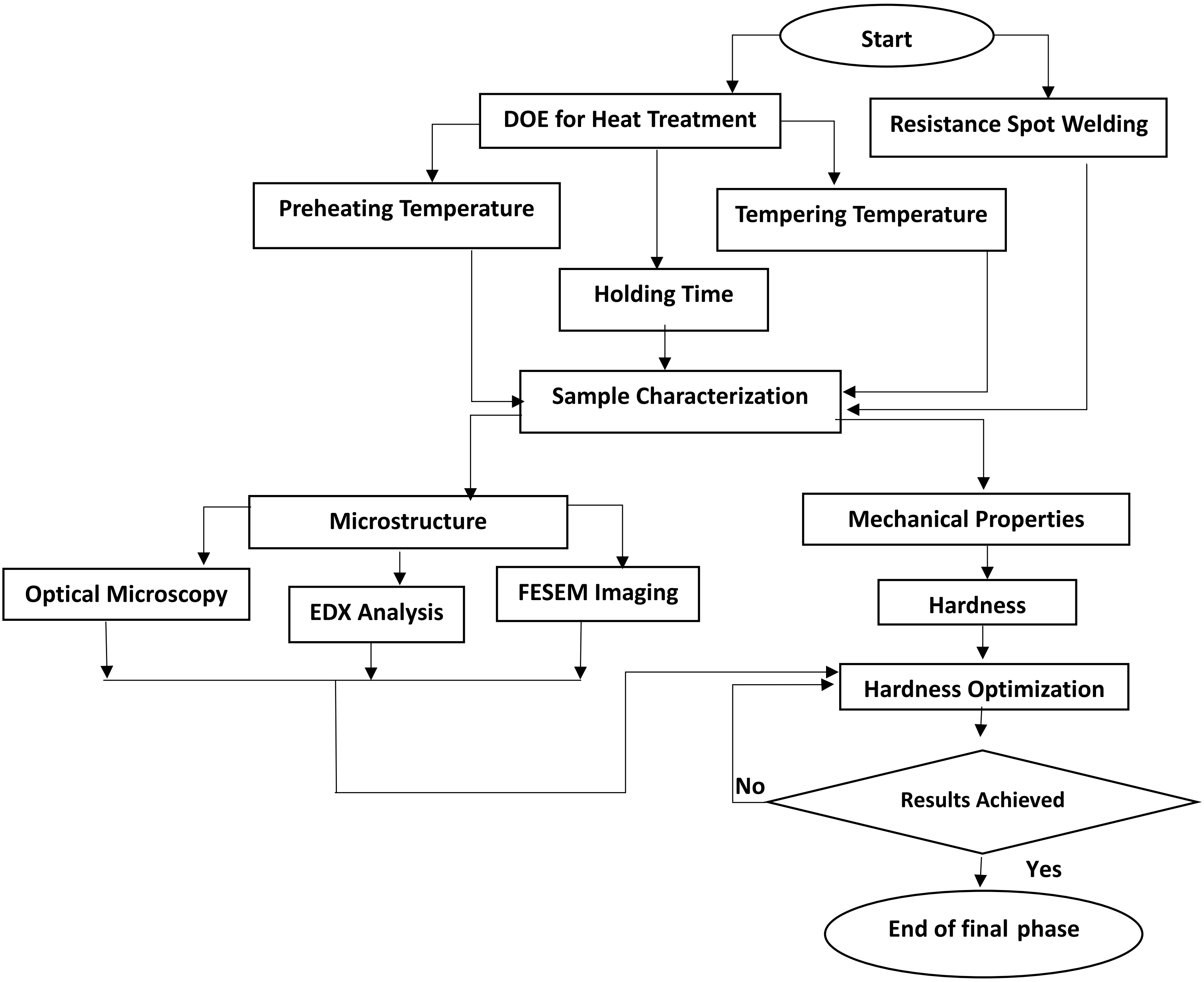

Figure 3.3: Process flow of the second stage showing experimental procedure

3.2 Material

The material used in this research work is the low carbon grade of 316 austenitic stainless steel (SUS 316L) with a thickness of 2 mm. The chemical composition of the samples was determined using Energy Dispersive X-ray (EDX) Spectroscopy, while microstructural imaging was achieved using Optical Microscopy (OM) and Field Emission Scanning Electron Microscopy (FESEM).

3.3 Design of Experiment (DOE) Using Response Surface Methodology (RSM)

The Design of Experiment, popularly known as DOE, is a problem-solving tool combining statistical and mathematical techniques with the common types being RSM, Artificial Neural Network (ANN) and factorial design. Incorporating axial and central points in RSM makes it sensitive to changes in the response surface when there are changes in the input variables. The DOE was carried out using Design Expert Software (Version 11.1.2.0).

The application of the RSM as carried out using the software is explained under the following sub-headings.

1. **Design Selection:** The RSM optimization process commences with selecting the design – type from a list of several designs, including factorial, response surface, supersaturated, split-plot, mixture, and custom designs. The Central Composite Design (CCD) of the Response Surface Methodology (RSM) was selected from other design – types such as Box-Behnken and Custom Design.
2. **Inputting Response Variables and Domain of Control Variables:** The design selection process is followed by specifying the number of numeric and categoric factors, inputting the domain of the selected factors, selecting the type and number of blocks, selecting CCD options and the value of α. The total number of experimental runs depends on the selected CCD options, the value of α and the block type. The selected factors (control variables) and response variables alongside the different levels for the experiment's first and second stages are summarised in Tables 3.1 and 3.2. The response variable for the first stage of the experiment is the average FZ hardness and the weld nugget diameter. But for the second stage, the average FZ hardness was the only response variable. The full-block design was adopted with a singular block. The factorial and axial points were un-replicated, while the number of centre points was 6, which is the standard default setting. Alpha was set to be rotatable (i.e., $k < 6$), having a value of 1.68179.

Table 3.1: Experimental design domain and levels for the spot welding parameters (First Stage Control Variables)

Welding Current (KA)	**Welding Time (Cycles)**	**Electrode Pressure (Bar)**				
6-11	10-30	4-6				
Variables	**Symbol**	**Level**				
		1	2	3	4	5
		-α	-1	0	1	α
Variable 1: Welding Current (KA)	x_1	4.3	6	8.5	11	12.7
Variable 2: Welding Time (Cycles)	x_2	3.18	10	20	30	36.82
Variable 3: Electrode Pressure (Bar)	x_3	3.32	4	5	6	6.68

Table 3.2**:** Experimental design domain and levels for the post-weld treatment parameters (Second Stage Control Variables)

Preheating Temperature (^oC)	**Tempering Temperature (^oC)**	**Holding Time (Hours)**				
100-200	400-600	2-4				
Variables	**Symbol**	**Level**				
		1	2	3	4	5
		-α	-1	0	1	α
Variable 1: Preheating Temperature (^oC)	x_1	65.91	100	150	200	234.09
Variable 2: Tempering Temperature (^oC)	x_2	331.82	400	500	600	668.18
Variable 3: Holding Time (Hours)	x_3	1.32	2	3	4	4.68

3. **Experimental Design:** Selecting the abovementioned options and proceeding to the next stage yields the design matrix of the experiment. Based on the selected options, a total of 20 experimental runs was obtained for each phase of the experiment, as represented in Tables 3.3 and 3.4.

Table 3.1: Experimental central composite design matrix for the spot welding parameters.

No.	Process parameters					
	Actual Variable Values			Coded Variable values		
	A: Welding Current (KA)	B: Welding Time (Cycles)	C: Electrode Pressure (Bar)	x_1	x_2	x_3
1	8.5	36.8	5	0	1.682	0
2	6	10	6	-1	-1	1
3	8.5	20	5	0	0	0
4	8.5	3.2	5	0	-1.682	0
5	8.5	20	5	0	0	0
6	4.3	20	5	-1.682	0	0
7	8.5	20	5	0	0	0
8	11	30	6	1	1	1
9	11	30	4	1	1	-1
10	8.5	20	5	0	0	0
11	11	10	6	1	-1	1
12	8.5	20	5	0	0	0
13	12.7	20	5	1.682	0	0
14	11	10	4	1	-1	-1
15	8.5	20	5	0	0	0
16	6	30	6	-1	1	1
17	8.5	20	6.7	0	0	1.682
18	6	10	4	-1	-1	-1
19	8.5	20	3.3	0	0	1.682
20	6	30	4	-1	1	-1

Table 2: Experimental central composite design matrix for the post-weld treatment parameters

No.	Process parameters					
	Actual Variable Values			Coded Variable values		
	A: Preheating Temperature (^oC)	B: Tempering Temperature (^oC)	C: Holding Time (Hours)	x_1	x_2	x_3
1	150	331.8	3	0	-1.682	0
2	65.91	500	3	-1.682	0	0
3	150	500	4.7	0	0	1.682
4	150	500	3	0	0	0
5	200	400	2	1	-1	-1
6	100	400	2	-1	-1	-1
7	150	500	3	0	0	0
8	150	500	1.3	0	0	-1.682
9	100	600	2	-1	1	-1
10	234	500	3	1.682	0	0
11	150	500	3	0	0	0
12	100	600	2	-1	1	-1
13	100	400	4	-1	-1	1
14	200	400	4	1	-1	1
15	150	668.2	3	0	1.682	0
16	150	500	3	0	0	0
17	150	500	3	0	0	0
18	150	500	3	0	0	0
19	200	600	4	1	1	1
20	200	600	2	1	1	-1

4. **Experimental Execution and Analysis:** Generation of the design matrix is followed by execution of the experiment as contained in the matrix. This is then followed by the analysis of the results using statistical techniques such as ANOVA, which is combined with intuition for proper decision making.

5. **Optimization and Validation:** The process is concluded with the optimization of variables by selecting desired conditions. The optimization objective of the first stage of the experiment is to minimize the average FZ hardness and maximize the weld nugget diameter. But for the second stage, the sole objective is to minimize the average FZ hardness. This is then followed by experimental validation of the results where necessary. The explanations of the RSM optimization procedure have been documented in the preceding chapter. However, a summary of the procedure is depicted by the flow chart in Figure 3.4.

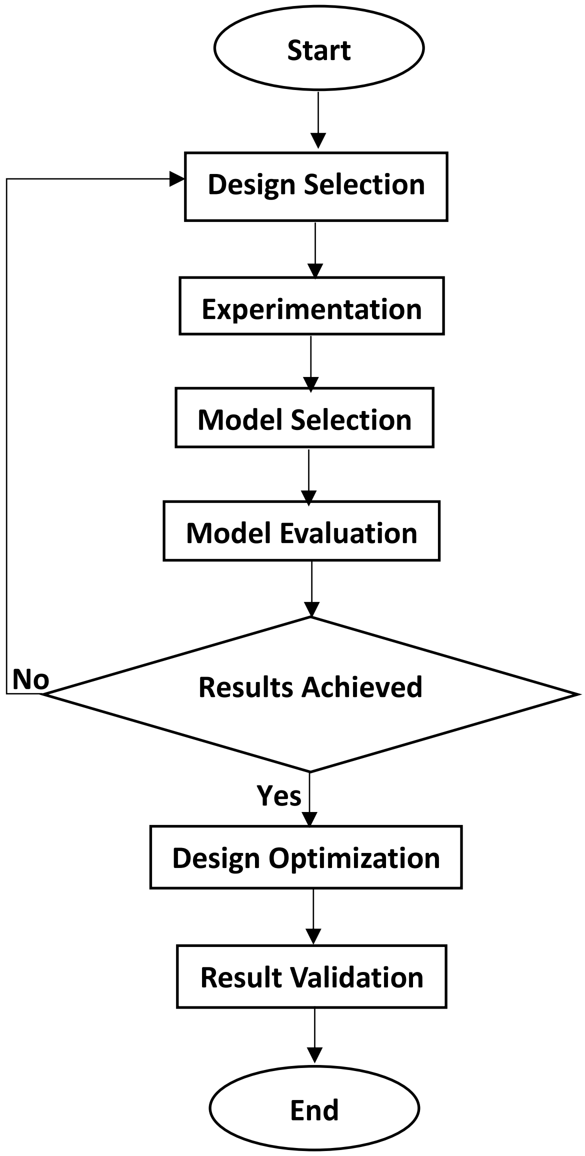

Figure 3.4: Flow chart showing the optimization process using response surface methodology.

3.4 Experimental Procedure

The design of experiment was succeeded by the actual experimental process, which commences with the preparation of standard specimen and encompasses other activities such as resistance spot welding, preheating, and tempering. The following sub-headings provide more details about each of the processes.

3.4.1 Preparation of Standard Specimen

The preparation of samples began with the sectioning of a 2 mm thick SUS 316L austenitic stainless steel to different dimensions using a CNC Metal Yag Laser Cutting Machine. This machine has a computer numerical control (CNC) coupled with the high-performance laser technology, which focuses the laser beam on the material, thereby cutting through it by melting or vaporizing parts of the material to produce a good surface finish. The machine can be seen in Figure 3.5 (Appendix). The samples for the optimization of resistance spot welding parameters were cut into 110 × 25 mm, while those for post-weld treatment were cut into 55 mm × 25 mm.

3.4.2 Resistance Spot Welding

Resistance spot welding of the samples was achieved using a single-phase (AC) 91 KVA Daiden spot welder (model: SL-AJ 35 - 600) manufactured by Daihen Industrial Machinery Corporation. It is a pedestal-type, pneumatically actuated, and equipped with a programmable logic controller to set the current and welding time cycle. The water-cooled electrodes are 45^{o} truncated cone made of copper alloy with a face diameter of 11 mm. Electrode cooling was achieved by using water as the cooling medium. The spot welding machine can be seen in Figure 3.6 (Appendix). The welding process was carried out under room temperature and pressure conditions. The spot welds for optimising spot welding parameters were uniformly distributed over the 110 mm × 25 mm × 2 mm forming a lap joint and maintaining sufficient distance to eliminate current shunting phenomenon, as shown in Figure 3.7 [236]. Figure 3.8 shows the lap joint of the samples for post-weld treatment.

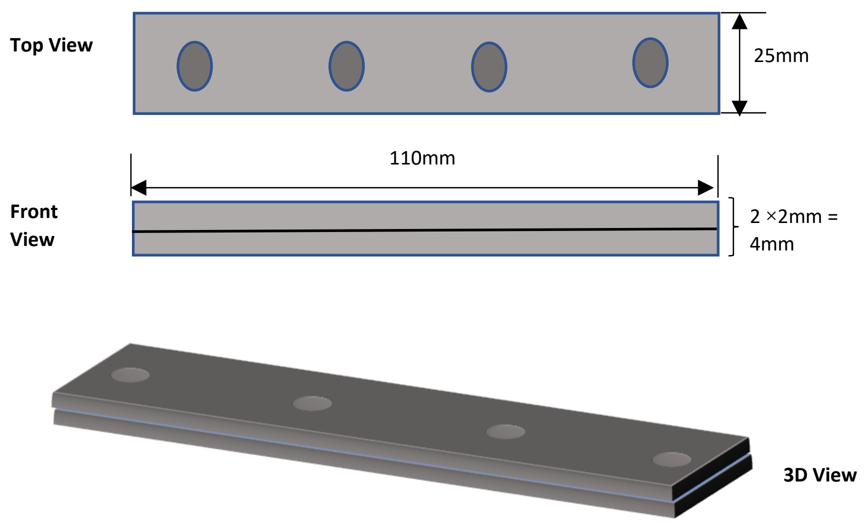

Figure 3.7: Specimen dimension for optimization of RSW parameters**.**

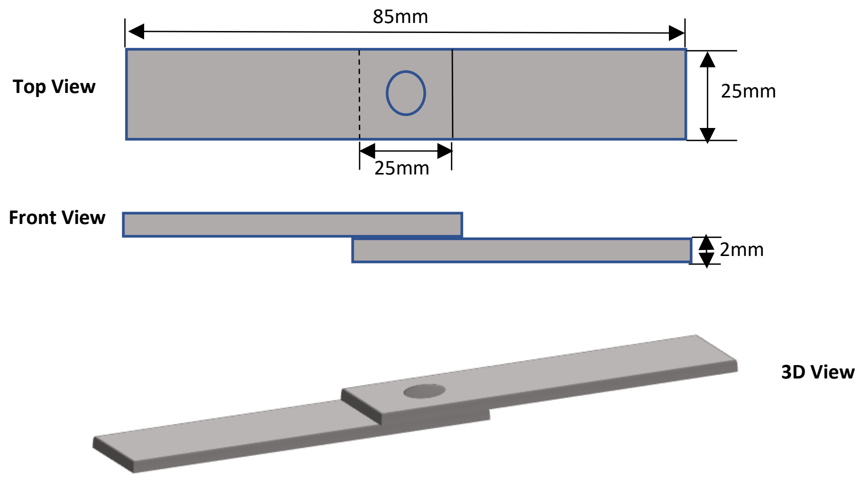

Figure 3.8: Specimen dimension for post weld treatment parameters.

3.4.3 Preheating

Preheating samples was achieved using a 240V AC bench oven (model: BE150M) with a heating capacity of 50 – 400 ^{o}C. The temperature in the oven was allowed to rise to the set temperature before the samples were placed inside. The samples were kept in the oven for about 3 minutes since heat transfer through the material is at the rate of 30 minutes per inch. This ensured that the entire specimen was heated up to the desired temperature. In addition, temperature tolerance of 10 ^{o}C was considered to account for losses to the atmosphere before the commencement of the welding process [237]. The bench oven can be seen in Figure 3.9 (Appendix).

3.4.4 Tempering

The heat treatment process was carried out using a carbolite heat treatment furnace, as shown in Figure 3.10 (Appendix). The samples for heat treatment were placed in the furnace; afterwards, it was switched on and set to the desired temperature following the design matrix obtained from the DOE. The samples were subsequently cooled in the air to room temperature.

3.5 Sample Characterization

Spot welded samples were characterized after the optimization of spot welding parameters and after post-weld treatment. Microstructural, mechanical, and geometrical characterization of the properties of the weld joints were conducted. Microstructural characterization was achieved using optical microscopy, energy dispersive x-ray and field emission scanning electron microscopy. Geometrical property characterization predominantly involves measuring the nugget diameter from the metallographic cross-section, while the mechanical property (microhardness) was determined using Vickers microhardness tester. The characterization process was preceded by metallographic sample preparation. The succeeding sections carefully elucidate each of these processes.

3.5.1 Metallographic Sample Preparation

This involves the preparation of samples followed by microstructural examination and analysis to ascertain their microstructural composition. The preparation of the samples for microstructural characterization was carried out following the ASTM/E3 standard [238]. The processes involved in metallographic sample preparation are discussed in the following sub-headings.

1. Sectioning: It involves cutting out the section of the material whose property is to be investigated. In this case, the area of interest is the spot weld region. A transverse cross-sectional cut through the spot weld was made through the spot weld using Electrical Discharge Machine (EDM) wirecut. The dimension chosen for the cross-sectional cut was based on the acceptable size of the mounting machine. Figure 3.11 (Appendix) shows the EDM machine.

2. Mounting: After sectioning, the next step is to keep the samples in a stationary position to make other metallographic processes easy. This process is termed mounting. Mounting of the sectioned samples was achieved using an Automatic Mounting Press (model: Simplet 1000) manufactured by Buehler ((Figure 3.12(a) (Appendix)). The mounting process commences with the careful setting of the specimen on the press, followed by hot mounting by embedding the sample in phenolic resin ((Figure 3.12(b) (Appendix)). The whole mounting process takes place in three stages, namely, heating, compression, and cooling. After introducing the phenolic resin to the sample to be mounted, the sample was compressed at a pressure of 4200 psi; this was followed by heating for one minute and 30 seconds and cooled for three minutes. Figures 3.12(c) (Appendix) and 3.12(d) (Appendix) show the sample before and after mounting, respectively.

3. Grinding: The idea behind grinding the mounted samples is to eliminate the rough surfaces generated from the cross-sectional cutting. The resultant surface obtained after grinding is relatively flat and smoother than the initial surface prior grinding. The grinding was carried out using Buehler Metaserv 250 twin-grinder-polisher, as shown in Figure 3.13 (Appendix). The grinding medium employed was silicon carbide paper starting with the coarse grit size of 120 and progressively increasing to 180, 240, 320, 400, 600, 800, 1200 and 4000 grit sizes until a mirror-like surface was obtained. When switching from one grit size to another, the specimen is rotated perpendicular to the direction of the previous grinding. Grinding was carried out at a constant speed of 350 rpm while running water was also supplied to prevent excessive heating, flushing of metal particles to prevent scratching, and keeping the samples free of any particles after concluding the grinding process.

4. Polishing: It involves producing a reflective mirror-like surface by applying pressure on the material to be polished against a rotating wheel impregnated with a polishing abrasive. The same twin-grinder-polisher used for grinding was also employed for polishing, except that the silicon carbide paper was replaced with a short-nap cloth. The polishing fluid used was MetaDi supreme polycrystalline diamond suspension manufactured by Buehler. Polishing was carried out mechanically by applying intermediate pressures, with a rotating wheel speed of 350 rpm starting with a polishing fluid of 6 μm and progressively increasing to 3 μm and finally 1 μm. As done before, the direction of polishing for a given grit size was orthogonal to the previous grit size. The polishing process was concluded by washing the polished samples with distilled water and drying off the water with a drybox. Figure 3.14(a) (Appendix) shows the polishing fluid, and 3.14(b) (Appendix) shows the drybox.

5. Etching: The metallographic process is concluded by etching the polished surface using an appropriate etchant to reveal microstructural features such as grain boundaries by differentiating grains in terms of their size, shape, and orientation. The polished samples were etched by swabbing with Adler’s reagent (9 g of copper ammonium chloride, 150 ml of hydrochloric acid, 45 g of ferric chloride and 75 ml od distilled water) for about 3 – 5 seconds and immediately rinsed with water to wash off particles which are the product of the reaction between the etchant and polished surface. After rinsing off the particles, the water was dried off using the drybox.

3.5.2 Optical Microscopy

This involves viewing the etched microstructure under a microscope with a high magnification using reflected light rays. Optical microscopy was achieved using a metallurgical microscope manufactured by Leica (model: DM 2700 M). The microstructural examination began by placing the sample under the lens. This was then followed by adjusting the light intensity and focus until a clear image was obtained. It is conventional to begin with the lens with the lowest magnification and gradually increase until the desired image is obtained. Figure 3.15 (Appendix) shows the metallurgical microscope.

3.5.3 Field Emission Scanning Electron Microscopy (FESEM)

FESEM, just like optical microscopy, allows the sample's microstructure to be examined at very high magnification. The difference between optical microscopy and FESEM lies in the replacement of the light with a beam of electrons, and the glass lens is replaced with an electromagnetic or electrostatic field [239]. A subtle difference also exists between the SEM and FESEM which lies in the electron generation system and high energy range that produces images with much higher resolution [240]. The FESEM microscope also has an energy dispersive x-ray (EDX) analyzer for elemental mapping. Figure 3.16 shows the FESEM microscope. The FESEM used for this research work was manufactured by Zeiss (model: SUPRA 55VP). The microscope operates by focusing an electron beam on the material, revealing microstructural features by passing through the sample unaffected or interacting with the material. A typical FESEM apparatus is shown in Figure 3.16 (Appendix).

3.5.4 Microhardness Measurement

The microhardness of a material is the hardness obtained on a microscale and provides other relevant information about the wear resistance of the material and the ductility. The microhardness of the weld joint was measured following the guidelines outlined in ASTM-E384-05a [241]. The microhardness was conducted using a Vickers microhardness testing machine (LM - 700 AT) manufactured by Leco corporation, Michigan, USA. The microhardness tester uses a square-based diamond pyramid indenter having an angle of 136 degrees. The test was carried out using a load of 200 gf, which was applied for a dwell time of 15 seconds, making a minimum of 20 indentations on each sample. Figure 3.17 shows the microhardness Vickers tester.

CHAPTER 4

RESULTS AND DISCUSSION

4.1 Experimental Results on Optimization of Resistance Spot Welding Parameters.

The results of the experiment on the optimization of resistance spot welding parameters (welding current, electrode pressure and welding time) were conducted following the design matrix presented in the previous chapter involving the nugget diameter and average FZ hardness as the response variables are presented in Table 4.1.

Table 4.1: Experimental results for the first stage of the experiment showing the average FZ hardness and the weld nugget diameter for all experimental runs.

Standard Order (Std)	Factor 1 A: Electric Current (KA)	Factor 2 B: Welding Time (Cycle)	Factor 3 C: Electrode Pressure (Bar)	Response 1: Nugget Diameter (mm)	Response 2: Hardness (HV)
1	8.5	36.8	5.0	7.0	202.65
2	6.0	10.0	6.0	5.7	207.56
3	8.5	20.0	5.0	6.5	198.42
4	8.5	3.2	5.0	0	194.23
5	8.5	20.0	5.0	7.0	190.73
6	4.3	20.0	5.0	6.0	198.84
7	8.5	20.0	5.0	6.7	200.4
8	11.0	30.0	6.0	9.0	199.56
9	11.0	30.0	4.0	8.5	204.29
10	8.5	20.0	5.0	6.8	178.23
11	11.0	10.0	6.0	5.0	196.6
12	8.5	20.0	5.0	7.7	203.89
13	12.7	20.0	5.0	9.8	209.19
14	11.0	10.0	4.0	7.0	202.5
15	8.5	20.0	5.0	7.9	195.66
16	6.0	30.0	6.0	5.8	165.84
17	8.5	20.0	6.7	7.2	209.87
18	6.0	10.0	4.0	5.5	189.6
19	8.5	20.0	3.3	7.8	180.02
20	6.0	30.0	4.0	6.4	205.88

4.2 Statistical Analysis of the Effect of Resistance Spot Welding Parameters on the Nugget Diameter

The results presented in Table 4.1 show different nugget diameters for the experimental runs. The maximum and minimum values were 9.8 mm (sample 13) and 5.5 mm (sample 18), respectively, while no fusion was observed in sample 4; hence, the value of the nugget diameter. The results of the ANOVA of the different mathematical models for the nugget diameter in terms of the spot welding parameters are summarized in Table 4.2.

Table 4.2: ANOVA of the generated models.

Source	Sequential p-value	Lack of Fit p-value	R^2	Adj. R^2	Pred. R^2	Std. Dev.	PRESS	
Linear	0.0003	0.0053	0.6862	0.6274	0.4613	1.74	83.27	
2FI	0.3921	0.0047	0.7488	0.6329	0.3806	1.73	95.74	
Quadratic	**0.0129**	**0.0225**	**0.9107**	**0.8304**	**0.3794**	**1.17**	**95.92**	**Suggested**
Cubic	0.0421	0.0765	0.9791	0.9339	-1.3058	0.7333	356.41	Aliased

The primary criteria used for evaluating the models are the p-value and the lack of fit test. Generally, a significant value of $p < 0.05$ (5 %) is usually desired with an insignificant lack of fit having p values greater than 0.05. In addition, R^2, standard deviation, and Predicted Residual Sum of Squares (PRESS) are sometimes used. The R^2 value denotes the predictive power of the model, and values close to 1 are desired. The PRESS, on the other hand, provides how well the model fits the selected design points. To sum up, a model with a significant p value, an insignificant lack of fit, R^2 close to unity, minimum standard deviation, and PRESS is desired.

A closer look at the models presented in Table 4.2, starting with the first model, which is linear, reveals that the model has a significant sequential p-value (0.0003 < 0.05), but the lack of fit is also significant (0.0053 < 0.05). Moving on to the next model, 2FI (two-factor interaction) model, the sequential p-value is insignificant (0.3921 > 0.05) while the lack of fit significant is (0.0047 < 0.05). The quadratic model has a significant sequential p-value (0.0129 < 0.05) and also a significant lack of fit (0.0225 < 0.05). Lastly, the cubic model has a significant sequential p-value and an insignificant lack of fit.

Despite the cubic model meeting the requirements of significant sequential p-value and insignificant lack of fit, the model was aliased hence, not appropriate. An aliased model is usually not recommended as it might contain redundant terms over the unique points. Model aliasing also results from incomplete experimental runs or missing data; thus, it might be misleading [58]. Eliminating the cubic model leaves us with linear, 2FI and quadratic models.

The factorial model is further eliminated since it has an insignificant p-value and a significant lack of fit antithetical to the initial desired requirement. The linear and quadratic models have the same conditions regarding the sequential p-value and the lack of fit. However, considering other criteria like R^2 and adjusted R^2 values, it becomes clear while the quadratic model was suggested as it has better predictive accuracy. The standard deviation and PRESS of both models are also within acceptable limits.

As shown from Table 4.3, the quadratic model is generally perceived as significant, having a p value of 0.0004, less than 5 %. This implies that there is a 0.04 % chance that the F-value of the model is attributed to noise which also connotes a very high confidence level.

Table 4.3: ANOVA results of the quadratic model showing all the coefficients

Source	Sum of Squares	df	Mean Square	F-value	p-value	
Model	140.77	9	15.64	11.33	0.0004	significant
A-Electric current	58.57	1	58.57	42.44	< 0.0001	
B-Welding time	42.08	1	42.08	30.49	0.0003	
C-Electrode pressure	5.43	1	5.43	3.93	0.0755	
AB	0.1800	1	0.1800	0.1304	0.7255	
AC	2.64	1	2.64	1.92	0.1964	
BC	6.84	1	6.84	4.96	0.0501	
A^2	5.69	1	5.69	4.12	0.0698	
B^2	18.18	1	18.18	13.17	0.0046	
C^2	1.22	1	1.22	0.8847	0.3691	
Residual	13.80	10	1.38			
Lack of Fit	12.18	5	2.44	7.52	0.0225	significant
Pure Error	1.62	5	0.3240			
Cor Total	154.57	19				
Mean						6.08
Adequate Precision						12.8233
% Coefficient of Variation						19.32

Further examination of the primary factors, namely, welding current, welding time and electrode pressure, it is obvious that the most significant parameter affecting the weld nugget diameter is the electric current, with the electrode pressure being the least significant parameter. This result corresponds to the findings of Zhao et al. [58]. Figure 4.1 depicts the hierarchy of these factors based on their level of significance.

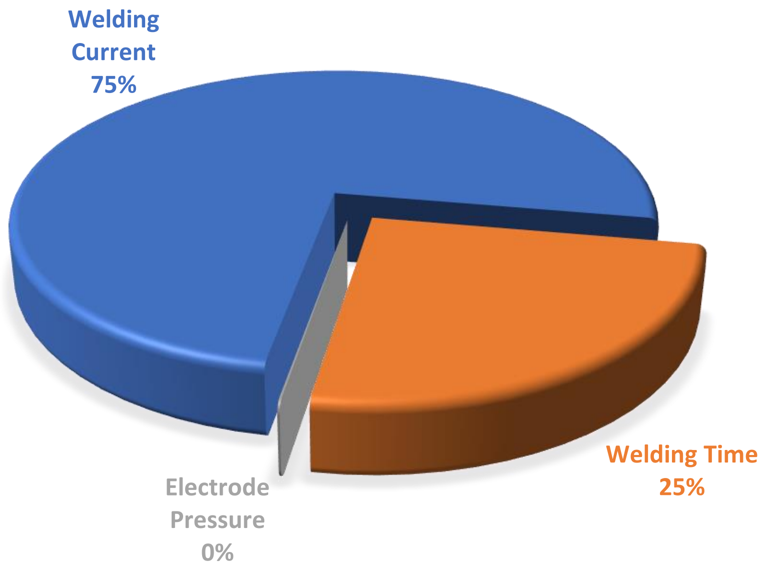

Figure 4.1: Percentage contribution of resistance spot welding parameters to the nugget diameter based on their significance value.

Further evaluation of the results reveals that all the interaction terms, i.e., AB, BC and AC, have significance with a confidence level less than 95 % except for BC, which is approximately 95 %. Generally, terms having probability values greater than 0.1 are considered insignificant. In addition, the quadratic factor B^2 was found to be significant, while A^2 and C^2 were insignificant. Despite their insignificance, they were not eliminated from the model because their p values were not greater than 0.1, and they also function as elements of support hierarchy.

As mentioned earlier, the R^2, adjusted R^2, predicted R^2, PRESS, and adequate precision provide relevant information regarding the model's predictive power and fitting efficiency. The results in Table 4.2 reveal that the model has an R^2 value of 0.9107 and 0.8304 as the adjusted R^2. This implies that the model can account accurately for 91.07 % of the experimental values of the nugget diameter, while about 9 % of the values are not accounted for. The model's adequate precision provides the accuracy of a model by measuring the signal to noise ratio. As a rule of thumb, its value should be greater than 4. A more detailed ANOVA of the quadratic model selected showing all the terms in the model is presented in Table 4.3. From Table 4.3, it can be seen that the model has an adequate precision of 12.8233, which implies that the model can successfully navigate the design space.

The final equation obtained for the prediction of nugget diameter in terms of welding current, welding time and electrode pressure is given as:

Nugget Diameter = +13.20520 + 0.213289 × Welding time - 7.34616 × Electrode pressure - 0.006000 × Electric current × Welding time + 0.230000 × Electric current × Electrode pressure + 0.092500 × Welding time × Electrode pressure - 0.100506 × Electric current^2 - 0.011231× Welding time^2 + 0.291077 × Electrode pressure^2.

In coded form, the equation can be written as:

Nugget Diameter = +7.08 + 2.07A + 1.76B - 0.6304C - 0.15AB + 0.575AC + 0.925BC - 0.6282A^2 - 1.12B^2 + 0.2911C^2.

The above equation will function more accurately within the initial specified domain whose mathematical form is given below.

$6 \leq$ welding current (KA) ≤ 11,

$10 \leq$ welding time (cycles) ≤ 30

$4 \leq$ electrode pressure (bar) ≤ 6.

Figure 4.2(a) shows the plot of the predicted nugget diameter and the actual nugget diameter. As can be seen from the graph, the plots are uniformly distributed along the straight line, and a more uniform scatter of error plots was observed on the normal plot of residuals (Figure 4.2(b)), indicating the correctness and flexibility of the derived mathematical model. Figure 4.2(c) shows the predicted and actual nugget diameter error for each experimental run.

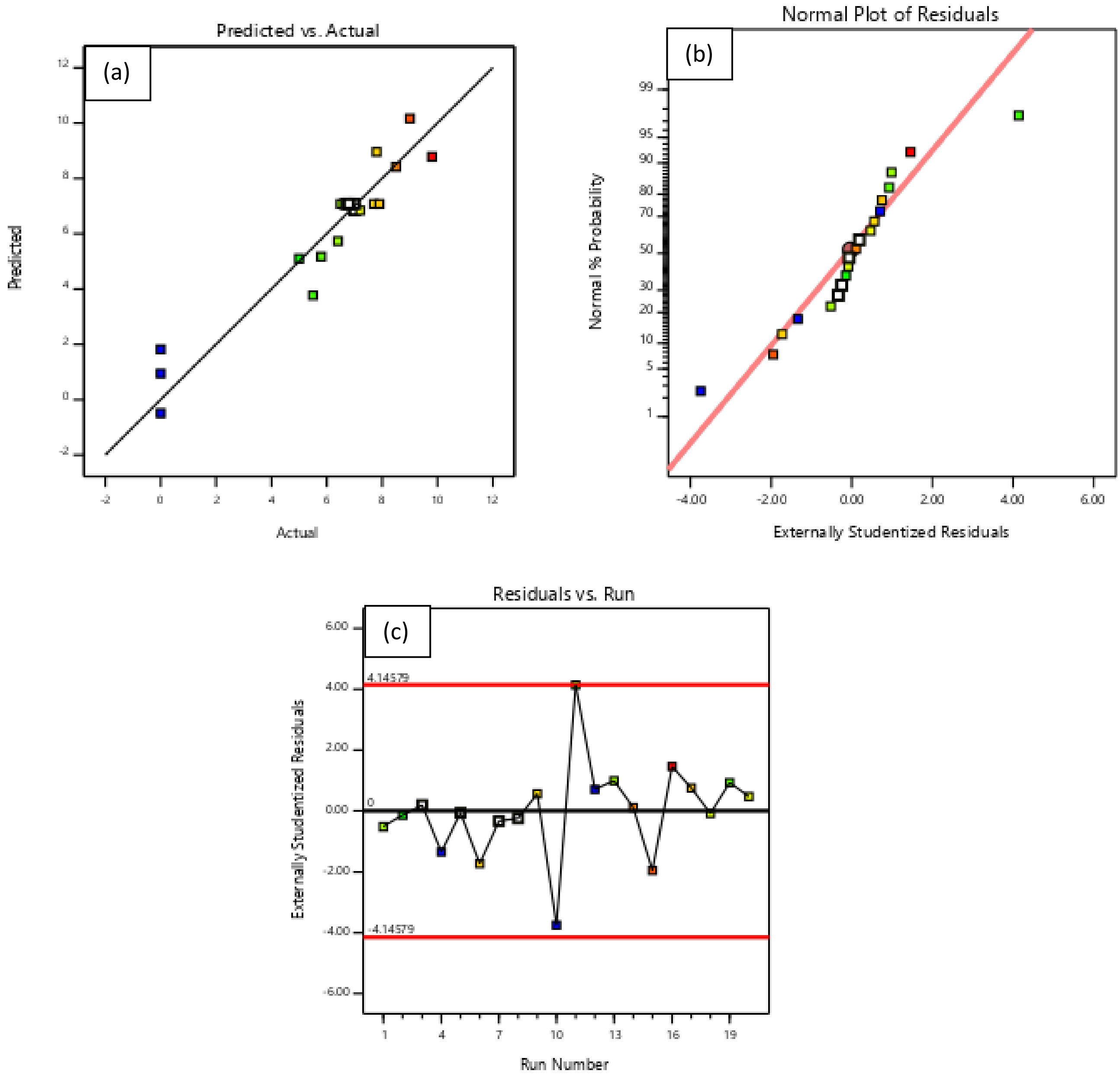

Figure 4.2: (a) Plot of predicted nugget diameter against the actual nugget diameter; (b) Normal plot of residuals for the regression model; (c) Plot of residuals against the experimental runs for all values of the nugget diameter

4.2.1 Process Parameters Analysis Using Model Graphs.

A perturbation plot depicts the combined effect of all the factors on the response variable, which implies the nugget diameter. In other words, it provides a measure of the sensitivity of the nugget diameter to changes in the resistance spot welding parameters [242]. The perturbation plot for the derived quadratic model obtained at welding current of 8.5 KA, welding time of 20 cycles and electrode pressure of 5 bar is presented in Figure 4.3.

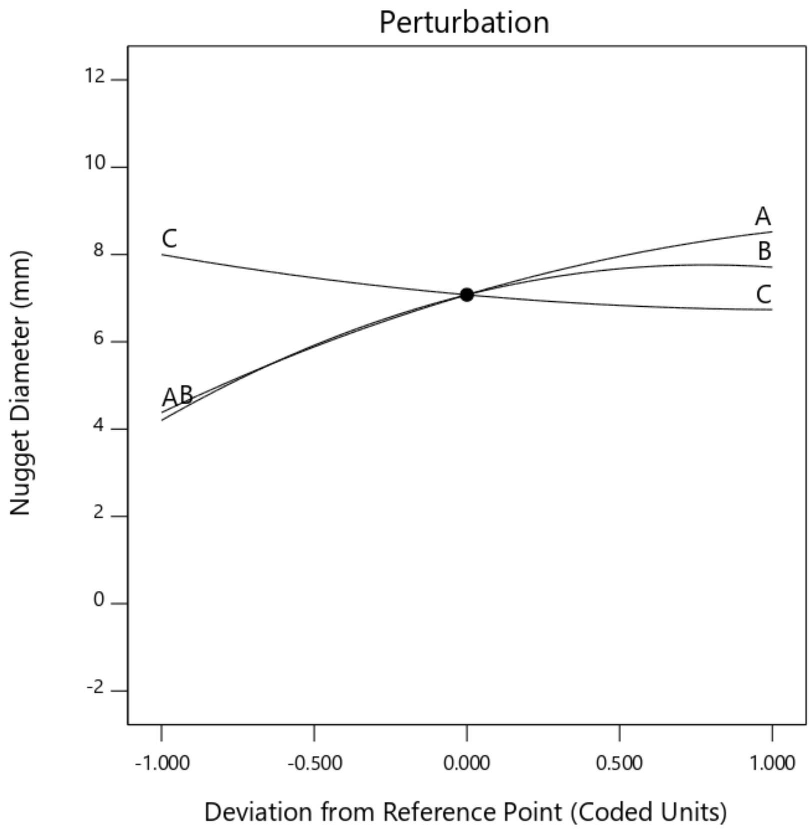

Figure 4.3: A perturbation plot showing the combined effect of resistance spot welding parameters on the nugget diameter.

As can be seen from the plot, the welding current and the welding time are positively correlated with the nugget diameter. The strength of this correlation was found to be 0.616 for welding current and 0.522 for the welding time, as represented by the scatter plot in Figures 4.4(a) and 4.4(b), respectively. On the other hand, the electrode pressure was found to be negatively correlated with the nugget diameter. The strength of the correlation was - 0.182 with the scatter plot represented in Figure 4.4(c).

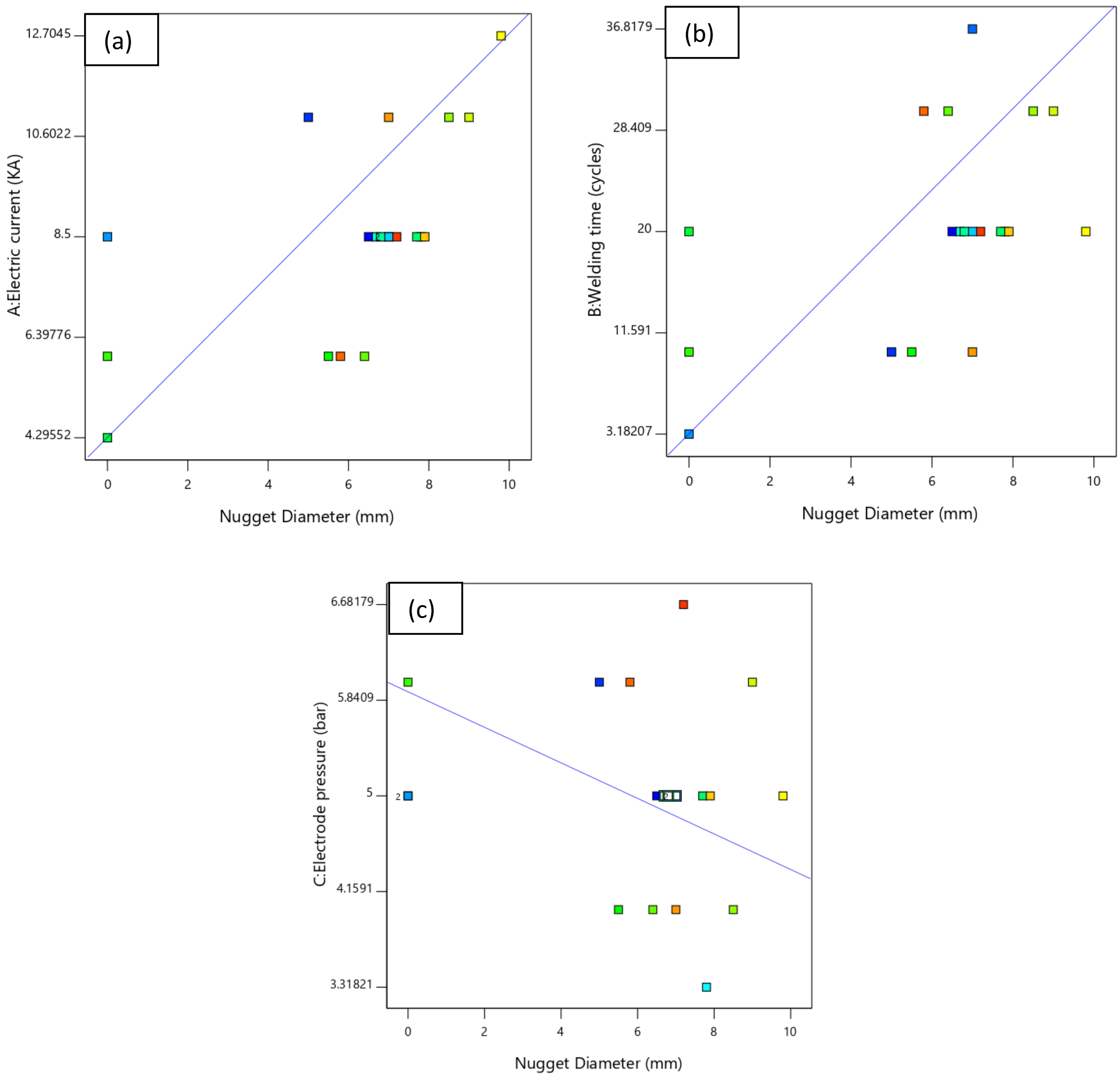

Figure 4.4: Scatter plot showing the correlation between the nugget diameter and (a) Electric current; (b) Welding time. (c) Electrode pressure

Figure 4.5 summarizes the correlation between the nugget diameter and the RSW parameters. The effect of the process parameters correlations explains the increase in nugget diameter when welding current and time were increased and the slight depletion upon increasing the electrode pressure till the reference point 0. Further reduction in the nugget diameter was observed with an increase in electrode pressure beyond the reference point 0 to 1. However, it is imperative to point out that the sensitivity of the nugget diameter to the process parameters is primarily governed by their level of significance provided by the ANOVA analysis. The correlation coefficient provides additional information regarding the nature of the changes in the nugget diameter in response to the changes in the RSW parameters. Correspondingly, the increment in the overall nugget diameter brought about by increasing the welding current and welding time outweighs its reduction by increasing the electrode pressure as vice versa. In the light of the abovementioned argument, considering studies 3 and 13, about 0.96 % changes in the welding current creates 1 % changes in the nugget diameter. However, much higher changes in electrode pressure amounting to about 9.3 % are required to cause a similar reduction in the nugget diameter, taking studies 16 and 20 as a case study.

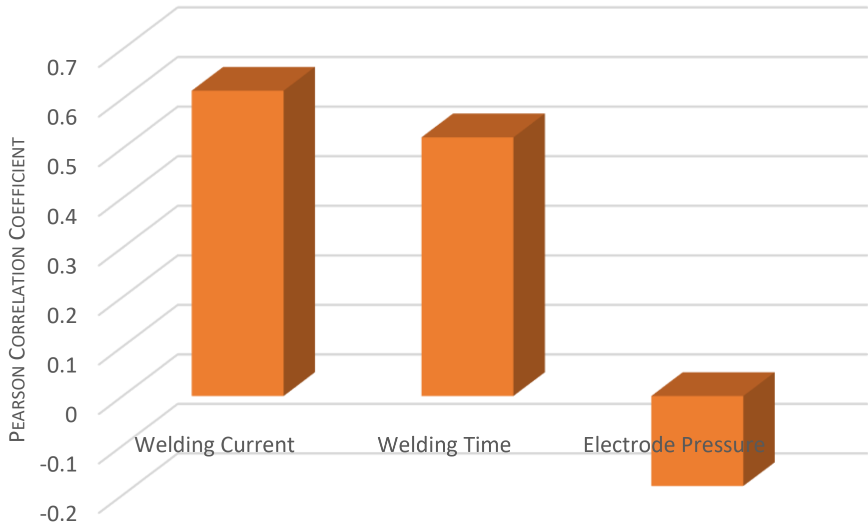

Figure 4.5: Summary of the correlation coefficient between the resistance spot welding parameters and nugget diameter

A study of the interaction between the process parameters can be effectively achieved using a two-dimensional contour plot. This plot is a graph comprising two RSW parameters on the horizontal and vertical axes, while the last parameter is represented by contour lines within the confined space [58]. The 3D surface combined with the 2D contour plot provides a clearer image of the interaction of process parameters and their effect on the response variable. Figure 4.6 shows the 3D response surface and 2D contour plot of the nugget diameter as a function of the welding current and welding time.

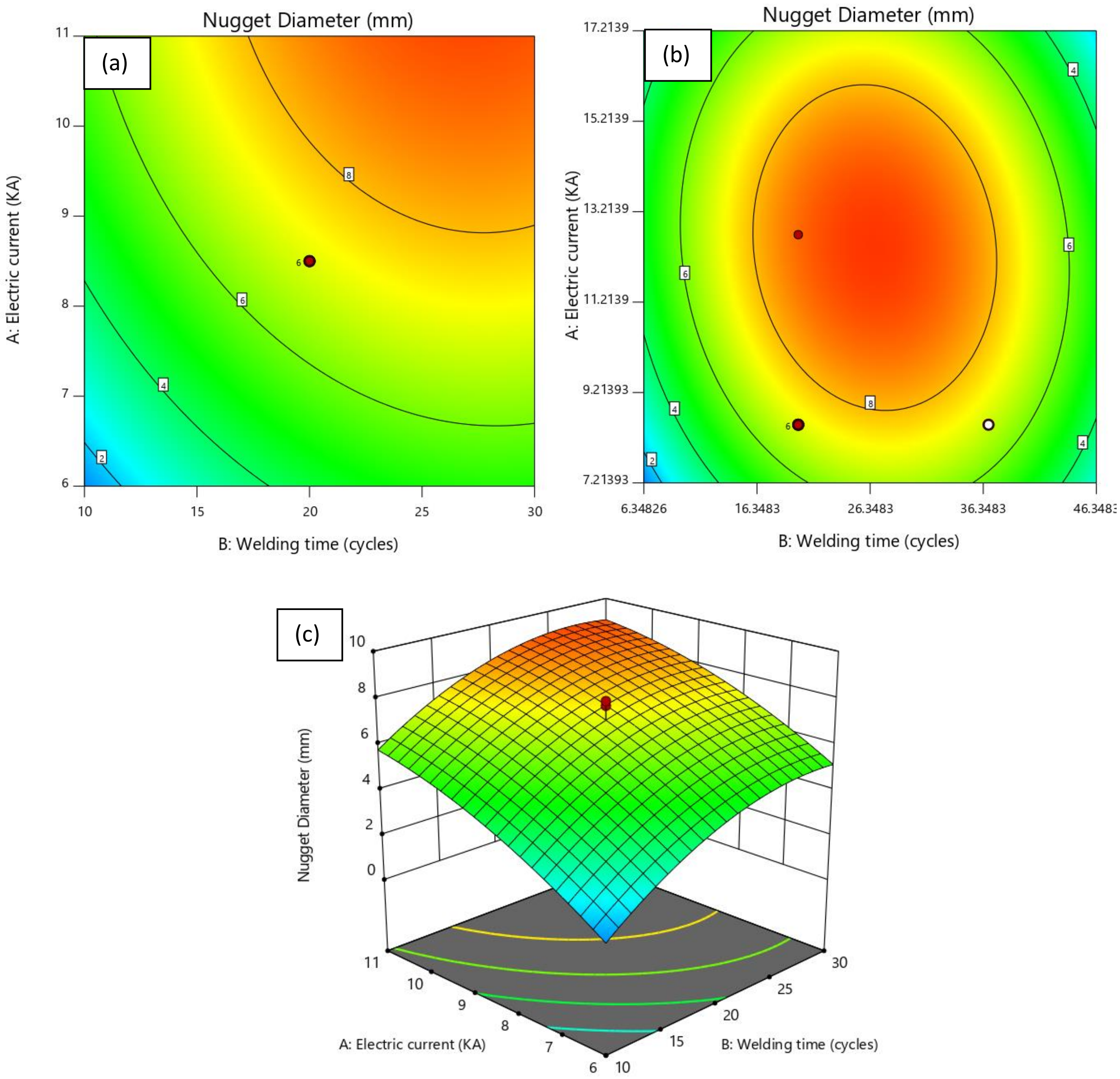

Figure 4.6: Interaction effect of welding current and welding time on the nugget diameter using: (a) and (b) 2D contour plot; (c) 3D response surface plot.

At the origin in Figure 4.6(a), where the welding time and electric current are 10 cycles and 6 KA, respectively, the nugget diameter is relatively small (less than 2 mm), which is below the acceptable limit ($4\sqrt{t}$). A similar scenario to the above condition is observed in sample 2, where incomplete fusion was observed due to insufficient heat input. If the electric current is further increased to a value of 8 - 9 KA, the maximum nugget diameter that can be achieved is about 8 mm. In the same light, increasing the welding time to a value between 20 - 25 cycles, the maximum nugget diameter that can be achieved is about 9 mm. This further justifies the argument that the weld nugget is more sensitive to the welding current predicted by the ANOVA test. The maximum diameter obtainable from the combination of these RSW parameters is 9.3 mm with a welding current of 12.4 KA and a welding time of 26 cycles. Other combinations of welding current and time are possible within the designated area, as revealed by Figure 4.6(b). The increase in nugget diameter with increasing welding current and welding time is attributed to the increase in heat input according to joules law ($H = I^2RT$). This relationship also justifies the greater sensitivity of weld nugget diameter to welding current than the welding time as the heat input.

Furthermore, increasing the heat supply above certain critical limits, as shown from Figure 4.6(b), would reduce nugget diameter. For instance, the maximum weld nugget obtained at a welding current of 17 KA is about 6 mm. The reduction in weld nugget diameter may be attributed to weld expulsion resulting from excessive heating. Expulsion in weld joints has been reported to reduce weld nugget diameter in different grades of stainless steel [61]. This phenomenon is also observed when the welding time is increased to about 45 cycles. The response surface of the interaction between these parameters and the weld nugget is represented in Figure 4.6(c).

Figure 4.7(a) shows the 2D contour plot of the interaction between the electrode pressure and the welding current, while Figure 4.7(b) shows the 3D response surface of the interaction at a welding time of 20 cycles. As can be seen from the contour plot, at the origin where the pressure is relatively low, having a magnitude of 3bar and the welding current is relatively low (about 3.5 KA), the nugget diameter is relatively low (about 5 mm). But slightly increasing the welding current to a moderate amount around 8 KA reveals that a very high value of nugget diameter of 10 mm is obtainable. However, the maximum attainable nugget size is restricted to about 2 mm at a very low electric current and moderate electrode pressure. Again, increasing the electrode force to about 7 bar and maintaining a very low 3.5 KA, it is observed that the nugget diameter drastically reduced from about 5 mm to 0, which indicates a condition of no fusion between the base metals on account of low heat input. However, compensation for the reduction in heat input brought about by increasing the electrode pressure can be catered for by increasing the welding current to about 11 – 13 KA, hence obtaining the maximum nugget diameter of about 10 mm as before. The above explanations justify the negative correlation between electrode pressure and nugget diameter. In other words, optimum values of nugget diameter are obtainable at low electrode pressures and high welding time. Zhao et al. [58] opined that increasing the electrode pressure increases the contact area at the faying surfaces, implying a reduction in contact resistance as a negative correlation exists between them (R=L/A). The reduction in the contact resistance ultimately reduces the heat input, as evident in joules expression for heating. It can also be observed from the response surface diagram (Figure 4.7(b)) that the maximum nugget diameter attainable by increasing the welding current (about 13.5 KA) and high electrode pressures is greater than that obtained at low electrode pressures and high welding current. This is due to the greater sensitivity of welding current to nugget diameter than electrode force. To sum up, optimum nugget diameter is obtained at either low electrode pressure and moderate to high values of welding current or at very high electrode pressure and high value of welding current.

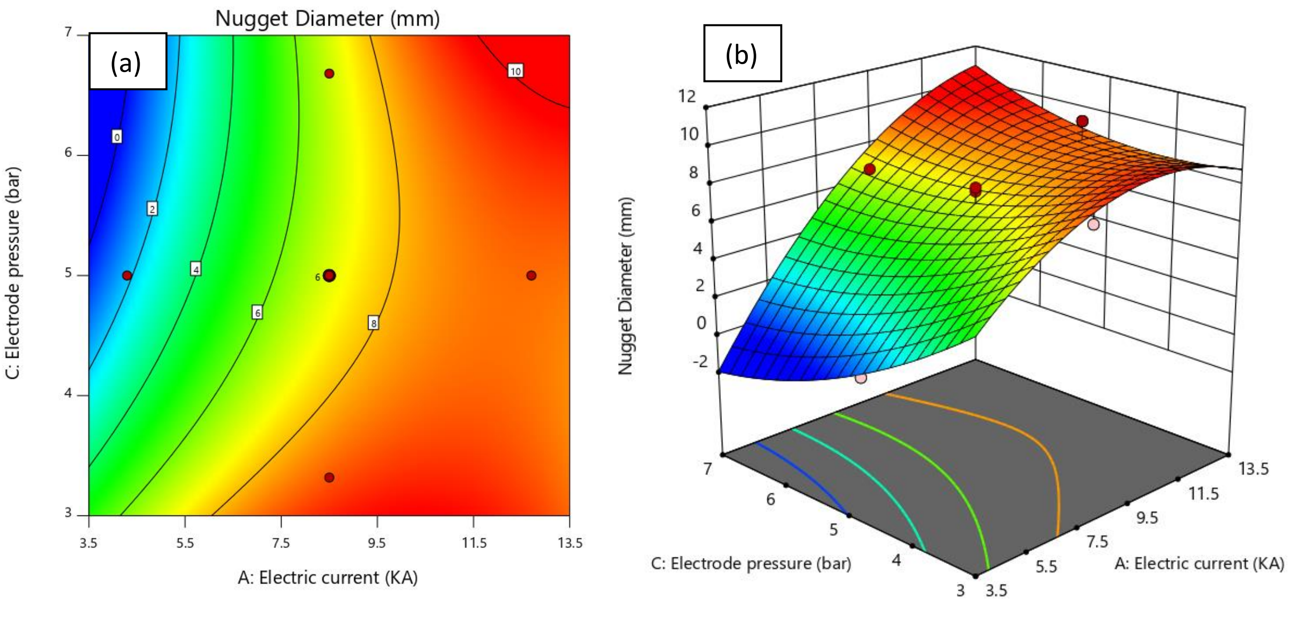

Figure 4.7: Interaction effect of welding current and electrode pressure on the nugget diameter; (a) 2D contour plot; (b) 3D response surface plot.

The interaction between electrode force and welding time is presented by the 2D contour plot and 3D response surface plot in Figures 4.8(a) and 4.8(b), respectively. From the contour plot, it can be seen that increasing the electrode pressure from 1.8 bar to 5.8 bar resulted in decreasing nugget diameter from about 6 mm to 0, indicating no fusion. However, a reverse phenomenon was observed on the welding time axis, as the nugget diameter drastically increases from about 6 mm to a maximum of 10 mm irrespective of the low electrode pressure. This further explains the positive correlation between the nugget diameter and the welding time and the negative correlation between the nugget diameter and electrode pressure. Furthermore, it was also observed that maximum nugget diameter is attainable between low and high values of welding time and low electrode force not exceeding 3 bar. As observed previously, increasing the electrode pressures to a value as high as 5.8 bar will require an extremely high amount of welding time (> 35 cycles). The response surface of the optimum region can be seen in the 3D response plot in Figure 4.8(b). As explained earlier, the reduction in nugget diameter with electrode pressure and lower welding time is due to a reduction in heat input. This implies that if welding is carried out at higher electrode pressures, there is a reduction in heat input and if optimum weld quality is desired, this reduction should be minimized.

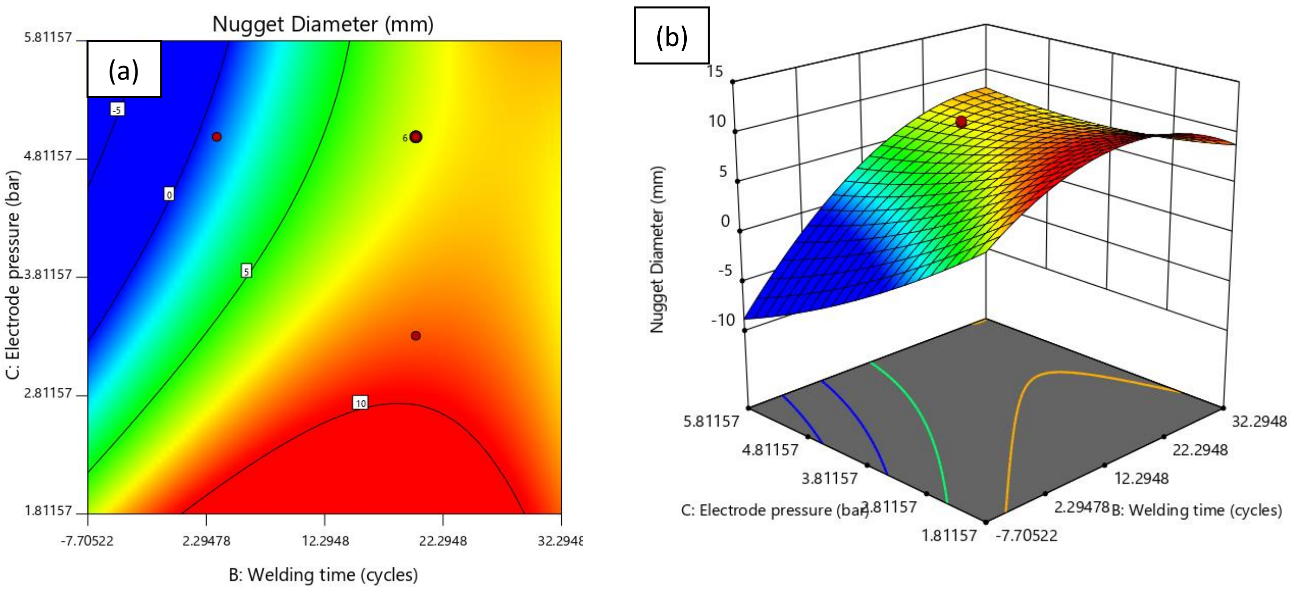

Figure 4.8: Interaction effect of welding current and electrode pressure on the nugget diameter using; (a) 2D contour plot; (b) 3D response surface plot.

4.3 Statistical Analysis of the Effect of Resistance Spot Welding Parameters on the Hardness

From Table 4.1, it is evident that the average FZ hardness varies from 165.84 HV to 209.87 HV for the experimental runs. Table 4.4 presents the models generated for the average FZ hardness prediction using ANOVA.

Table 4.4: ANOVA of the generated mathematical model

Source	***Sequential p-value***	***Lack of Fit p-value***	***Adjusted R^2***	***Predicted R^2***	***Std. Dev.***	***PRESS***	
Mean	**< 0.0001**						**Suggested**
Linear	0.6647	0.2455	-0.0792	-0.5481	11.67	3712.98	
2FI	0.2855	0.2616	-0.0028	-1.9059	11.25	6969.40	
Quadratic	0.8534	0.1544	-0.2097	-3.0485	12.36	9709.83	
Cubic	0.0781	0.5877	0.4103	-1.8301	8.63	6787.77	Aliased

As shown from Table 4.4, the linear model, two factorial model, and quadratic model have an insignificant lack of fit, which is desirable. However, their sequential p-values are all greater than 0.05, implying insignificance, making them inappropriate models for hardness prediction. On the other hand, the cubic model was aliased, making it unsuitable as selecting such a model can result in overfitting. Apart from that, the adjusted R^2 and the predicted R^2 are negative, indicating their low predictive accuracy. The PRESS values for the models are also on the high side. All these put together makes the mean of the hardness a more suitable predictor of the hardness of the weld joint.

A detailed analysis of the effect of the resistance spot welding parameters on the hardness of the weld joint is provided by the ANOVA results presented in Table 4.5.

Table 4.5: ANOVA of the effect of spot welding parameters on the average FZ hardness.

Source	Sum of Squares	df	Mean Square	F-value	p-value	
Model	0.0	0	0	0.0	<0.0001	significant
A-Electric current	322.708	4	80.677	0.581	0.681	
B-Welding time	95.711	4	23.928	0.155	0.958	
C-Electrode pressure	588.552	4	147.138	1.215	0.345	
Residual	2398.39	19	126.23			
Lack of Fit	1979.79	14	141.41	1.69	0.2935	not significant
Pure Error	418.6	5	83.72			
Cor Total	2398.39	19				
Mean						196.71
%Coefficient of Variation						5.71

The results of the ANOVA revealed that the probability values of the welding current, welding time and electrode pressure are 0.681, 0.958 and 0.345, respectively. This implies that 68.1 %, 95.8 % and 34.5 % of the respective F-values are due to noise. In addition, the p-value of the lack of fit indicates that there is a 29.35 % chance that the F-value of lack of fit is due to noise. Though the resistance spot welding parameters have p-values greater than 0.05, the electrode pressure seems to have a more considerable effect on the hardness of the weld joint, with the welding time having the least significance value, as depicted in Figure 4.9.

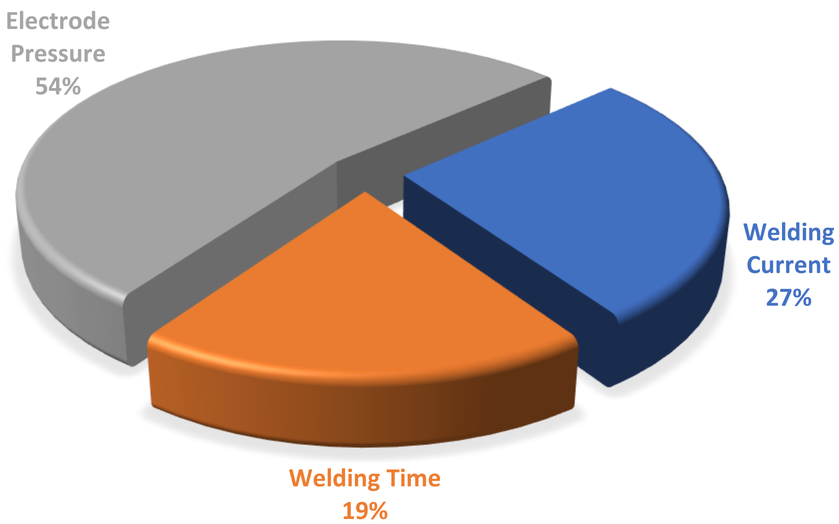

Figure 4.9: Percentage contribution of resistance spot welding parameters to the hardness of the weld joint based on their significance value.

The significance values also imply that the hardness of the weld joint is more sensitive to changes in electrode pressure than the welding current and time. However, the nature of this effect is presented by the scatter plot in Figure 4.10 with the summary of the correlation between resistance spot welding parameters and the hardness presented in Figure 4.11.

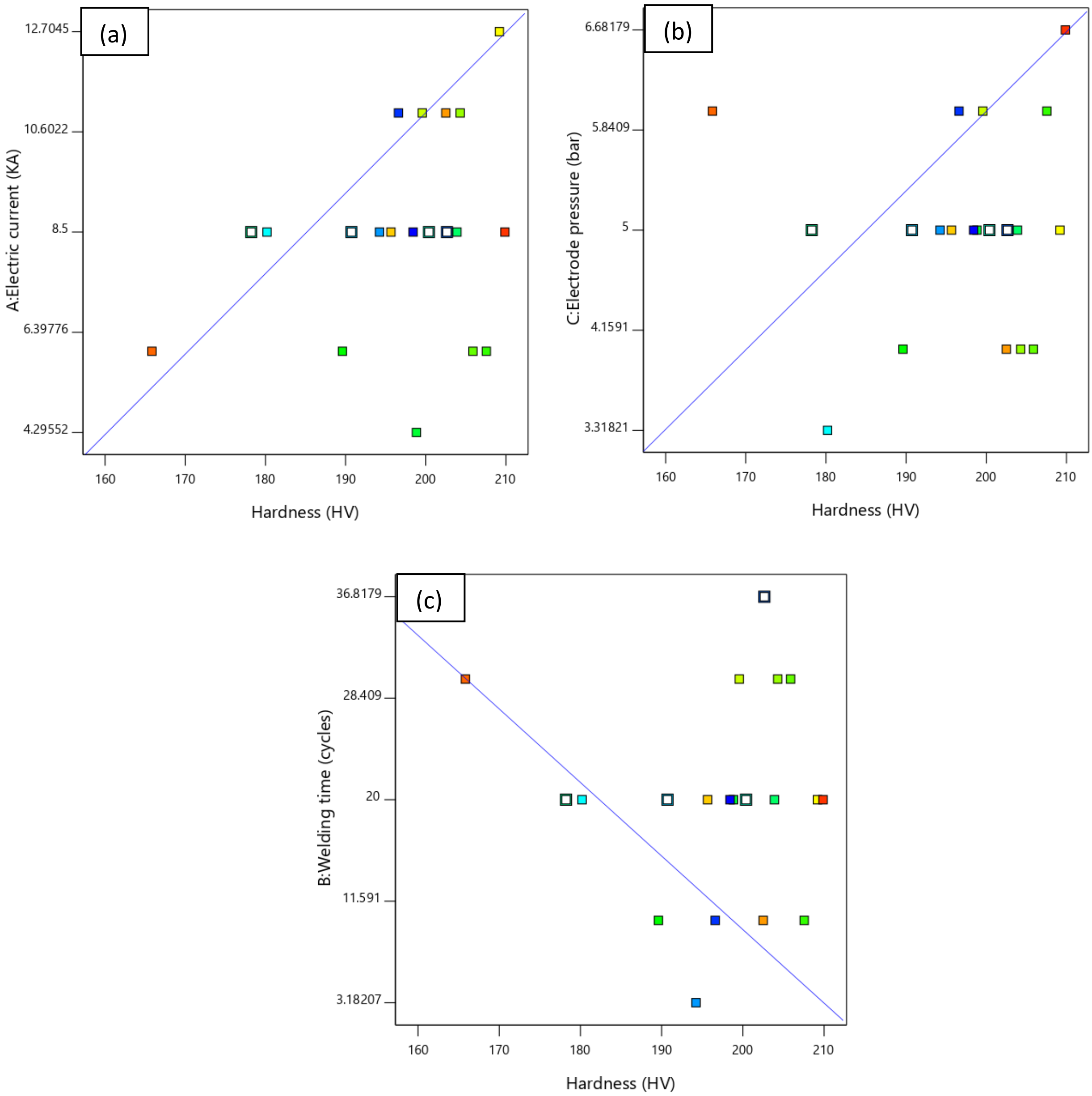

Figure 4.10: Scatter plot showing the correlation between hardness: (a) Electric current; (b) Electrode pressure (c) Welding time

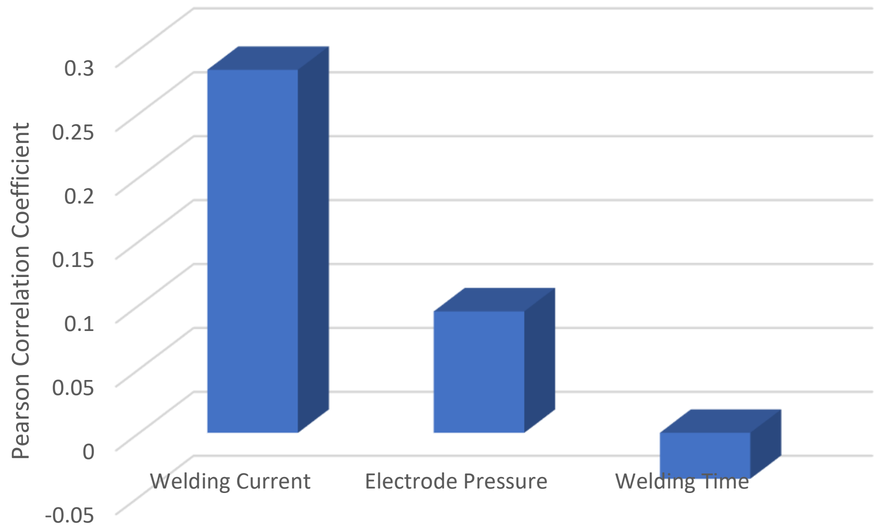

Figure 4.11: Summary of the correlation coefficient between the resistance spot welding parameters and hardness

The suggested mathematical model for hardness prediction was the mean of the hardness of the experimental runs, which was 196.71 HV with validity within the abovementioned domain. As can be seen from the normal plot of residuals in Figure 4.12(a), the errors are almost aligned with the straight line indicating the model's suitability. The residual plot against the experimental runs (Figure 4.12(b)) further reveals the deviation of the predicted hardness from the actual values obtained for each experimental run.

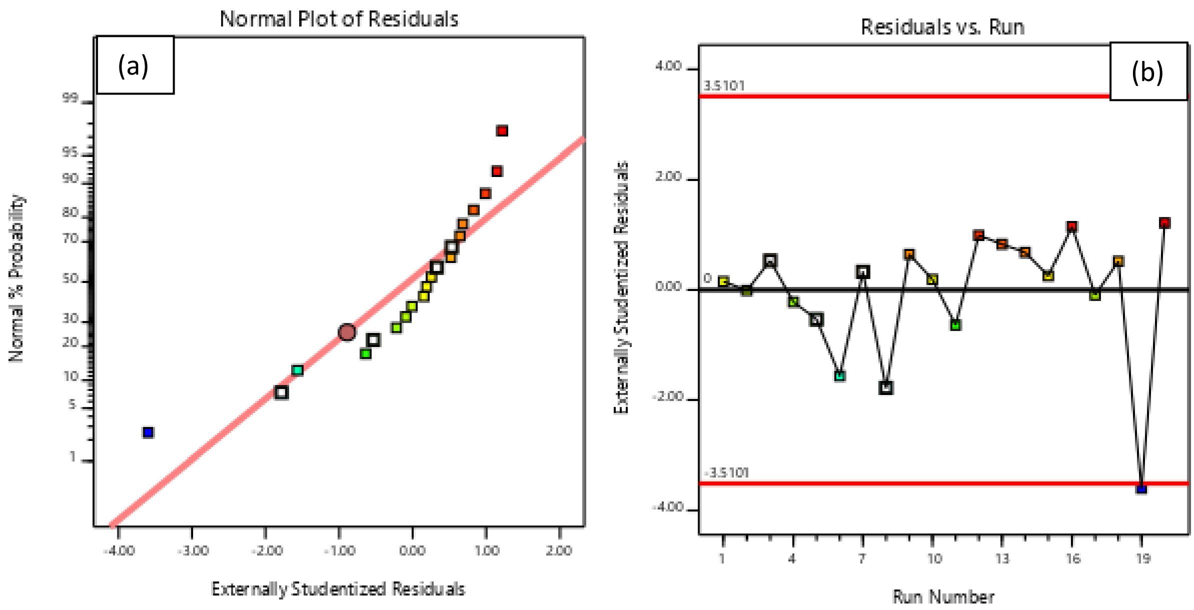

Figure 4.12: (a) Normal plot of residuals for the regression model; (c) Plot of residuals against the experimental runs for all values of the nugget diameter

4.4 Optimization of Resistance Spot Welding Parameters

Following the statistical analysis of the effect of spot welding parameters on the weld nugget diameter and average FZ hardness of the weld joint, the next phase is to optimize these parameters to minimize the average FZ hardness and maximizing the nugget diameter. The welding current and welding times were within the specified domain with a default significance of 60 %, while the nugget diameter and hardness were given a significance of 100 %. A total of 84 solutions with various combinations of spot welding parameters were generated with the optimum solution having desirability of 0.547, as shown in Figure 4.13. The corresponding spot welding parameters are 10.884 KA, 30 cycles and 5.822 bar for the welding current, welding time and electrode pressure, respectively. The optimum parameters obtained for the nugget diameter and hardness are 9.837 mm and 196.707 HV, respectively. Figure 4.14(a) - (c) shows 2D contour plots of the optimum conditions obtained, which entails the desirability, Nugget diameter and hardness against the different spot welding parameters. Figure 4.14(a) depicts a 2D contour plot of the desirability, nugget diameter and average FZ hardness in terms of the welding current and welding time. Figure 4.14(b) is a plot of the desirability, nugget diameter and FZ hardness against the welding current and electrode pressure, while Figure 4.14(c) shows a plot of the nugget diameter, desirability and FZ hardness as a function of the electrode pressure and welding time.

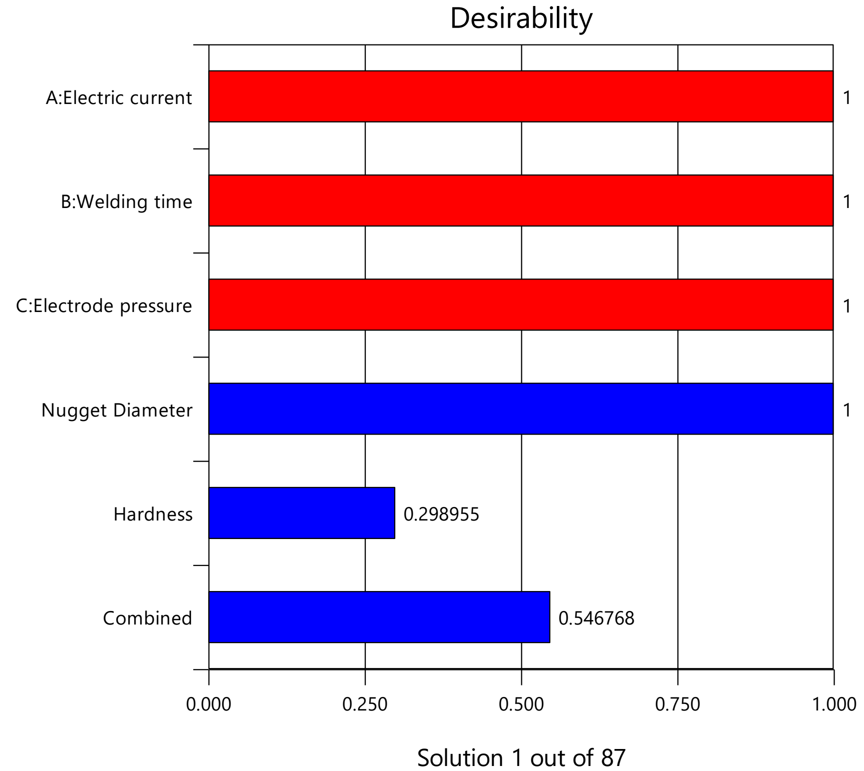

Figure 4.13: Desirability of the optimum solution which minimizes the hardness of the weld joint and maximizes the nugget diameter.

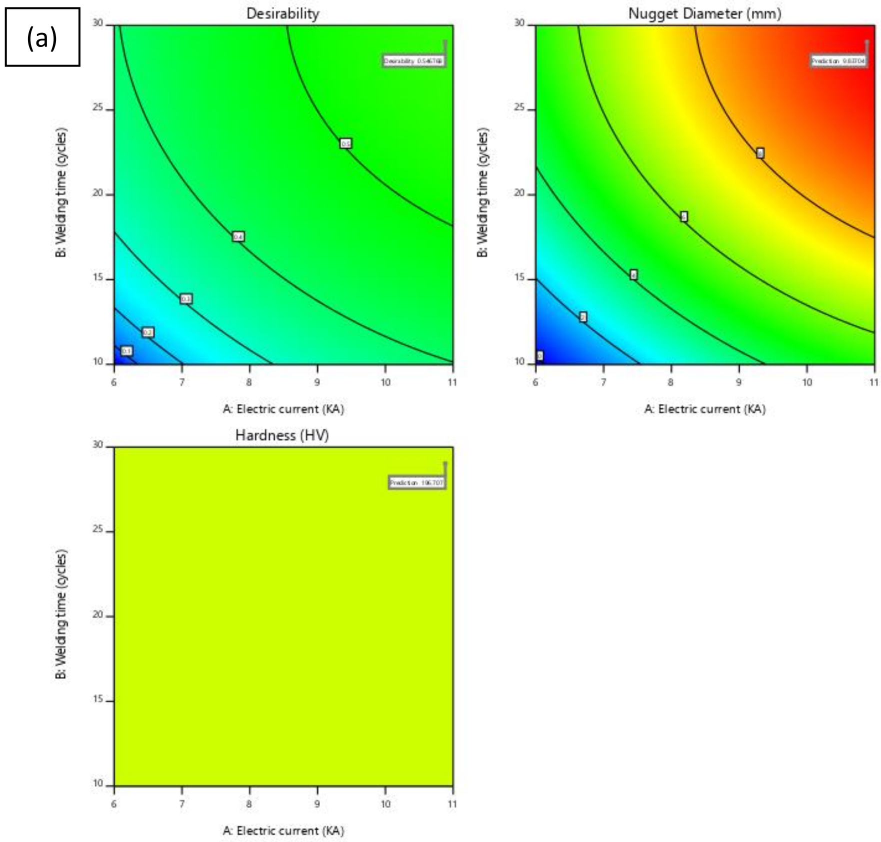

(b)

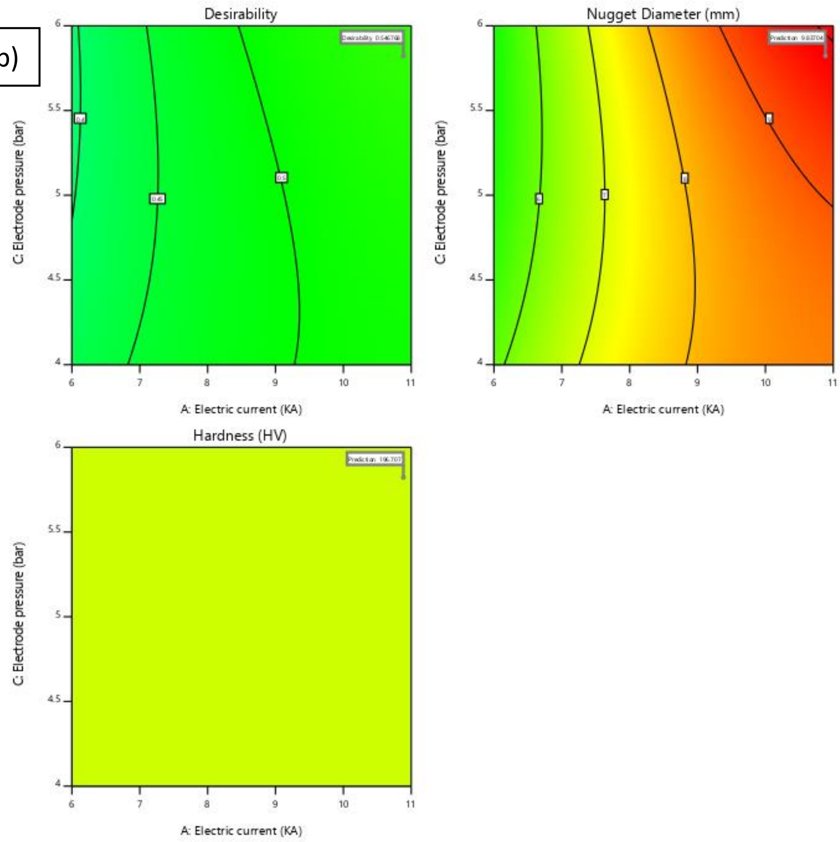
Desirability
Nugget Diameter (mm)
Hardness (HV)
C: Electrode pressure (bar)
A: Electric current (KA)

(c)

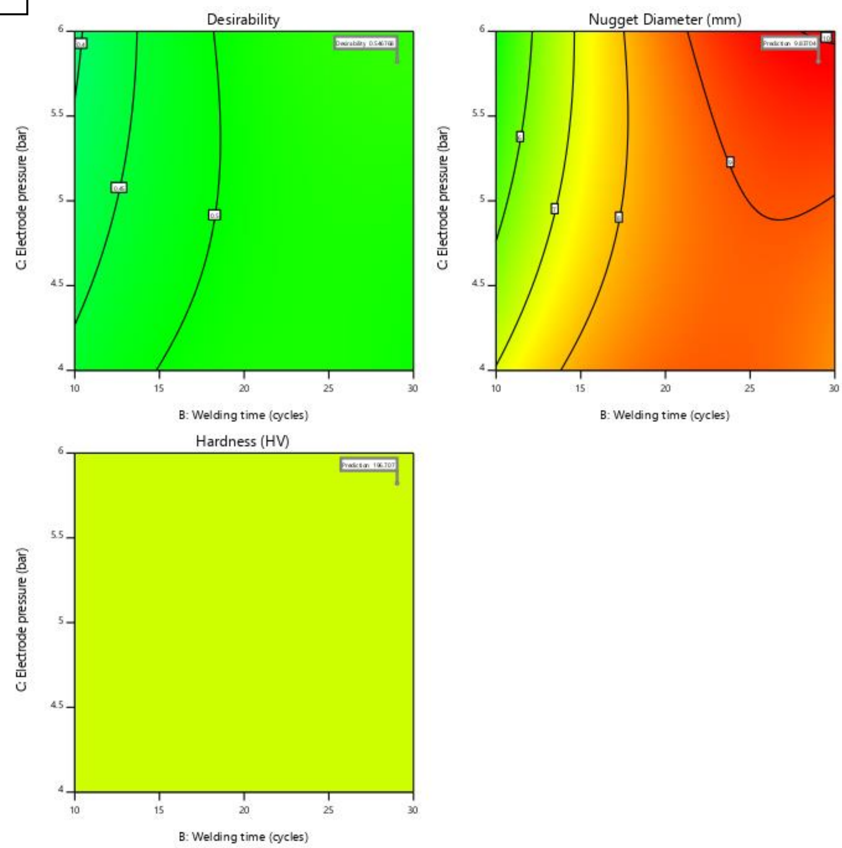
Desirability
Nugget Diameter (mm)
Hardness (HV)
C: Electrode pressure (bar)
B: Welding time (cycles)

Figure 4.14: 2D contour Plot showing the desirability, optimum nugget diameter and hardness as functions of (a) Welding current and welding time; (b) Welding current and electrode pressure; (c) Welding time and electrode pressure.

4.5 Model Prediction and Experimental Validation

The optimization of the spot welding parameters was followed by the experimental validation of the obtained optimum parameters in the previous section. Table 4.6 provides details of the predicted optimum parameters and weld properties alongside the ones obtained experimentally. The validation was repeated twice to ensure reproducibility, and the average of the results was obtained.

Table 4.4: Predicted and actual values of nugget diameter and hardness using the regression model

	Electric current (KA)	**Welding Time (cycles)**	**Electrode Pressure (bar)**	**Nugget Diameter (mm)**	**Hardness (HV)**
Predicted	10.85	29.03	5.822	9.837	196.7
Actual	10.85	29.03	5.800	9.200	204.3

As shown from Table 4.6, the difference between the predicted nugget diameter and the experimental nugget diameter is about 0.637 mm, corresponding to 6.9 %, implying a confidence level of about 93 %. The error obtained in the hardness prediction is about 7.6 HV, corresponding to 3.7 %. This also implies a confidence level of about 96 %. The high confidence levels obtained in predicting these properties using this regression model make it a suitable model. The complexity of the hardness of the weld joint may account for the slight deviation obtained for the predicted values, but residuals less than 10 % are generally acceptable.

4.6 Effect of Resistance Spot Welding Parameters on the Hardness

The results from the previous sections revealed that the significance of the spot welding parameters regarding their effect on the hardness of the weld joint all have probability values greater than 0.05, indicating that their effect on the weld hardness has a confidence level far below 95 %. This further implies that the correlation between the hardness and these parameters will also be insignificant, further supported by the weak correlations obtained in the previous section. Similar results have been reported by Wan et al. [73].

The above findings imply that the average hardness of the weld joint is not predominantly dependent on the spot welding parameters despite their pertinence in the fusion process. Nonetheless, the average FZ hardness of the weld joints might be attributed to other factors such as the chemistry and phase transformations (metallurgical factors) taking place at the weld joint during the welding process and the rate of cooling. High cooling rates between 7800 – 8000 K/s have been reported in some spot welded joints that significantly affect the hardness [19]. Figure 4.15 depicts the factors influencing the hardness of the weld joint, categorising them into two broad categories; metallurgical and resistance spot welding parameters based on the ANOVA results obtained previously in Table 4.5.

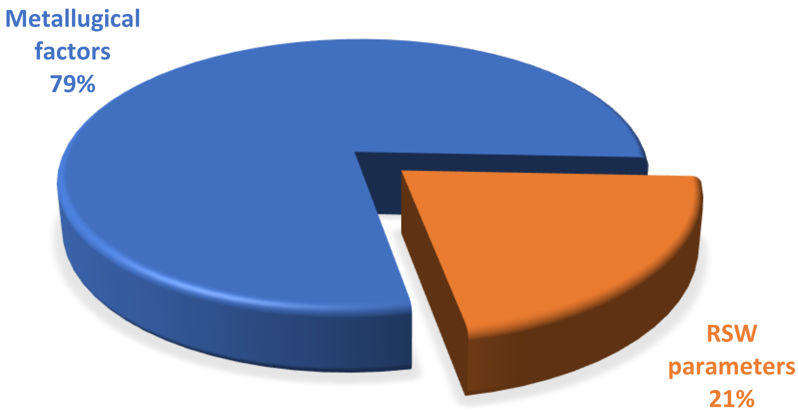

Figure 4.15: Percentage contribution of resistance spot welding parameters and metallurgical factors to the average hardness of the weld joint based on their significance value.

Examination of the hardness results in Table 4.1 revealed that at relatively low pressures, such as in sample 19, having the least electrode pressure of 3.3 bar, the average hardness was 180.02 HV reaching a maximum of 197.2 HV. Comparing this sample with sample 17 having the highest electrode pressure, the average hardness was 209.87 HV, with the maximum being 220.6 HV, as represented in Figure 4.16. Thus, at a constant electric current of 8.5 KA and welding time of 20 cycles, increasing the electrode pressure also increased the hardness of the weld joint above that of the as-received base metal (202 HV). A similar result was obtained when sample 3 having an electrode pressure of 5 bar is considered. This accounts for the positive correlation obtained in the previous analysis.

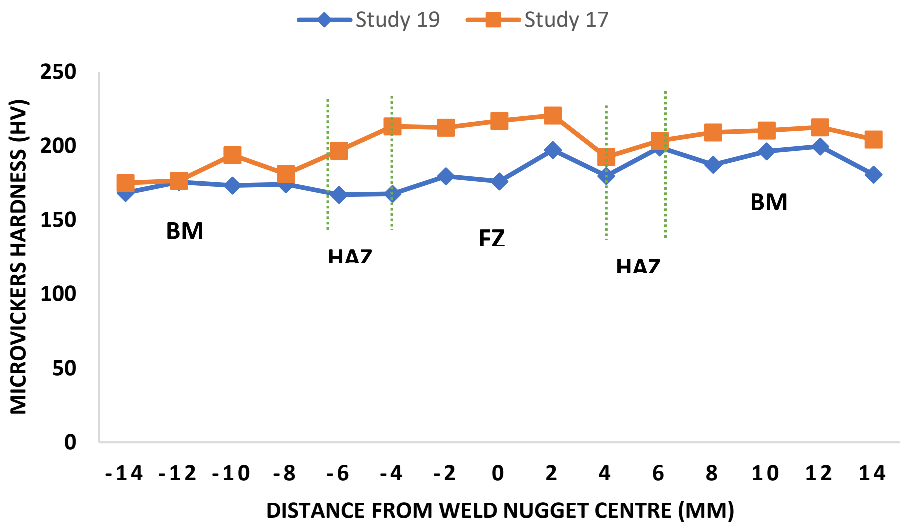

Figure 4.161: MicroVickers hardness distribution profile for study 19 and 17.

To study the effect of welding time on the hardness of the weld joint, sample 1 and sample 4 were taken into consideration. The hardness profiles of these studies are presented in Figure 4.17 below. In sample 1, the average hardness is 202.65 HV reaching a maximum value of 207 HV, while in sample 4, with the least welding time, the average hardness is 194.23 HV reaching a maximum value of 202.2 HV. The result revealed that increasing the welding time correspondingly raised the hardness level above the as-received base metal. Comparism with the hardness value in sample 7 revealed a similar trend.

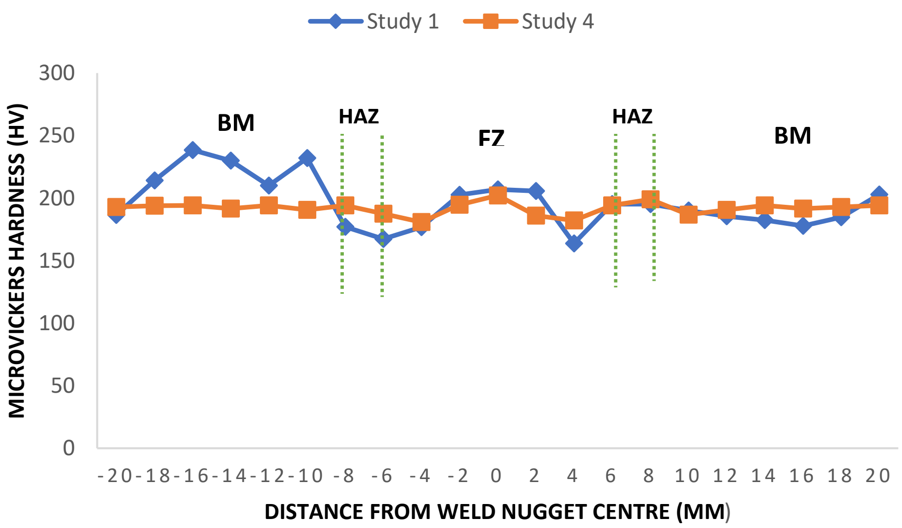

Figure 4.17: MicroVickers hardness distribution profile for study 1 and 4

Figure 4.18 shows the hardness profiles for studies 6 and 13. In these studies, the electrode pressure and welding time are maintained at 5 bar and 20 cycles, with the welding current being 4.3 KA and 12.7 KA, respectively. The average hardness of the fusion zone in sample 6 is about 198 HV reaching a maximum value of 212 HV, but a higher hardness value (average = 209.19 HV, maximum = 226.7 HV) was obtained in sample 13 with an increased value of welding current. However, a reverse trend was observed for sample 7 with an intermediate welding current.

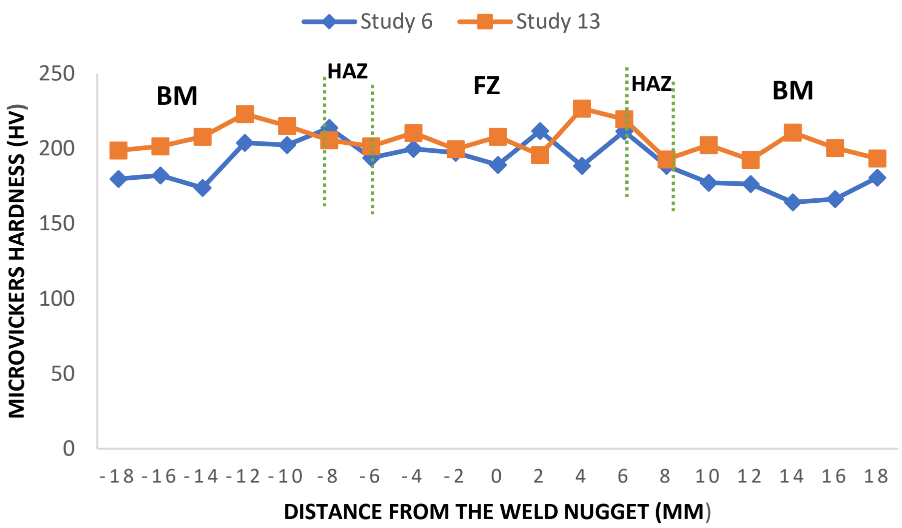

Figure 4.18: MicroVickers hardness distribution profile for study 6 and 13

4.7 Morphological Analysis of Phase 1

Morphological evolution in spot welded joints is primarily controlled by the metallurgical factors alongside the resistance spot welding parameters. The post-weld solidification of austenitic stainless steel involves precipitation of the delta ferrite phase, which is gradually transformed to the austenite phase. During the transformation, the liquid metal, delta ferrite, and the austenite phase co-exist. Ideally, the austenitic stainless steel, after transformation, solidifies into the austenite phase. However, due to the non-uniform and fast cooling rate associated with the spot welding process, most transformation processes retain a certain amount of untransformed delta ferrite alongside the austenite phase [19]. The transformation process is summarized by the equation below.

Liquid (L)→ Liquid (L) + delta ferrite (δ)→ Liquid (L) + delta ferrite (δ) + Austenite (γ)→ delta ferrite (δ) + Austenite (γ).

In addition to the cooling rate, the chromium and nickel equivalent ratio is another primary factor influencing the mode of solidification, i.e. A, AF, FA, and F modes. It has been reported that increasing this ratio or the cooling rate increases the tendency of solidification from A - F mode with 316L austenitic stainless steel having a greater tendency to undergo the FA solidification due to its chromium-nickel equivalent ratio in the range of 1.6 - 1.7 [243]. Furthermore, the abovementioned factors also influence the delta ferrite transformation from eutectic, vermicular, lathy, acicular to widmanstätten austenite. Attempts have been made to predict the post-weld solidification phases in austenitic stainless steel using the Schaeffler diagram, WRC-1992 diagram and the pseudo-binary diagram. Though a certain level of accuracy was achieved, discrepancy still existed between the predicted phases and those obtained. The variation might be attributed to the non-equilibrium cooling rate, chemical composition, ferrite morphology and phase dissolution [244]. The following paragraphs present the effect of the welding parameters on the weld morphology.

The investigation of the effect of welding current on the weld morphology was achieved using studies 6 and 13 as case studies having a welding current of 4.3 KA and 12.7 KA with a constant welding time and electrode pressure of 5 bar and 20 cycles, respectively. Figure 4.19(a) and (b) represents the outer weld appearance, 4.19(c) and (d) depicts the entire weld metallographic surface of the entire weld region, while 4.19(e) and (f) delineates the fusion zone.

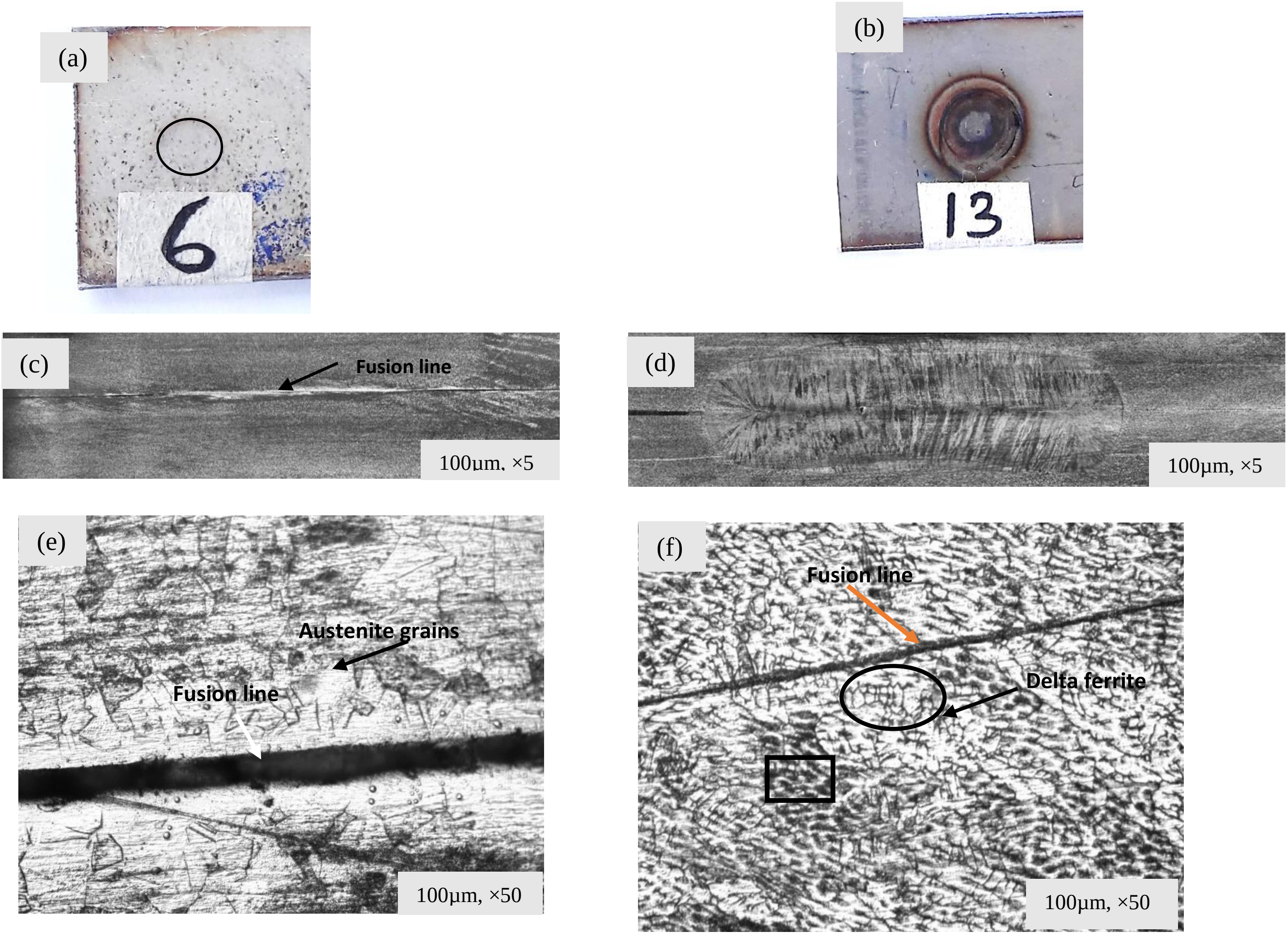

Figure 4.19: Weld morphology of study 6 and 13 showing the outer weld appearance, entire weld cross section and the fusion zones.

The outer weld surface of sample 6 having the least welding current revealed that the weld nugget is almost invisible (the circled region in Figure 4.19(a)) but increasing the welding current as observed in sample 13 revealed a visible weld nugget (Figure 4.19(b)). Increasing the welding current also led to the formation of columnar dendrite with grains enlarged parallel to the direction of the applied electrode force. No shrinkage cavities, cracks or porosities were observed, indicating the absence of excessive heating of weld joint (Figure 4.19(d)). The absence of the columnar dendrite in sample 6 results from the low heat input attributed to the low welding current leading to incomplete fusion (arrow in Figure 4.19(c)). The base metals are not properly fused, as evident in the large separation gap (represented by white arrow) between the base metals, as can be seen in Figure 4.19(e).

Consequently, such a joint will have very poor tensile shear load bearing capacity coupled with the small weld nugget. On the contrary, proper fusion and solidification were observed in sample 13, as evident in the presence of columnar dendrite and the small separation gap (golden arrow in Figure 4.19(f)) between base metals relative to the former. Certainly, this sample will have better mechanical properties and exhibit superior service performance. Further examination revealed no significant microstructural evolution occurred in sample 6 as the microstructure contains untransformed austenite grains similar to those in the unwelded base metal (black arrow in Figure 4.19(e)). On the other hand, increasing the heat input led to the transformation of austenite grains to delta ferrite, mainly lathy ferrite (the oval enclosed area), as can be seen in Figure 4.19(f). In addition, a region of partially transformed austenite (enclosed in the rectangle) was observed. The formation of lathy ferrite may be attributed to the fast cooling rate induced by the increase in welding current facilitating the transformation process. The slightly increased hardness observed in sample 13 may be attributed to the formation of lathy ferrite and partially transformed austenite grains. The fine grain size in sample 13 also gives it superior tensile and yield strength in accordance with the principles of hall Petch.

The effect of welding time on the weld joint morphology was studied using studies 1 and 4 having welding times of 36.8 and 3.2 cycles, respectively. As observed previously, Figure 4.20(a) revealed that no visible weld nugget was formed in sample 4 in the outer weld surface, but in and Figure 4.20(b), an obvious nugget was observed in sample 1 as there was sufficient heat input following the duration of welding time. Also, the indentation from the electrode was visible, and a ring of HAZ was formed around the weld nugget. A further examination of the metallographic surface in Figure 4.20(c) and 4.20(d) revealed that no fusion occurred in sample 4, contrary to the full columnar dendrite solidification observed in sample 1 characterized by the formation of shrinkage cavity centrally located at the fusion zone (arrow in Figure 4.20(d)). Studies revealed that stresses in weld joints having such cavities are insignificant and thus, have no effect on the overall properties of the weld joint [6]. As expected, no phase transformation was observed in sample 4 as the welding time is too short to supply the necessary heat energy to initiate the transformation process; hence, the microstructure comprised austenite phase majorly as in the base metal (arrow in Figure 4.20(e)). Antithetically, acicular lathy ferrite was observed in sample 1 (the area enclosed in the rectangle in Figure 4.20(f)), whose formation may be attributed to the restriction of low-temperature diffusion of delta ferrite over long distances due to the increased cooling rate. A comparism of the average hardness values of the two studies revealed that a subtle difference of 8.42 HV, with sample 1 exhibiting a greater hardness. Increasing heat input during the spot welding leads to ferritization of the weld joint, as observed by Kianersi et al. [6]. Despite the ferritization observed in sample 1, the greater hardness may be attributed to the reformation of the austenite grains.

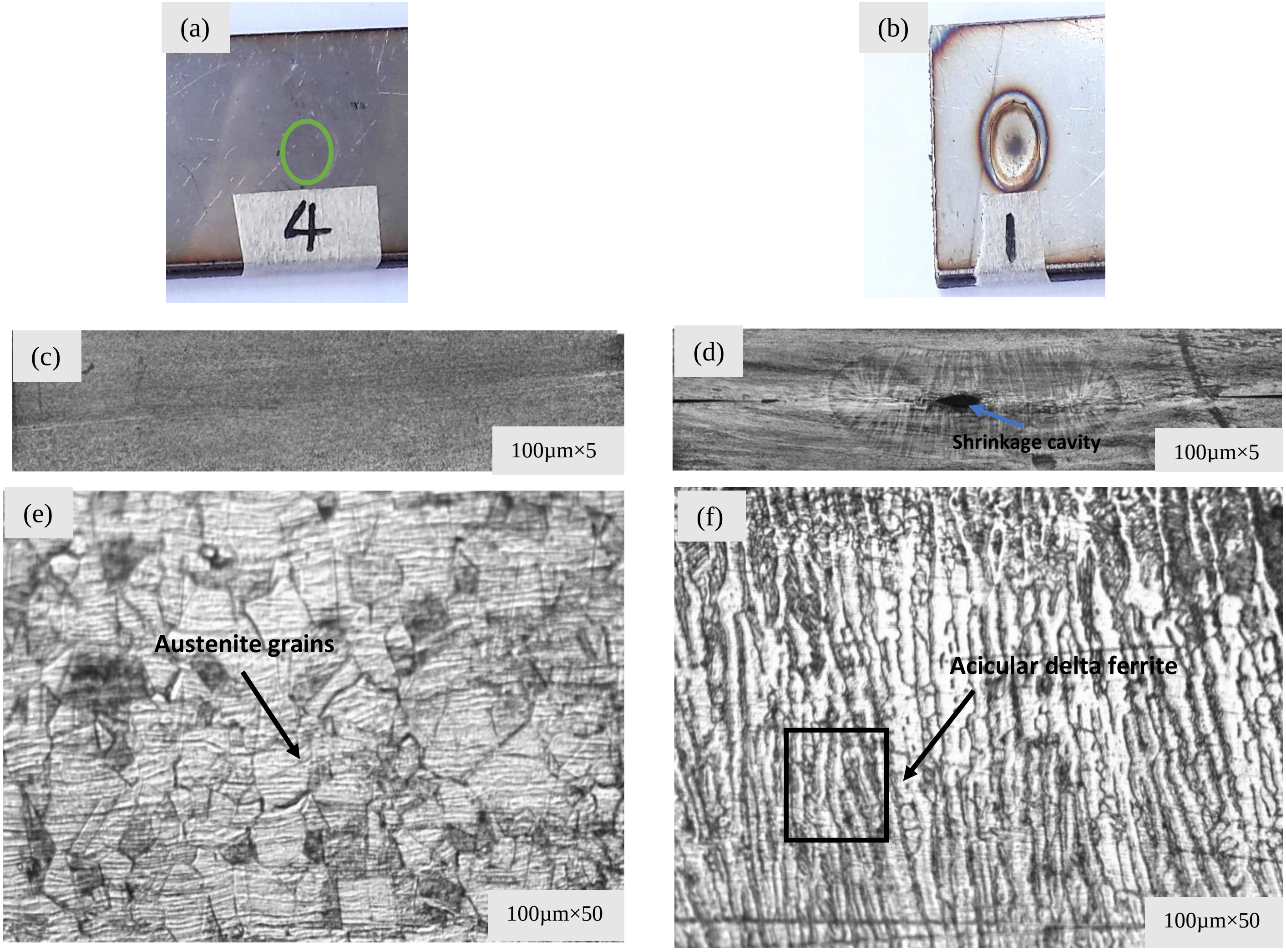

Figure 4.20: Weld Morphology of Study 1 and 4 showing the outer weld appearance, entire weld cross section and the fusion zones.

The effect of electrode pressure was investigated using studies 17 and 19. Figure 4.21(a) and (b) represent the outer appearance of the weld joints, Figure 4.21(c) and (d) present an aerial view of the fusion zone, while Figure 4.21(e) and (f) is a magnified view of the fusion zones.

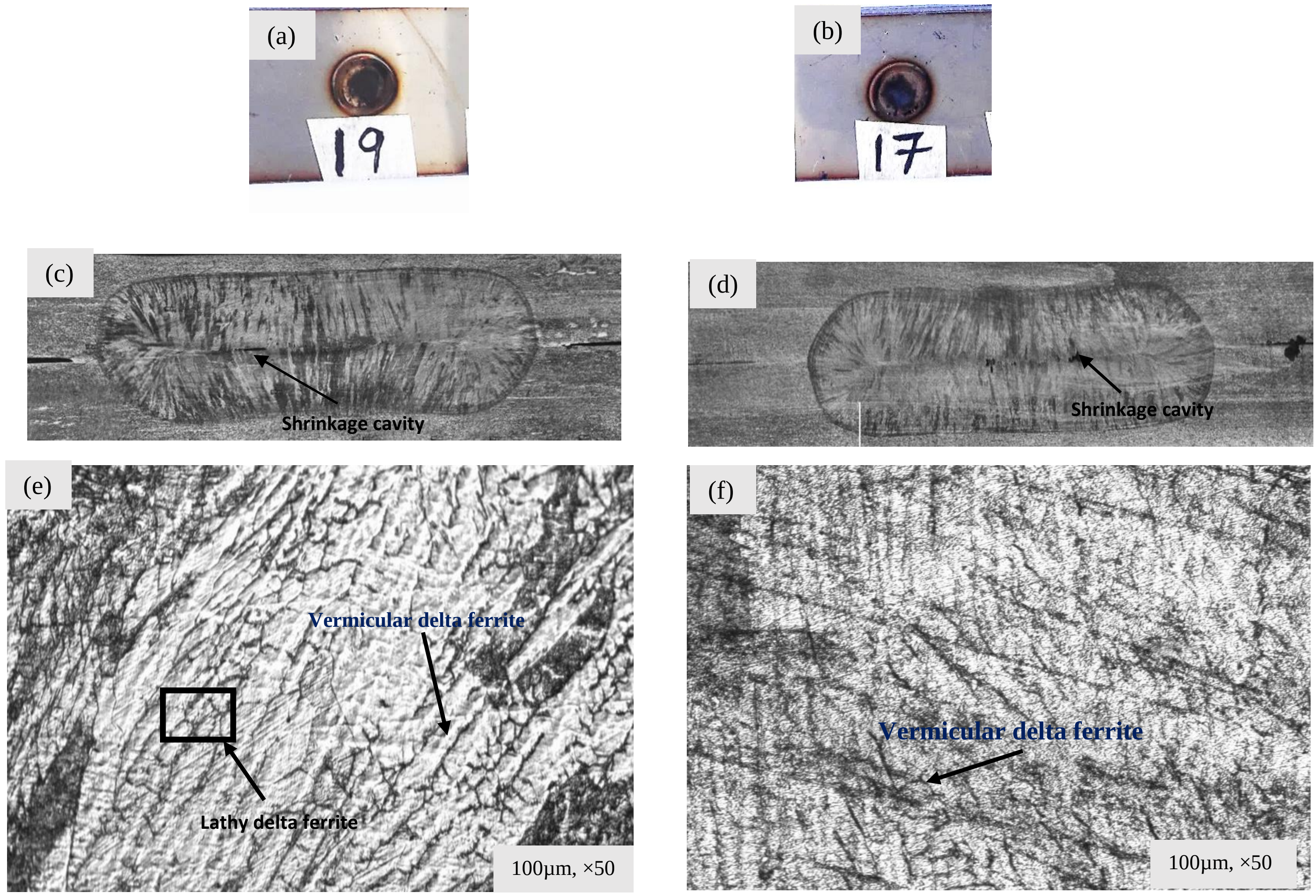

Figure 4.21: Weld morphology of study 17 and 19 showing the outer weld appearance, entire weld cross section and the fusion zones**.**

A minuscule contrast was observed in the exterior weld appearance when electrode pressure was increased from 3.3 bar (Figure 4.21(a)) to 6.7 bar (4.21(b)) as rings of HAZ was formed in both welds and the indentations from the electrode are both discernible. However, Figure 4.21(c) and (d) revealed that the weld nugget was reduced by 8 % with increasing electrode pressure and grain elongation parallel to the direction of electrode force was also less evident. This may be attributed to the reduction in heat input due to the increase in contact area at the base metals' faying surface, which consequently reduces the overall joint resistance. Full columnar dendrite solidification was also evident as centrally located shrinkage cavities were observed in both studies. The evaluation of the metallographic cross-section of the fusion zone of both studies further revealed that ferritization occurred at the fusion zones, which was characterized by lathy and vermicular delta ferrite and vermicular delta ferrite for studies 19 and 17, respectively, as revealed by Figure 4.21(e) and (f). Consequently, the reformation of austenite grains and reduction in ferritization may account for the lower hardness observed in sample 19 relative to sample 17.

Figure 4.22 shows the micrographs of the cross-sectional view of the sample's microstructure for the experimental validation of the optimum spot welding parameters alongside those of the as-received base metal.

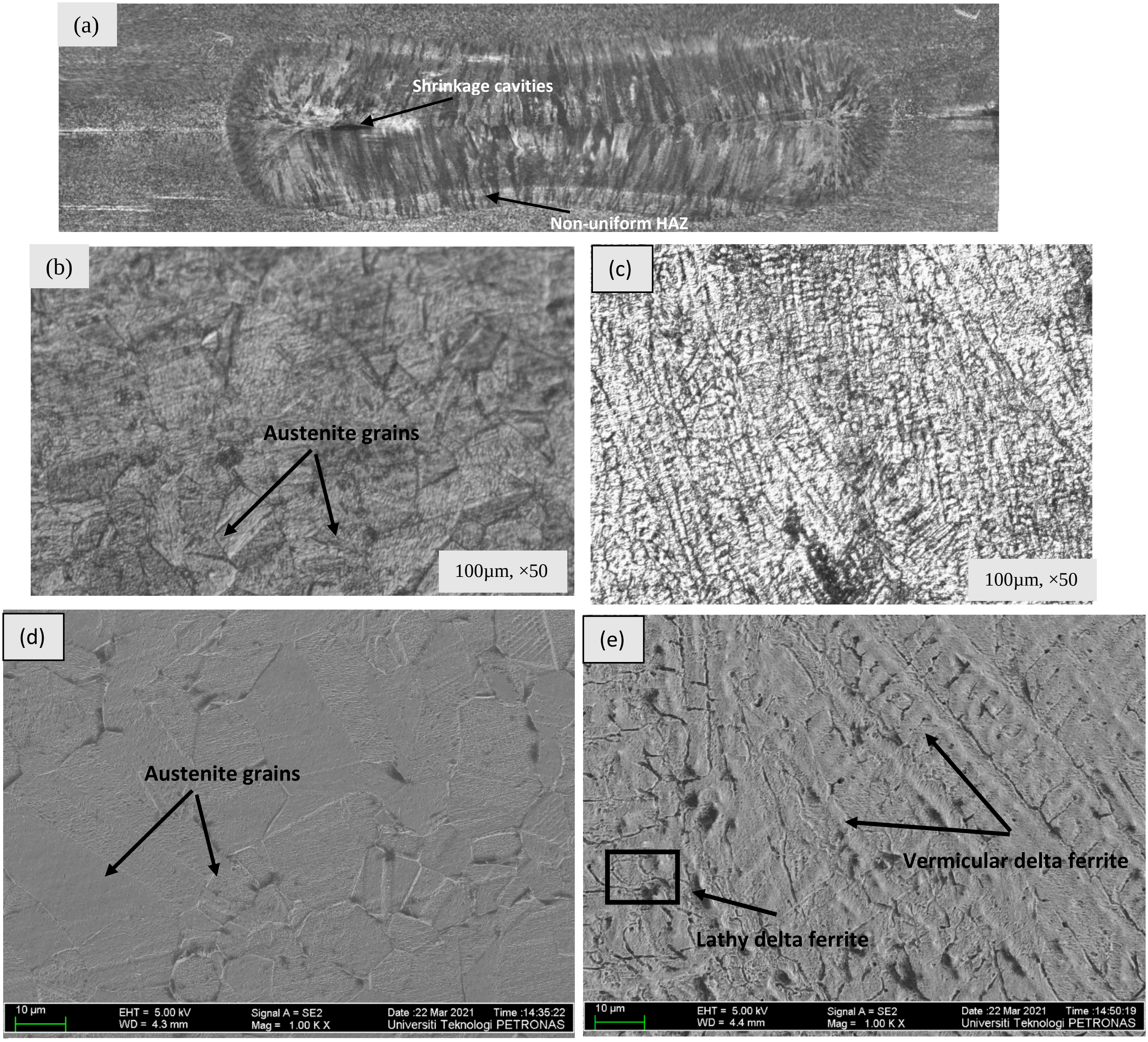

Figure 4.22: Weld morphology showing the entire weld cross section and the fusion zones of study the experimental validation sample.

Figure 4.22(a) reveals that the experimental sample for the validation of the optimum parameters underwent a complete columnar dendrite solidification characterized by shrinkage cavity and a non-uniform heat affected zone (indicated by white arrows). The austenite-delta ferrite grain elongation parallel to the direction of the electrode force appears to be more distinct. Further examination of the fusion zone reveals that the microstructure comprises lathy delta ferrite (enclosed rectangular area) and vermicular delta ferrite (two black arrows) dispersed in austenite matrix, as revealed by Figure 4.22(e). The formation of lathy delta ferrite and shrinkage cavity is an indication of a very fast cooling rate due to the high energy input during the welding process. Comparism between the microstructure of the as-received metal and the fusion zone of the validation sample revealed that that the base metal is typically made of austenite grains (two black arrows in Figure 4.22(b) and (d)) while the latter has delta ferrite precipitated in the microstructure. One might expect the average fusion zone of the latter to be lower due to ferritization induced by the welding process. However, the hardness values were found to be approximately the same. The increase in hardness of the fusion zone may be attributed to the refined austenite grains, which have a much finer microstructure than the latter, compensating for the reduction induced by ferritization. Consequently, the optimized sample would have increased tensile shear load bearing capacity evident in the size of the nugget diameter while having an average hardness similar to the as-received base metal.

4.8 Energy Dispersive X-ray (EDX) Elemental Analysis of the First Stage

Table 4.7 summarises the elemental composition of the as-received base metal and the validation sample for the optimum RSW parameters.

Table 4.7: EDX analysis showing the phase stabilizers % composition in the as-received base metal and the optimum parameter validation sample.

Sample	**Cr**	**Mo**	**Si**	**Ni**	**Mn**	**Fe and others**
AS-Received BM	16.33	2.63	0.50	9.36	1.83	65.10
Validation Sample	16.07	2.25	0.38	8.65	1.64	64.22

The results in Table 4.7 revealed that an infinitesimal difference in elemental chemical composition exists between the as-received base metal and the fusion zone of the validation sample, further justifying the result of the hardness values obtained in the previous section. However, a slight reduction was observed in both austenite and ferrite stabilizers after welding.

A plausible explanation for the observation lies in the discrepancy in microstructural phase composition, as the as-received base metal comprises austenite phase majorly while the validation sample comprises delta ferrite/austenite phase interfaces and is thus susceptible to the mechanism of partitioning [126]. During the welding process, the fast cooling rate induced by the spot welding process causes austenite stabilizers such as Cr, Mo and Si are consumed by the austenite phase leading to the reduction of delta ferrite in those regions while delta ferrite stabilizers such as Ni and Mn enriches the delta ferrite phase and consequently leading to the depletion of austenite. Moreover, the findings reported by other experimenters revealed that increasing the heat input during spot welding results increase in ferrite phase stabilizers, mainly chromium, while austenite phase stabilizers such as nickel are reduced connoting ferritization. Figure 4.23 shows the EDX analysis of the optimum validation sample as well as the as-received base metals.

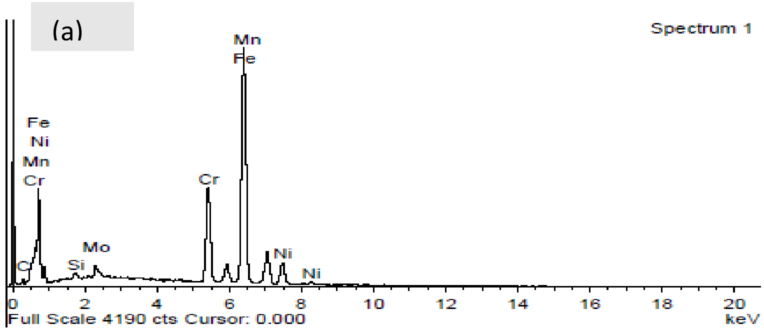

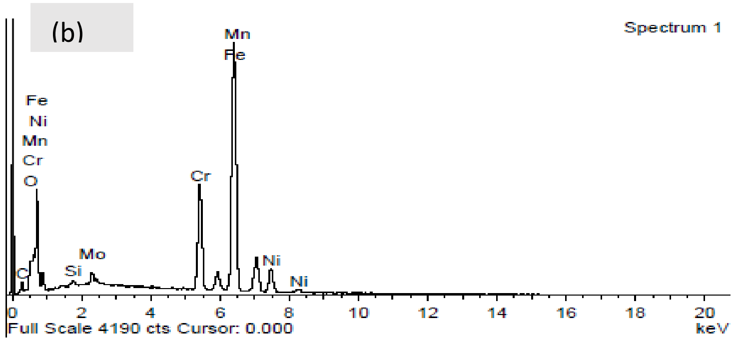

Figure 4.23: EDX analysis showing the peaks of the different elements present in the fusion zone of: (a) As-received base metal; (b) Optimum parameter validation sample.

4.9 Statistical Analysis of the Effect of Weld Treatment Parameters on Hardness

Table 4.8 shows the average hardness of the fusion zone for the different experimental runs involving different weld treatment parameters. As can be seen from the table, the maximum hardness occurred in sample 19 (210.3 HV), while the minimum was found in sample 11 (149.2 HV).

Table 4.5: Design matrix for weld treatment parameters and experimental results obtained for the response.

Std	Factor 1 A: Preheating Temperature (ºC)	Factor 2 B: Tempering Temperature (ºC)	Factor 3 C: Holding Time (hours)	Response: Hardness (HV)
1	150	500	3	176.3
2	150	500	1.31821	169.6
3	100	600	2	180.8
4	150	500	3	176.9
5	100	400	2	165.1
6	150	500	3	179.5
7	150	500	3	186.7
8	65.9104	500	3	187.1
9	150	331.821	3	180.8
10	100	400	4	191.1
11	150	500	4.68179	149.2
12	150	500	3	176.7
13	200	400	4	190.4
14	150	500	3	179.7
15	150	668.179	3	178.4
16	234.09	500	3	182.6
17	100	600	4	174.4
18	200	400	2	180.3
19	200	600	4	210.3
20	200	600	2	171.7

Table 4.9 presents the different mathematical models generated for the average FZ hardness in terms of the preheating temperature, tempering temperature and holding time using ANOVA. From the table, we can see that the linear, two factorial and quadratic models all have insignificant p-values and a significant lack of fit, making them inapposite models. On the contrary, the cubic model has a significant probability value and lack of fit. The insignificant lack of fit makes it unsuitable, coupled with the tendency of overfitting. Based on these

underlying facts, the mean of the hardness was suggested as the p-value is very significant. In addition, their R^2 values are all negative, with very high PRESS values.

Table 4.9: Different mathematical models generated for hardness using ANOVA.

Source	Sequential p-value	Lack of Fit p-value	Adj. R^2	Pred. R^2	Std. Dev.	PRESS	
Mean	**< 0.0001**						**Suggested**
Linear	0.7787	0.0043	-0.1113	-0.7003	12.48	4525.06	
2FI	0.8723	0.0025	-0.2982	-2.7130	13.48	9881.57	
Quadratic	0.2813	0.0024	-0.1712	-3.7756	12.81	12709.44	
Cubic	0.0247	0.0107	0.6227	-18.9714	7.27	53150.86	Aliased

A detailed analysis of the effect of weld treatment parameters on the hardness of the weld joint is provided by the ANOVA results presented in Table 4.10.

Table 4.10: ANOVA of the effect of weld treatment parameters on the hardness

Source	Sum of Squares	df	Mean Square	F-value	p-value	
Model	0.0	0	0	0.0	<0.0001	significant
A-Preheating temperature	548.738	4	137.185	0.974	0.451	
B-Tempering temperature	208.824	4	52.206	0.319	0.861	
C-Holding time	1707.034	4	426.758	6.708	0.03	
Residual	2661.35	19	140.07			
Lack of Fit	2584.87	14	184.63	12.07	0.0062	significant
Pure Error	418.6	5	83.72			
Cor Total	2661.35	19				
Mean						179.38
%Coefficient of Variation						6.6

The results presented in Table 4.10 reveal that the most significant parameter having the greatest influence on the hardness of the weld joint is the holding time having a probability value of 0.03 indicating that 3 % of the F-value is due to noise also implies a confidence level of about 97 %. On the other hand, the preheating temperature and the tempering temperature are less significant having p-values of 0.451 and 0.861 and confidence levels of 54.9 % and 13.9 %, respectively. In addition, the p-value of the lack of fit indicates that there is a 0.62 %

chance that the F-value of lack of fit is due to noise. Figure 4.24 shows the weld treatment parameters' significance level based on the weld joint's hardness.

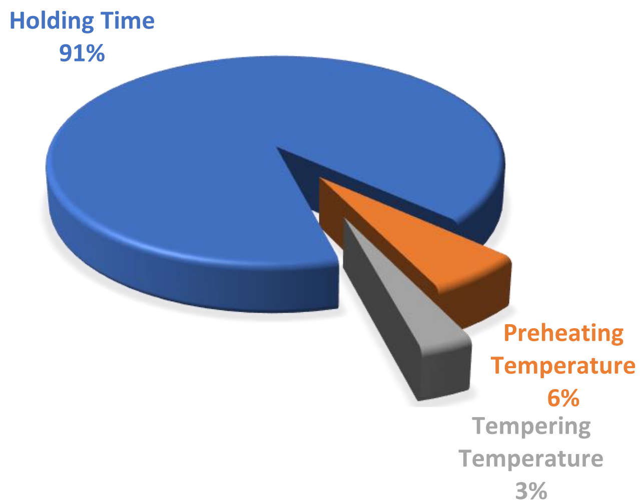

Figure 4.24: Percentage contribution of weld treatment parameters to the hardness of the weld joint based on their significance value.

The nature of the effect of these parameters on the average FZ hardness of the weld joint can be determined using correlation analysis. The scatter plot showing the relationship between these weld treatment processes can be seen in Figure 4.25. The results of the correlation analysis, as can be seen on the scatter plots, revealed that positive correlations (0.177, 0.033 and 0.178) exist between the hardness of the weld joint and the weld treatment parameters, namely, preheating temperature, tempering temperature, and holding time respectively. These correlations infer that increasing the abovementioned parameters is likely to bring about a corresponding increase in the average FZ hardness of the weld joint. However, their overall contribution to the weld joint hardness is a function of their significance levels. It is important to point out that, despite the low significance levels of the other two parameters within the specified domain, greater significance levels can be obtained with a smaller domain, a subset of the specified domain.

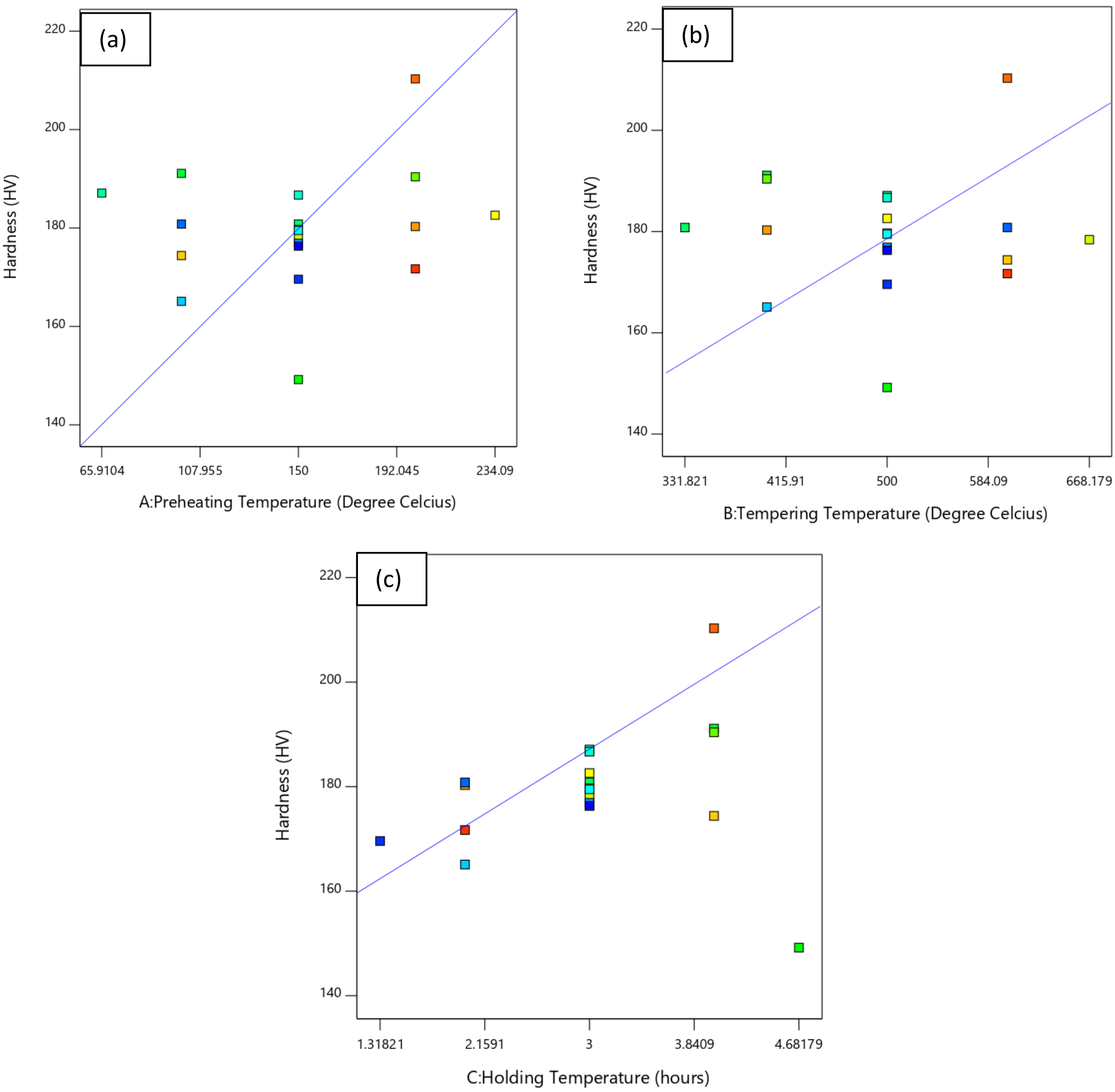

Figure 4.252: Scatter plot showing the correlation between hardness and; (a) Preheating temperature; (b) Tempering temperature (c) Holding time.

The suggested mathematical model for hardness prediction was the mean of the hardness of the experimental runs, which was 179.38 HV with validity within the abovementioned domain. As can be seen from the normal plot of residuals (Figure 4.26(a)), the errors are almost aligned with the straight line indicating the model's suitability. The residual plot against the experimental runs (Figure 4.26(b)) further reveals the deviation of the predicted hardness from the actual values obtained for each experimental run.

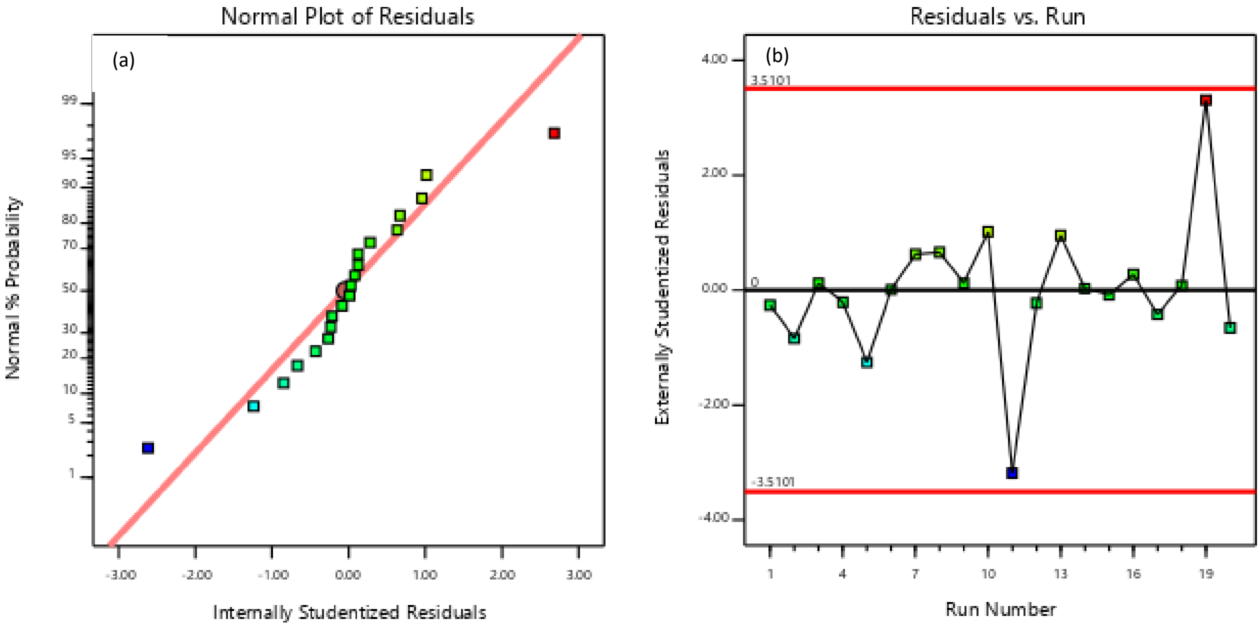

Figure 4.26: (a) Normal plot of residuals for the fusion zone hardness; (c) Plot of residuals against the experimental runs of average fusion zone hardness.

With the objective of minimizing the hardness of the weld joint, the experimental sample with the least hardness is sample 11 with weld treatment parameters 150 ^{o}C, 500 ^{o}C and 4.7 hours. The corresponding hardness of the weld joint is 149.2 HV.

4.10 Effect of Weld Treatment Parameters on the FZ Hardness

The results of the ANOVA revealed that the holding time significantly affects the hardness of the weld joint while the effect of the preheating temperature and tempering temperature have confidence levels less than 90 %. The nature of this effect revealed by the correlation analysis shows that these parameters are all positively correlated with the hardness of the weld joint. Combining the two results, we can infer that increase in the holding time is more likely to bring about a corresponding increase in the hardness of the weld joint than any of the weld treatment parameters.

In order to sample the effect of holding temperature on the hardness of the weld joint by comparing the experimental results with those obtained from ANOVA and correlation, sample 2 and 11 were taken into consideration. As presented in Table 4.8, their respective holding times are 1.3 and 4.7 hours, respectively. Increasing the holding time from 1.3 hours to 4.7 hours reduced the average hardness of the weld joint from 169.6 HV to 149.2 HV, which was contrary to the predicted correlation. However, considering studies 3 and 17, a positive correlation was observed, as the average hardness was found to increase with increasing holding time. But comparing these hardness values with those of the as-received metal and the optimized sample in the first stage, we can infer that there is a considerable reduction in weld joint hardness. The hardness profiles of these studies can be found in Figure 4.27.

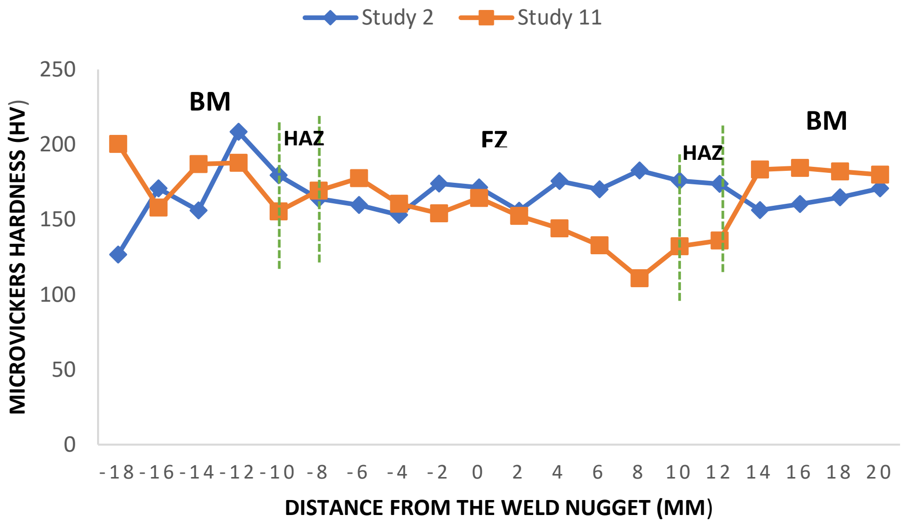

Figure 4.27: MicroVickers hardness distribution profile for study 2 and 11

Studies 8 and 16 were taken into consideration in evaluating the effect of preheating temperature on the hardness of the weld joint. The hardness results revealed that increasing the preheating temperature from 65 to 234 ^{o}C brought about a corresponding reduction in the hardness value from 187.1 HV - 178.4 HV, antithetical to the predicted correlation. The hardness profiles of these studies can be seen in Figure 4.28. On the contrary, a positive correlation was observed between studies 5 and 18 as the hardness was found to increase from 165.1 HV to 180.3 HV with increasing preheating temperature. And if we also compare with the optimum hardness obtained from the first stage, there is an overall hardness reduction.

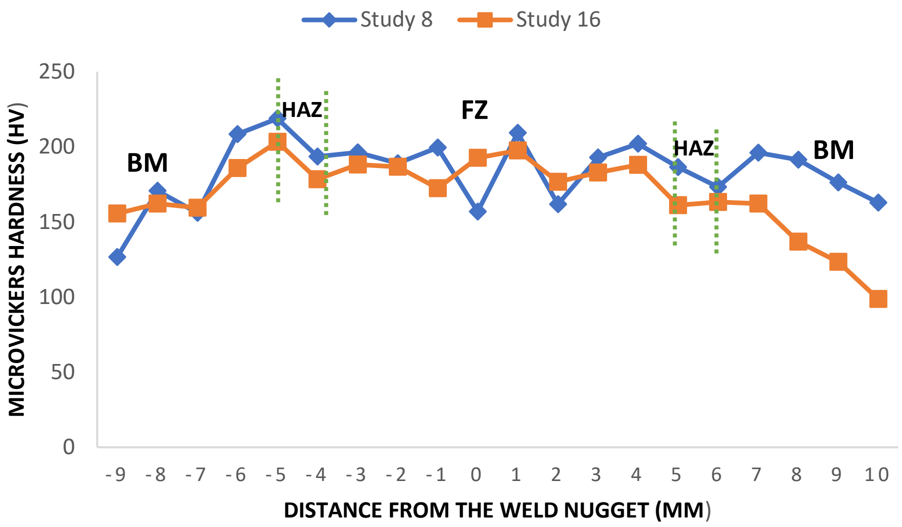

Figure 4.28: MicroVickers hardness distribution profile for study 8 and 16.

It was observed in studies 9 and 15 that increasing the tempering temperature reduced the hardness from 180.8 HV to 178.4 HV at a constant preheating temperature and holding time. But an expected positive correlation was observed between studies 3 and 5, as the reduction in tempering temperature was accompanied by a corresponding reduction in the hardness values from 180.8 HV to 165.1 HV. Figure 4.29 shows the hardness profiles of these studies. As also observed previously, the average hardness of these studies were lower than the optimum hardness obtained in the first phase. Going by this, we can also infer that there was a general reduction in the hardness of the weld joint.

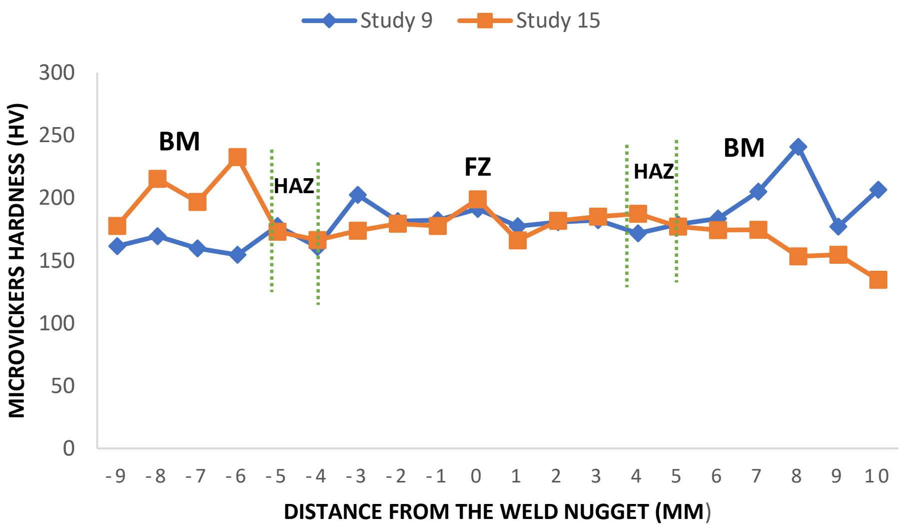

Figure 4.29: MicroVickers hardness distribution profile for study 9 and 15**.**

4.11 Morphological Analysis of the Second Experimental Stage

As done in the previous section, we will examine the effect of preheating temperature, tempering temperature, and holding time on the morphology of the weld joint using different case studies.

The effect of preheating temperature on the microstructural evolution of the weld joint was investigated using studies 8 and 16. Figure 4.30 shows the optical and FESEM micrographs of the cross-sectional views of the base metals and fusion zone. Figure 4.30(a) and (c) represents the base metals of sample 8, while sample 16 is represented by Figure 4.30(b) and (d). Their respective fusion zones are represented in Figure 4.30(e) and (f). The micrographs of the base metals revealed that no significant changes occurred in the base metal when the preheating temperature was increased from 65.91 ^{o}C to 234 ^{o}C. However, a subtle difference was observed in the microstructure of the respective fusion zones. The fusion zone of sample 8 contains a combination of partially transformed austenite grains (oval enclosed area in Figure 4.30(e)) and lathy delta ferrite (rectangular enclosed area in Figure 4.30(e)) relative to the vermicular lathy ferrite in the form of skeletal lathy ferrite (oval enclosed area in Figure 4.30(f)) observed in sample 16. The formation of lathy ferrite and partially transformed austenite in the sample may be attributed to the relative fast cooling due to the low preheating temperature. But on increasing the preheating temperature in the latter, the cooling rate was reduced, forming vermicular ferrite. The transformation of delta ferrite from lathy to vermicular may be attributed to the migration of the austenite-delta interface in the direction of decreasing interfacial energy between the two phases induced by preheating [25]. Another benefit of preheating reported by experimenters is the release of residual stresses by reducing the temperature gradient between the weld joint and base metals.

Furthermore, the reduction in the austenite-delta ferrite interfaces induced by preheating has been reported to improve the corrosion behaviour of welded joints as the interfaces serve as sites for the initiation of pitting corrosion [237]. In other words, the deferritization of welded joints induced by preheating is a good measure for enhancing their corrosion resistance. Contrastingly, researchers have also reported that preheating increases the tendency of carbide precipitation as sufficient time is made available due to a reduction in cooling rate. However, carbide precipitation was not observed in these studies because the post-weld treatment was carried out at temperatures below 650 ^{o}C coupled with the low carbon composition of austenitic stainless steel. Furthermore, deferritization also reduces the overall strength of the weld joint as resistance to dislocation movement offered by the presence of delta ferrite is eliminated by preheating.

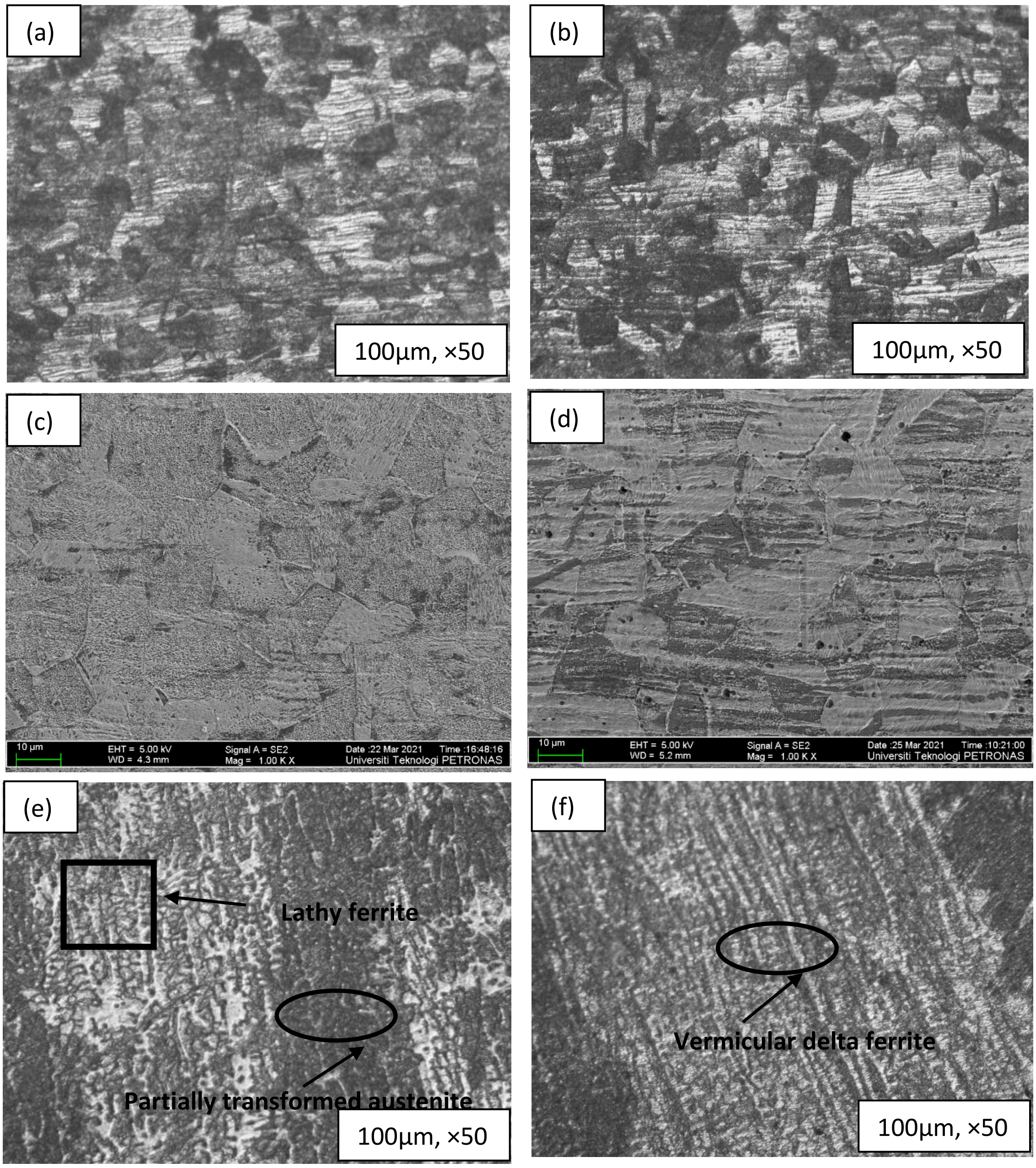

Figure 4.30: FZ and BM region of study 8 and 16; (a) and (c) BM of study 8; (b) and (d) BM of study 16; (e) FZ of study 8 (f) FZ of study 16.

The hardness of the base metal region of sample 8 was found to be higher than that of sample 16 with increased preheating temperature. This reduction in hardness may be attributed to the reduction in residual stresses offered by increasing the preheating temperature as both base metals have the same microstructural composition comprising coarse austenite grains. However, a subtle difference of about 5 HV was found to exist between the average hardness of the fusion zones of both studies, with the latter also exhibiting the lower hardness. The increased hardness observed in the former may be attributed to the relatively high level of retained residual stresses coupled with the interaction between the austenite, lathy delta ferrite and partially transformed austenite phases. The quotient of the hardness values of the fusion zone to the base metals for both studies, which is termed the hardening ratio, was considerably affected by increasing the preheating temperature. The hardening ratio was found to be 1.01 and 1.23 for studies 8 and 16, respectively. Thus, the preheating temperature is positively correlated with the hardening ratio of the weld joints.

The effect of post-weld treatment temperature was investigated using studies 9 and 15 with tempering temperatures of 331.8 ^{o}C and 668.2 ^{o}C, respectively. The cross-sectional views of the base metals and fusion zones of the studies are presented in Figure 4.31. Figure 4.31(a) and (b) represent the base metal region of sample 9 and 15, respectively, while Figure 4.31(c) and (e) and Figure 4.31(d) and (f) represent their respective fusion zones. The base metal micrographs revealed that the austenite grains are generally finer than those of the as-received base metals without post-weld treatment. The precipitation of delta ferrite was not evident due to the relatively slow cooling rate induced by tempering. The fine austenite grains in these regions account for the hardness observed in this region, with an average value of 184.3 HV and 179.9 HV for studies 9 and 15, respectively. The reduction of austenite grain size by tempering will result in an increased yield and tensile strength, as proposed by Hall Petch. In the fusion zone, a river-like pattern of austenite phase and delta ferrite was precipitated, as can be seen in Figure 4.31(c), while the FESEM micrographs in Figure 4.31(e) reveals that both vermicular delta ferrite (oval enclosed area) and lathy delta ferrite (rectangular enclosed area) were precipitated. But in sample 15, with increased tempering temperature, the lathy delta ferrite was absent as the microstructure comprised skeletal delta ferrite (indicated by the arrow in Figure 4.31(f)) dispersed in austenite matrix. Thus, increasing the temperature facilitated the dissolution of the lathy delta ferrite phase by providing the energy for the high-temperature transformation. Despite the deferritization by increased post-weld temperature, both studies' average hardness was almost the same, with sample 9 slightly higher by 2 HV. Consequently, the hardening ratio of both studies was not significantly influenced by increasing the post-weld temperature.

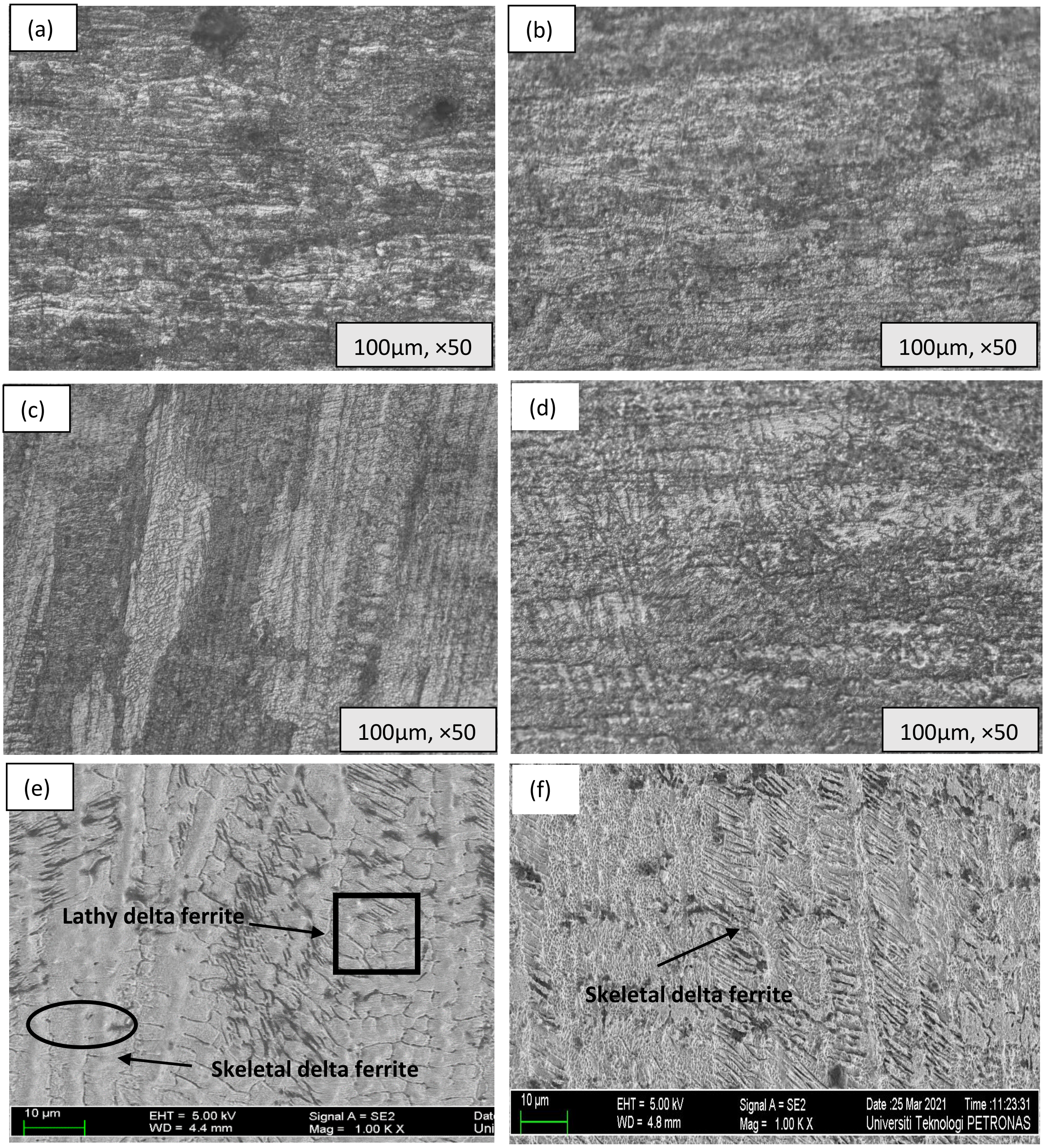

Figure 4.31: FZ and BM region of Study 9 and 15; (a) BM of study 9; (b)BM of study 15; (c) and (e) FZ of study 9; (d) and (f) FZ of study 8

Although delta ferrite was evolved after welding, the sigma phase was not precipitated when the post-weld treatment temperature was elevated. This might be attributed to the relatively slow transformation kinetics required for their formation. This is also evident in the relatively low average hardness of the fusion zone as sigma phase precipitation increases the hardness of the weld joint. Furthermore, carbides precipitation at the austenite - delta ferrite interface was also not observed. Nonetheless, carbide precipitation was reported in STS 304 austenitic stainless steel by Ma et al. [32]. The absence of carbides may be attributed to austenitic stainless steel's relatively low carbon content and partly due to the relatively low post-weld temperature. The probability that they were precipitated and dissolved due to the sufficient post-weld holing time is unlikely.

The effect of post-weld holding time was studied using sample 2 and 11 with holding times of 1.3 and 4.7 hours, respectively, at a constant preheating temperature and tempering temperature of 150 ^{o}C and 500 ^{o}C, respectively. Figure 4.32 shows the micrographs of the base metal and fusion zone of both studies.

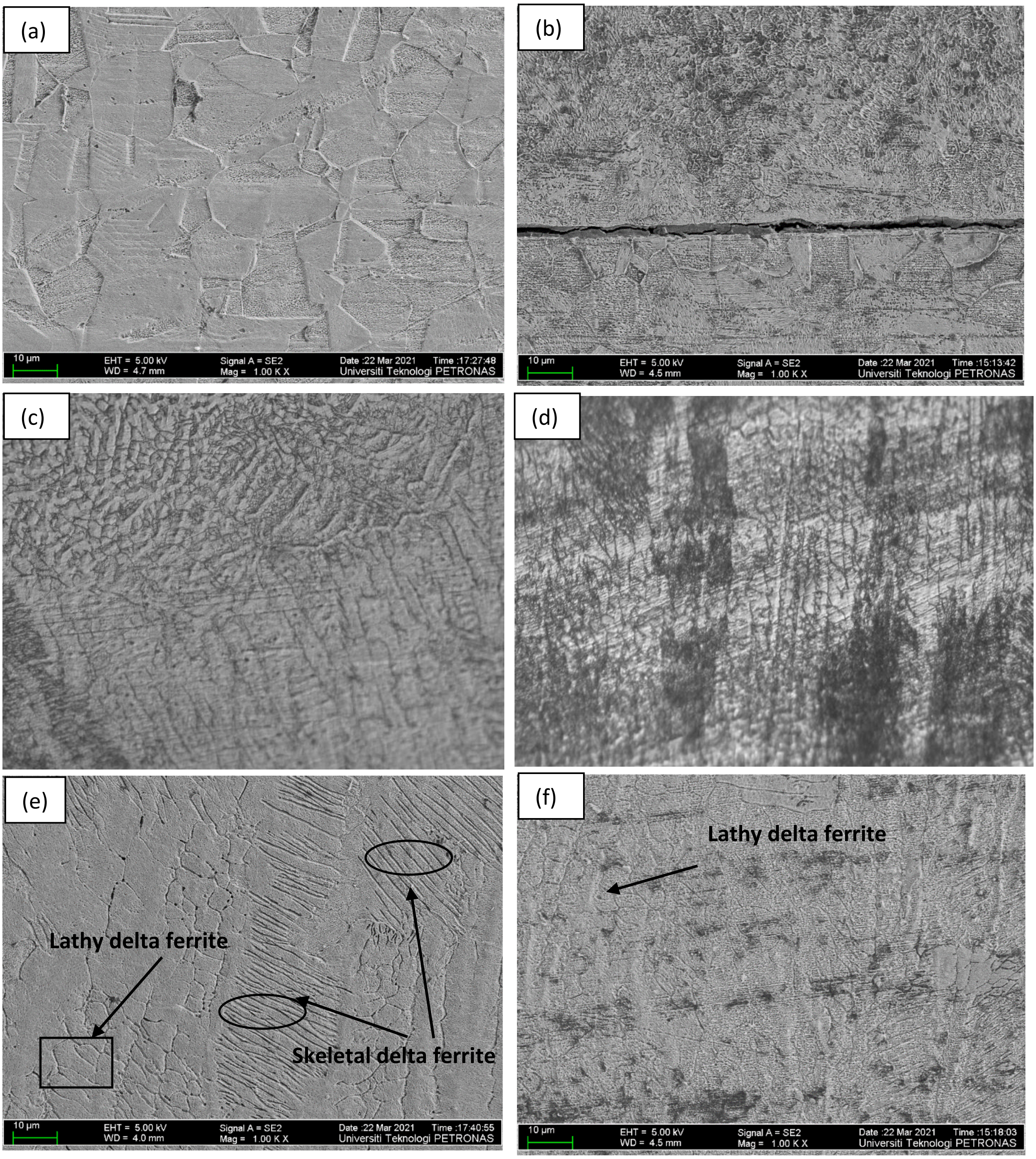

Figure 4.32: FZ and BM region of Study 11 and 2; (a) BM of study 11; (b) BM of study 2; (c) and (e) FZ of study 11; (d) and (f) FZ of Study 8

As shown in Figure 4.32(a) and (b) representing the base metal region of sample 11 and 2 respectively, the austenite grains appear to be relatively coarser in the former with increased holding time. The increased holding time facilitated the thermal-assisted migration of the austenite grain boundaries, thus, resulting in their growth. In addition to the release of residual stress induced by preheating, the hardness reduction in the base metal region in these studies accounts for the general reduction in hardness. The supplemental increment observed in the austenite grains accounts for the lower base metal average hardness. Despite reducing the hardness of the base metal, the increment in austenite grain size has a detrimental effect on the yield strength and tensile strength, as related by Hall Petch.

Accordingly, the fusion zone micrographs in Figure 4.32(e) revealed that sample 11 comprises both lathy delta ferrite (rectangular enclosed area) and skeletal delta ferrite (oval enclosed area); a form of vermicular delta ferrite, while sample 2 comprise mainly refined austenite grains and relatively finer lathy delta ferrite (arrow in Figure 4.32(f)) compared to the former. This implies that increasing the holding time by 3.4 hours provided sufficient time for the growth of the delta ferrite grains, which were precipitated during the initial welding process. The lower holding time in the latter resulted in the finer delta ferrite, as shown in Figure 4.32(e) and (f), respectively. It can be deduced that the holding time had no significant effect on phase transformation; rather, it only aided the growth of the already precipitated phases. Consequently, we can infer that the hardness reduction in the fusion zone observed in sample 11 is attributed primarily to the growth of delta ferrite phases and, secondarily, ferritization and release of residual stresses. Comparing the average hardness values of both studies, as expected, sample 11 exhibited a much lower hardness than the latter by 20.4 HV. This sample also exhibited the least (optimum) average fusion zone hardness (149.2 HV). It was also observed that the hardening ratio increased from 0.814 to 1.03 with increasing holding time. We can therefore imply that the holding time had a more significant effect on the hardening ratio than the temperature, but the former had a more significant effect on phase transformation.

4.12 Energy Dispersive X-ray (EDX) Elemental Mapping Analysis of Phase 2

Table 4.11 summarises the EDX elemental composition of the fusion zone of studies 8 and 16, 9 and 15, 2 and 11 used in the previous section to sample the effect of weld treatment parameters on the microstructural evolution.

Table 4.11: EDX analysis showing the phase stabilizers composition of different studies.

Sample	Cr	Mo	Si	Ni	Mn	Fe and others
8	14.80	2.26	0.49	8.20	1.71	73.03
16	15.18	1.65	0.49	8.24	1.72	72.72
9	16.10	2.26	0.43	8.44	1.61	71.16
15	15.56	2.29	0.46	7.91	1.71	72.07
2	16.22	2.44	0.39	9.26	1.60	70.09
11	17.69	-	0.47	9.37	1.78	70.69

The results obtained from the EDX analysis revealed that increasing the preheating temperature affected majorly the delta ferrite phase stabilizers causing an increase in the chromium content and a reduction in the molybdenum content, while no significant effect was recorded for the austenite phase stabilizers as observed in studies 8 and 16. The increment recorded in the chromium content is an indication of an increase in corrosion resistance which might be attributed to the reduction in phase interfaces as explained in the previous section. On the other hand, the constant composition of the austenite phase stabilizers implies that no major phase transformation in the phase was induced by preheating. Figure 4.33(a) and (b) depict the different elements' peaks in studies 8 and 16, respectively.

Thereafter, considering the elemental composition of studies 9 and 15 revealed that increasing the tempering temperature resulted in a reduction in both austenite and delta-ferrite stabilizers (chromium and nickel). The silicon content was fairly constant, while a slight increment was observed in the manganese composition. The reduction in chromium content may be attributed to the reduction in delta ferrite phase fraction induced by increasing the tempering temperature leading to deferritization. The peaks of the elemental composition of both studies are depicted in Figure 4.33(c) and (d), respectively.

Lastly, the elemental composition of studies 2 and 11, as shown in Table 4.11, revealed that increasing the holding time resulted in an increase in austenite (Nickel and Manganese) and delta ferrite phase stabilizers (chromium and silicon). The respective peaks are depicted in Figure 4.33(e) and (f). This justifies the explanation provided in the previous section regarding the grain growth of both phases with increasing time. This further shows that, in addition to a reduction in hardness of the fusion zone, increasing the holding time improves the corrosion resistance of the weld joint.

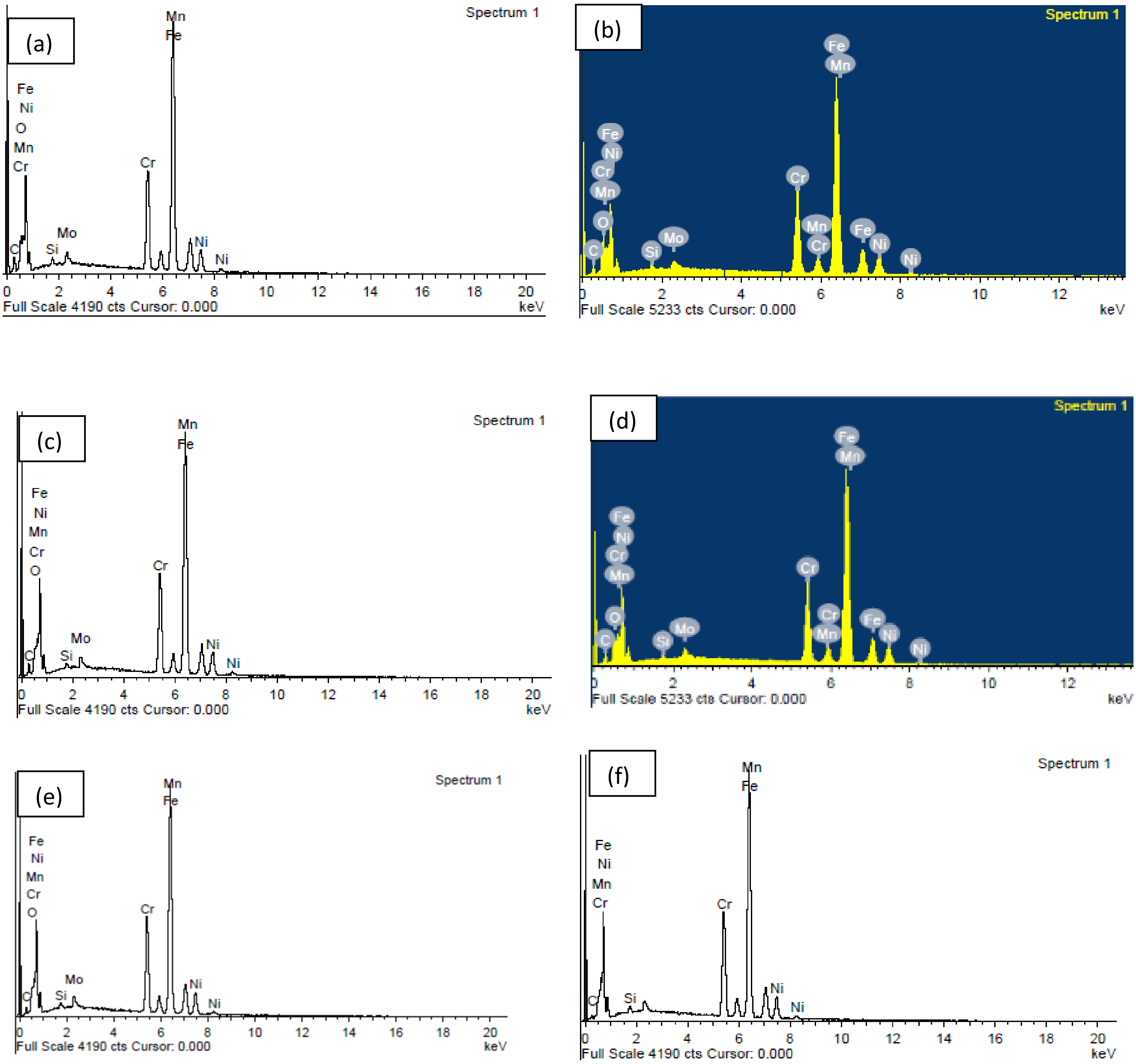

Figure 4.33**:** EDX analysis showing the peaks of the different elements present in the fusion zone of; (a) Study 8; (b) Study 16; (c) Study 9; (d) Study 15 (e) Study 2 (f) Study 11.

4.13 Chapter Summary

The analysis of the experimental results revealed that the most significant parameter affecting the nugget diameter is the welding current, followed by the welding time and then the electrode pressure. The Bivariate correlation analysis revealed that the nugget diameter is positively correlated with the welding current and time, while a negative correlation was observed for the electrode pressure. On the other hand, the average FZ hardness was not significantly influenced by the spot welding parameters, but their effect on the hardness was in the order of electrode pressure > welding current > welding time. Subsequently, the optimum parameters that simultaneously maximized the weld nugget diameter and minimized the FZ hardness of the weld joint were found to be 10.884 KA, 30 cycles and 5.822 bar for the welding current, welding time and electrode pressure, respectively, producing a weld joint with an average hardness of 196.707 HV and weld nugget of 9.837 mm. A subtle discrepancy between the predicted and experimental values was found to be 6.9 % and 3.7 % for weld nugget diameter and hardness, respectively.

Nonetheless, the most significant weld treatment parameter affecting the hardness of the weld joint is the holding time, then the preheating temperature and lastly, the tempering temperature. A positive correlation was also found between these parameters and the average hardness of the weld joint. The optimum parameters that minimise the hardness of the weld joints were 150 ^{o}C, 500 ^{o}C and 4.68 hours for the preheating temperature, tempering temperature, and holding time, respectively, producing an average weld hardness of 149.2 HV. The morphological analysis further revealed that the reduction in hardness is attributed to the ferritization of the fusion zone, the growth of austenite and delta ferrite grains and the release of residual stresses.

CHAPTER 5

CONCLUSION AND RECOMMENDATION

5.1 Chapter Overview

This chapter concludes the research work and also provides recommendations for further studies. The chapter was concluded with the major findings regarding the objectives slated out in the opening chapter. The proposed direction for further studies is a culmination of the findings of this research work which would serve as a substantial contribution to literature.

5.2 Conclusion

Following the results obtained from the experimentation and statistical analysis in the preceding section, the following conclusions were made.

The most significant parameter affecting the nugget diameter, in other words, the TSLBC, is the welding current followed by the welding time and least affected by the electrode pressure. The nugget diameter was found to increase with welding current and time, while a negative correlation was obtained for the electrode pressure. On the other hand, the hardness was dominantly affected by metallurgical factors relative to spot welding parameters. Consequently, the spot welding parameters that simultaneously optimize the nugget diameter and hardness were 10.884 KA, 30 cycles and 5.822 bar producing a nugget diameter and hardness of 9.2 mm and 204.3 HV, respectively and slightly different from the predicted by 6.9 % and 3.7 %, respectively.

The most significant weld treatment parameter affecting the weld joint's hardness was the holding time, with the least significant parameter being tempering temperature. The minimum weld hardness was found to be 149.2 HV at 150 ^{o}C, 500 ^{o}C and 4.68 hours preheating temperature, tempering temperature, and holding time, respectively. The overall hardness reduction was attributed to the ferritization of the fusion zone, the growth of austenite and delta ferrite grains and the release of residual stresses as revealed by the morphological analysis.

5.3 Recommendations

As a way of moving forward following the completion of this study, the following are suggestions for experimenters with similar research interests to explore:

1. To determine the spot welding parameters that would result in no fusion and expulsion in austenitic stainless steel, especially those with thickness greater than 1.5 mm (i.e., the minimum and maximum spot welding parameters) using RSM or other DOEs, as limited studies are available. Such information would come in handy in the construction of the welding lobe for the metal. In this study, only conditions of no fusion were observed.
2. To investigate the effect of increasing the holding time and the tempering temperature above 5 hrs and 700 ^{o}C, respectively, on the average FZ hardness of the weld joint using a suitable DOE. The scope of this study was limited to a tempering temperature of 668 ^{o}C and a holding time of 4.68 hours, where the optimum average FZ hardness was obtained.

REFERENCES

[1] E. F. W. Edward F. Wente, “Steel,” *Encylopeida Britannica*. 2019.

[2] “Handbook of Comparative Workd Steel Standards,” *Comp. Gen. Pharmacol.*, pp. 1–19, 2011.

[3] M. F. McGuire, “Austenitic Stainless Steels,” in *Encyclopedia of Materials: Science and Technology*, 2001.

[4] V. J. Badheka, S. K. Agrawal, and N. Shroff, “Resistance spot welding of martensitic stainless steel (SS420) - Part I,” *Int. J. Mech. Mater. Eng.*, vol. 4, no. 3, pp. 328–340, 2009.

[5] A. M. Al-Mukhtar, “Review of Resistance Spot Welding Sheets: Processes and Failure Mode,” *Adv. Eng. Forum*, vol. 17, pp. 31–57, 2016, doi: 10.4028/www.scientific.net/aef.17.31.

[6] B. Kocabekir, R. Kaçar, S. Gündüz, and F. Hayat, “An effect of heat input, weld atmosphere and weld cooling conditions on the resistance spot weldability of 316L austenitic stainless steel,” *J. Mater. Process. Technol.*, vol. 195, no. 1–3, pp. 327–335, 2008, doi: 10.1016/j.jmatprotec.2007.05.026.

[7] B. K. Srivastava, D. S. P. Tewari, and P. Jyoti, “A Review on the Effects of preheating and/or post weld treatment on the mechanical behaviour of Ferrous metals,” *Int. J. Eng. Sci. Technol.*, vol. 2, no. 4, pp. 625–631, 2010.

[8] S. Kumar, G. P. Chaudhari, S. K. Nath, and B. Basu, “Effect of preheat temperature on weldability of martensitic stainless steel,” *Mater. Manuf. Process.*, vol. 27, no. 12, pp. 1382–1386, 2012, doi: 10.1080/10426914.2012.700150.

[9] P. Gupta, G. Tenhundfeld, E. O. Daigle, and D. Ryabkov, “Electrolytic plasma technology: Science and engineering-An overview,” *Surf. Coatings Technol.*, vol. 201, no. 21 SPEC. ISS., pp. 8746–8760, 2007, doi: 10.1016/j.surfcoat.2006.11.023.

[10] C. Köse and R. Kaçar, “The effect of preheat & post weld heat treatment on the laser weldability of AISI 420 martensitic stainless steel,” *Mater. Des.*, vol. 64, pp. 221–226, 2014, doi: 10.1016/j.matdes.2014.07.044.

[11] F. Nikoosohbat, S. Kheirandish, M. Goodarzi, and M. Pouranvari, “Effect of Tempering on the Microstructure and Mechanical Properties of Resistance-Spot-Welded Dp980

Dual-Phase Steel," *Mater. Tehnol. / Mater. Technol.*, 2015, doi: 621.791.76/.79:539.4.016:621.785.72.

[12] R. D. SissonJr. *Encyclopedia of Materials Science and Technology*. 2001.

[13] M. Jayalakshmi, P. Huilgol, B. R. Bhat, and K. U. Bhat, "Microstructural characterization of low temperature plasma-nitrided 316L stainless steel surface with prior severe shot peening," *Mater. Des.*, vol. 108, pp. 448–454, 2016, doi: 10.1016/j.matdes.2016.07.005.

[14] A. U. Alkali, T. L. Gintar, H. Fawad, and A. M. Abdulrani, "Influence of preheat flux on the microstructure of 304 stainless steel," in *Applied Mechanics and Materials*, 2014, vol. 465–466, pp. 1287–1291, doi: 10.4028/www.scientific.net/AMM.465-466.1287.

[15] F. C. Liu, Y. Hovanski, M. P. Miles, C. D. Sorensen, and T. W. Nelson, "A review of friction stir welding of steels: Tool, material flow, microstructure, and properties," *J. Mater. Sci. Technol.*, vol. 34, no. 1, pp. 39–57, 2018, doi: 10.1016/j.jmst.2017.10.024.

[16] A. M. Al-Mukhtar and Q. M. Doos, "Cracking Phenomenon in Spot Welded Joints of Austenitic Stainless Steel," *Mater. Sci. Appl.*, vol. 04, no. 10, pp. 656–662, 2013, doi: 10.4236/msa.2013.410081.

[17] S. Fukumoto, K. Fujiwara, S. Toji, and A. Yamamoto, "Small-scale resistance spot welding of austenitic stainless steels," *Mater. Sci. Eng. A*, vol. 492, no. 1–2, pp. 243–249, 2008, doi: 10.1016/j.msea.2008.05.002.

[18] D. Kianersi, A. Mostafaei, and J. Mohammadi, "Effect of welding current and time on the microstructure, mechanical characterizations, and fracture studies of resistance spot welding joints of AISI 316L austenitic stainless steel," *Metall. Mater. Trans. A Phys. Metall. Mater. Sci.*, vol. 45, no. 10, pp. 4423–4442, 2014, doi: 10.1007/s11661-014-2421-z.

[19] Y. Zhang, J. Guo, Y. Li, Z. Luo, and X. Zhang, "A comparative study between the mechanical and microstructural properties of resistance spot welding joints among ferritic AISI 430 and austenitic AISI 304 stainless steel," *J. Mater. Res. Technol.*, vol. 9, no. 1, pp. 574–583, 2020, doi: 10.1016/j.jmrt.2019.10.086.

[20] M.Pouranvari, M. Alizadeh-Sh, and S. P. H. Marashi, "Welding metallurgy of stainless steels during resistance spot welding Part 1; fusion zone," *Inst. Mater. Miner. Min.*, vol. 20, no. 6, pp. 502–511, 2015, doi: 10.1179/1362171815Y.0000000015.

[21] F. Hayat and I. Sevim, “The effect of welding parameters on fracture toughness of resistance spot-welded galvanized DP600 automotive steel sheets,” *Int. J. Adv. Manuf. Technol.*, vol. 58, no. 9–12, pp. 1043–1050, 2012, doi: 10.1007/s00170-011-3428-x.

[22] H. Essoussi, S. Elmouhri, S. Ettaqi, and E. Essadiqi, “Microstructure and mechanical performance of resistance spot welding of AISI 304 stainless steel and AISI 1000 series steel,” *Procedia Manuf.*, vol. 32, pp. 872–876, 2019, doi: 10.1016/j.promfg.2019.02.296.

[23] H. L. Jaber, M. Pouranvari, R. K. Salim, F. A. Hashim, and S. P. H. Marashi, “Peak load and energy absorption of DP600 advanced steel resistance spot welds,” *Ironmak. Steelmak.*, vol. 44, no. 9, pp. 699–706, 2017, doi: 10.1080/03019233.2016.1229880.

[24] S. Richard, *The procedure handbook of arc welding*. 1995.

[25] T. H. Nam *et al.*, “Effect of post weld heat treatment on the microstructure and mechanical properties of a submerged-arc-welded 304 stainless steel,” *Metals (Basel).*, vol. 8, no. 26, pp. 1–13, 2018, doi: 10.3390/met8010026.

[26] S. S. M. Tavares, C. R. Rodrigues, J. M. Pardal, E. Da Silva Barbosa, and H. F. G. De Abreu, “Effects of post weld heat treatments on the microstructure and mechanical properties of dissimilar weld of supermartensític stainless steel,” *Mater. Res.*, vol. 17, no. 5, pp. 1336–1343, 2014, doi: 10.1590/1516-1439.299314.

[27] J. Luo, Y. Dong, L. Li, and X. Wang, “Microstructure of 2205 duplex stainless steel joint in submerged arc welding by post weld heat treatment,” *J. Manuf. Process.*, 2014, doi: 10.1016/j.jmapro.2013.06.013.

[28] M. Muhammed, M. Mustapha, T. L. Ginta, A. M. Ali, F. Mustapha, and C. C. Hampo, “Statistical Review of Microstructure-Property Correlation of Stainless Steel : Implication for Pre and Post-weld Treatment,” *MDPI Process.*, vol. 8, no. 7, pp. 1–32, 2020.

[29] Y. Murakami, *metal Fatigue*, Second Edi. 2019.

[30] J. R. Davis, “Alloy Digest Sourcebook: Stainless Steels,” *ASM Int.*, vol. 27, no. 9, pp. 624–635, 1999, doi: 10.2464/jilm.37.624.

[31] A. Foussat *et al.*, “Mechanical design and construction qualification program on ITER correction coils structures,” *Nucl. Eng. Des.*, vol. 269, pp. 116–124, 2014, doi: 10.1016/j.nucengdes.2013.08.016.

[32] H. Ma, G. Qin, P. Geng, F. Li, X. Meng, and B. Fu, "Effect of post-weld heat treatment on friction welded joint of carbon steel to stainless steel," *J. Mater. Process. Technol.*, vol. 227, pp. 24–33, 2016, doi: 10.1016/j.jmatprotec.2015.08.004.

[33] A. M. Al-Mukhtar, S. A. K. Al-Jumaili, and A. H. F. Al-Jlehawy, "Effect of Heat Treatments on 302 Austenitic Stainless Steel Spot Weld," *Adv. Eng. Forum*, vol. 29, pp. 19–25, 2018, doi: 10.4028/www.scientific.net/aef.29.19.

[34] "Chemical Compositions of AISI (ASTM/ASME) and UNS Austenitic Stainless Steel Grades," *British Stainless Steel Association*, 2021. [Online]. Available: https://bssa.org.uk/bssa_articles/chemical-compositions-of-aisi-astm-asme-and-uns-austenitic-stainless-steel-grades/. [Accessed: 16-Aug-2021].

[35] M. Theofanous and L. Gardner, "Experimental and numerical studies of lean duplex stainless steel beams," *J. Constr. Steel Res.*, vol. 66, no. 6, pp. 816–825, 2010, doi: 10.1016/j.jcsr.2010.01.012.

[36] M. De Abreu, M. Iordachescu, and A. Valiente, "Effects of hydrogen assisted stress corrosion on damage tolerance of a high-strength duplex stainless steel wire for prestressing concrete," *Constr. Build. Mater.*, vol. 66, pp. 38–44, 2014, doi: 10.1016/j.conbuildmat.2014.05.069.

[37] L. Yang, M. Zhao, T. M. Chan, F. Shang, and D. Xu, "Flexural buckling of welded austenitic and duplex stainless steel I-section columns," *J. Constr. Steel Res.*, vol. 122, pp. 339–353, 2016, doi: 10.1016/j.jcsr.2016.04.007.

[38] Z. Zhang, H. Zhang, L. He, D. Han, Y. Jiang, and J. Li, "Precipitation evolution in duplex stainless steel during isothermal aging at 700°C," *Mater. Sci. Technol. (United Kingdom)*, vol. 30, no. 4, pp. 451–457, 2014, doi: 10.1179/1743284713Y.0000000366.

[39] E. Medina, J. M. Medina, A. Cobo, and D. M. Bastidas, "Evaluation of mechanical and structural behavior of austenitic and duplex stainless steel reinforcements," *Constr. Build. Mater.*, vol. 78, pp. 1–7, 2015, doi: 10.1016/j.conbuildmat.2015.01.008.

[40] M. Martins and L. C. Casteletti, "Heat treatment temperature influence on ASTM A890 GR 6A super duplex stainless steel microstructure," *Mater. Charact.*, vol. 55, no. 3, pp. 225–233, 2005, doi: 10.1016/j.matchar.2005.05.008.

[41] J. D. Kordatos, G. Fourlaris, and G. Papadimitriou, "Effect of hydrogen and cooling rate on the mechanical and corrosion properties of SAF 2507 duplex stainless steel welds,"

Mater. Sci. Forum, vol. 318, pp. 615–620, 1999.

[42] C. Y. Chen, H. W. Yen, and J. R. Yang, "Sympathetic nucleation of austenite in a Fe-22Cr-5Ni duplex stainless steel," *Scr. Mater.*, vol. 56, no. 8, pp. 673–676, 2007, doi: 10.1016/j.scriptamat.2006.12.021.

[43] Y. C. Lin and S. C. Chen, "Effect of residual stress on thermal fatigue in a type 420 martensitic stainless steel weldment," *J. Mater. Process. Technol.*, vol. 138, no. 1–3, pp. 22–27, 2003, doi: 10.1016/S0924-0136(03)00043-8.

[44] V. Olden, C. Thaulow, and R. Johnsen, "Modelling of hydrogen diffusion and hydrogen induced cracking in supermartensitic and duplex stainless steels," *Mater. Des.*, vol. 29, no. 10, pp. 1934–1948, 2008, doi: 10.1016/j.matdes.2008.04.026.

[45] P. E. Kvaale and S. Olsen, "Experience with Supermartensitic Stainless Steels in Flowline Applications," in *Stainless Steel Word Conference, (The Netherlands)*, 1999, pp. 19–26.

[46] J. C. Lippold and D. J. Kotecki, *Martensitic Stainless Steel, Welding Metallurgy and Weldability Of Stainless Steels.*, First edit. New York: Wiley, 2005.

[47] C. Muthusamy, L. Karuppiah, S. Paulraj, D. Kandasami, and R. Kandhasamy, "Effect of heat input on mechanical and metallurgical properties of gas tungsten arc welded lean super martensitic stainless steel," *Mater. Res.*, vol. 19, no. 3, pp. 572–579, 2016, doi: 10.1590/1980-5373-MR-2015-0538.

[48] M. Sarkari Khorrami, M. A. Mostafaei, H. Pouraliakbar, and A. H. Kokabi, "Study on microstructure and mechanical characteristics of low-carbon steel and ferritic stainless steel joints," *Mater. Sci. Eng. A*, vol. 608, pp. 35–45, 2014, doi: 10.1016/j.msea.2014.04.065.

[49] H. H. Cho *et al.*, "Microstructural analysis of friction stir welded ferritic stainless steel," *Mater. Sci. Eng. A*, vol. 528, no. 6, pp. 2889–2894, 2011, doi: 10.1016/j.msea.2010.12.061.

[50] S. Elangovan, S. Balagopal, M. Timper, I. Bay, D. Larsen, and J. Hartvigsen, "Evaluation of ferritic stainless steel for use as metal interconnects for solid oxide fuel cells," *J. Mater. Eng. Perform.*, vol. 13, no. 3, pp. 265–273, 2004, doi: 10.1361/10599490419153.

[51] M. W. Dewan, J. Liang, M. A. Wahab, and A. M. Okeil, "Effect of post-weld heat

treatment and electrolytic plasma processing on tungsten inert gas welded AISI 4140 alloy steel," *Mater. Des.*, vol. 54, pp. 6–13, 2014, doi: 10.1016/j.matdes.2013.08.035.

[52] H. A. Nied, "The Finite Element Modeling of the Resistance Spot Welding Process An analytical tool is provided to predict the processing parameters needed to produce a spot weld with sufficient joint penetration," *Weld. Res. Suppl.*, pp. 123–132, 1984.

[53] Ó. Martín *et al.*, "Quality prediction of resistance spot welding joints of 304 austenitic stainless steel," *Mater. Des.*, vol. 30, no. 1, pp. 68–77, 2009, doi: 10.1016/j.matdes.2008.04.050.

[54] W. H. Zhang, X. M. Qiu, D. Q. Sun, and L. J. Han, "Effects of resistance spot welding parameters on microstructures and mechanical properties of dissimilar material joints of galvanised high strength steel and aluminium alloy," *Sci. Technol. Weld. Join.*, vol. 16, no. 2, pp. 153–161, 2011, doi: 10.1179/1362171810Y.0000000009.

[55] Y. B. Li, Q. X. Zhang, L. Qi, and S. A. David, "Improving austenitic stainless steel resistance spot weld quality using external magnetic field," *Sci. Technol. Weld. Join.*, vol. 23, no. 7, pp. 619–627, 2018, doi: 10.1080/13621718.2018.1443997.

[56] Miller, "Hand Book for Resistance Spot Welding," no. July, 2005.

[57] D. Kianersi, A. Mostafaei, and A. A. Amadeh, "Resistance spot welding joints of AISI 316L austenitic stainless steel sheets: Phase transformations, mechanical properties and microstructure characterizations," *Mater. Des.*, vol. 61, pp. 251–263, 2014, doi: 10.1016/j.matdes.2014.04.075.

[58] D. Zhao, Y. Wang, D. Liang, and P. Zhang, "Modeling and process analysis of resistance spot welded DP600 joints based on regression analysis," *Mater. Des.*, vol. 110, pp. 676–684, 2016, doi: 10.1016/j.matdes.2016.08.038.

[59] X. Q. Zhang, G. L. Chen, and Y. S. Zhang, "Characteristics of electrode wear in resistance spot welding dual-phase steels," *Mater. Des.*, vol. 29, no. 1, pp. 279–283, 2008, doi: 10.1016/j.matdes.2006.10.025.

[60] D. Özyürek, "An effect of weld current and weld atmosphere on the resistance spot weldability of 304L austenitic stainless steel," *Mater. Des.*, vol. 29, no. 3, pp. 597–603, 2008, doi: 10.1016/j.matdes.2007.03.008.

[61] I. S. Hwang, M. J. Kang, and D. C. Kim, "Expulsion reduction in resistance spot welding by controlling of welding current waveform," in *Procedia Engineering*, 2011, vol. 10,

pp. 2775–2781, doi: 10.1016/j.proeng.2011.04.461.

[62] H. Moshayedi and I. Sattari-Far, “Resistance spot welding and the effects of welding time and current on residual stresses,” *J. Mater. Process. Technol.*, vol. 214, no. 11, pp. 2545–2552, 2014, doi: 10.1016/j.jmatprotec.2014.05.008.

[63] Q. Fan, G. Xu, and X. Gu, “Expulsion characterization of stainless steel resistance spot welding based on dynamic resistance signal,” *J. Mater. Process. Technol.*, vol. 236, pp. 235–240, 2016, doi: 10.1016/j.jmatprotec.2016.05.026.

[64] M. Pouranvari, S. M. Mousavizadeh, S. P. H. Marashi, M. Goodarzi, and M. Ghorbani, “Influence of fusion zone size and failure mode on mechanical performance of dissimilar resistance spot welds of AISI 1008 low carbon steel and DP600 advanced high strength steel,” *Mater. Des.*, vol. 32, no. 3, pp. 1390–1398, 2011, doi: 10.1016/j.matdes.2010.09.010.

[65] M. Pouranvari, S. P. H. Marashi, and D. S. Safanama, “Failure mode transition in AHSS resistance spot welds. Part II: Experimental investigation and model validation,” *Mater. Sci. Eng. A*, vol. 528, no. 29–30, pp. 8344–8352, 2011, doi: 10.1016/j.msea.2011.08.016.

[66] M. Pouranvari and S. P. H. Marashi, “Failure mode transition in AHSS resistance spot welds. Part I. Controlling factors,” *Mater. Sci. Eng. A*, vol. 528, no. 29–30, pp. 8337–8343, 2011, doi: 10.1016/j.msea.2011.08.017.

[67] L. Han, M. Thornton, D. Boomer, and M. Shergold, “A correlation study of mechanical strength of resistance spot welding of AA5754 aluminium alloy,” *J. Mater. Process. Technol.*, pp. 513–521, 2011, doi: 10.1016/j.jmatprotec.2010.11.004.

[68] P. Pant, P. Dahlmann, W. Schlump, and G. Stein, “A new nitrogen alloying technique - a way to distinctly improve the properties of austenitic steel,” *Steel Research*, vol. 58, no. 1. pp. 18–25, 1987, doi: 10.1002/srin.198701482.

[69] S. Fukumoto, I. Lum, E. Biro, D. R. Boomer, and Y. Zhou, “Effects of electrode degradation on electrode life in resistance spot welding of aluminum alloy 5182,” *Weld. J. (Miami, Fla)*, vol. 82, no. 11, 2003.

[70] S. Fukumoto, Z. Chen, and Y. Zhou, “Interfacial phenomena and joint strength in resistance microwelding of crossed Au-plated Ni wires,” *Metall. Mater. Trans. A Phys. Metall. Mater. Sci.*, vol. 36, no. 10, pp. 2717–2724, 2005, doi: 10.1007/s11661-005-

0268-z.

[71] S. K. Khanna and X. Long, "Residual stresses in resistance spot welded steel joints," *Science and Technology of Welding and Joining*. 2008, doi: 10.1179/174329308X283884.

[72] V. A. Popovskiki and V. P. Berezienko, "Effect of resistance spot welding conditions on the distribution of residual stresses," *Weld. Int.*, vol. 2, no. 12, pp. 1058–1061, 1988, doi: 10.1080/09507118809447606.

[73] X. Wan, Y. Wang, and P. Zhang, "Modelling the effect of welding current on resistance spot welding of DP600 steel," *J. Mater. Process. Technol.*, vol. 214, no. 11, pp. 2723–2729, 2014, doi: 10.1016/j.jmatprotec.2014.06.009.

[74] A. Ramazani, K. Mukherjee, A. Abdurakhmanov, M. Abbasi, and U. Prahl, "Characterization of microstructure and mechanical properties of resistance spot welded DP600 steel," *Metals (Basel).*, vol. 5, no. 3, pp. 1704–1716, 2015, doi: 10.3390/met5031704.

[75] F. Badkoobeh, A. Nouri, H. Hassannejad, and H. Mostaan, "Microstructure and mechanical properties of resistance spot welded dual-phase steels with various silicon contents," *Mater. Sci. Eng. A*, vol. 790, no. January, p. 139703, 2020, doi: 10.1016/j.msea.2020.139703.

[76] I. Sevim, "Fracture toughness of spot-welded steel joints," *Kov. Mater.*, vol. 43, no. 2, pp. 113–123, 2005.

[77] I. Sevim, "Effect of hardness to fracture toughness for spot welded steel sheets," *Mater. Des.*, vol. 27, no. 1, pp. 21–30, 2006, doi: 10.1016/j.matdes.2004.09.008.

[78] D. W. Zhao, Y. X. Wang, L. Zhang, and P. Zhang, "Effects of electrode force on microstructure and mechanical behavior of the resistance spot welded DP600 joint," *Mater. Des.*, vol. 50, pp. 72–77, 2013, doi: 10.1016/j.matdes.2013.02.016.

[79] M. Alizadeh-Sh, S. P. H. Marashi, and M. Pouranvari, "Microstructure–properties relationships in martensitic stainless steel resistance spot welds," *Sci. Technol. Weld. Join.*, vol. 19, no. 7, pp. 595–602, 2014, doi: 10.1179/1362171814Y.0000000230.

[80] M. Tamizi, M. Pouranvari, and M. Movahedi, "Welding metallurgy of martensitic advanced high strength steels during resistance spot welding," *Sci. Technol. Weld. Join.*, vol. 22, no. 4, pp. 327–335, 2017, doi: 10.1080/13621718.2016.1240979.

[81] M. Pouranvari, S. Sobhani, and F. Goodarzi, "Resistance spot welding of MS1200 martensitic advanced high strength steel: Microstructure-properties relationship," *J. Manuf. Process.*, vol. 31, pp. 867–874, 2018, doi: 10.1016/j.jmapro.2018.01.009.

[82] M. Pouranvari, H. Aghajani, and A. Ghasemi, "Enhanced mechanical properties of martensitic stainless steels resistance spot welds enabled by in situ rapid tempering," *Sci. Technol. Weld. Join.*, vol. 25, no. 2, pp. 119–126, 2020, doi: 10.1080/13621718.2019.1641962.

[83] M. Alizadeh-Sh, S. P. H. Marashi, and M. Pouranvari, "Resistance spot welding of AISI 430 ferritic stainless steel: Phase transformations and mechanical properties," *Mater. Des.*, vol. 56, pp. 258–263, 2014, doi: 10.1016/j.matdes.2013.11.022.

[84] M. Alizadeh-Sh, M. Pouranvari, and S. P. H. Marashi, "Welding metallurgy of stainless steels during resistance spot welding part II –heat affected zone and mechanical performance," *Sci. Technol. Weld. Join.*, vol. 20, no. 6, pp. 512–521, 2015, doi: 10.1179/1362171815Y.0000000010.

[85] M. Pouranvari, M. Alizadeh-Sh, and S. P. H. Marashi, "Welding metallurgy of stainless steels during resistance spot welding part I: Fusion zone," *Sci. Technol. Weld. Join.*, vol. 20, no. 6, pp. 502–511, 2015, doi: 10.1179/1362171815Y.0000000015.

[86] A. Subrammanian, D. B. Jabaraj, and J. Jayaprakash, "Multi-objective optimization of resistance spot welding of AISI 409M ferritic stainless steel," *J. Sci. Ind. Res. (India).*, vol. 77, no. 5, pp. 276–281, 2018.

[87] M. Pouranvari and S. P. H. Marashi, "Critical review of automotive steels spot welding: Process, structure and properties," *Sci. Technol. Weld. Join.*, vol. 18, no. 5, pp. 361–403, 2013, doi: 10.1179/1362171813Y.0000000120.

[88] M. Vural, A. Akkuş, and B. Eryürek, "Effect of welding nugget diameter on the fatigue strength of the resistance spot welded joints of different steel sheets," *J. Mater. Process. Technol.*, vol. 176, no. 1–3, pp. 127–132, 2006, doi: 10.1016/j.jmatprotec.2006.02.026.

[89] L. Kolařík, M. Sahul, M. Kolaříková, M. Sahul, M. Turňa, and M. Felix, "Resistance spot welding of dissimilar steels," *Acta Polytech.*, vol. 52, no. 3, pp. 43–47, 2012, doi: 10.14311/1548.

[90] X. Yuan, C. Li, J. Chen, X. Li, X. Liang, and X. Pan, "Resistance spot welding of dissimilar DP600 and DC54D steels," *J. Mater. Process. Technol.*, vol. 239, pp. 31–41,

2017, doi: 10.1016/j.jmatprotec.2016.08.012.

[91] K. Kishore, P. Kumar, and G. Mukhopadhyay, “Resistance spot weldability of galvannealed and bare DP600 steel,” *J. Mater. Process. Technol.*, vol. 271, no. September 2018, pp. 237–248, 2019, doi: 10.1016/j.jmatprotec.2019.04.005.

[92] R. W. Rathbun, D. K. Matlock, and J. G. Speer, “Fatigue behavior of spot welded high-strength sheet steels,” *Weld. J. (Miami, Fla)*, vol. 82, no. 8, 2003.

[93] S. Dancette, D. Fabrègue, V. Massardier, J. Merlin, T. Dupuy, and M. Bouzekri, “Experimental and modeling investigation of the failure resistance of Advanced High Strength Steels spot welds,” *Eng. Fract. Mech.*, vol. 78, no. 10, pp. 2259–2272, 2011, doi: 10.1016/j.engfracmech.2011.04.013.

[94] M. Pouranvari and S. P. H. Marashi, “Failure of resistance spot welds: Tensile shear versus coach peel loading conditions,” *Ironmak. Steelmak.*, vol. 39, no. 2, pp. 104–111, 2012, doi: 10.1179/1743281211Y.0000000066.

[95] A. N. B. A. C. V. NIELSEN, K. S. FRIIS, W. ZHANG, “Welding of advanced high-strength sheet steels,” *Weld. Int.*, vol. 25, no. 5, pp. 389–396, 2011, doi: 10.1080/09507116.2011.554234.

[96] A. G. Thakur and V. M. Nandedkar, “Application of Taguchi method to determine resistance spot welding conditions of austenitic stainless steel AISI 304,” *J. Sci. Ind. Res. (India).*, vol. 69, no. 9, pp. 680–683, 2010.

[97] N. K. Singh and Y. Vijayakumar, “Application of Taguchi method for optimization of resistance spot welding of austenitic stainless steel AISI 301L,” *Innov. Syst. Des. Eng.*, vol. 3, no. 10, pp. 49–61, 2012.

[98] R. Kumar, J. S. Chohan, R. Goyal, and P. Chauhan, “Impact of process parameters of resistance spot welding on mechanical properties and micro hardness of stainless steel 304 weldments,” *Int. J. Struct. Integr.*, 2020, doi: 10.1108/IJSI-03-2020-0031.

[99] H. T. Sun, X. M. Lai, Y. S. Zhang, and J. Shen, “Effect of variable electrode force on weld quality in resistance spot welding,” *Sci. Technol. Weld. Join.*, vol. 12, no. 8, pp. 718–724, 2007, doi: 10.1179/174329307X251862.

[100] D. Zhao, Y. Wang, S. Sheng, and Z. Lin, “Multi-objective optimal design of small scale resistance spot welding process with principal component analysis and response surface methodology,” *J. Intell. Manuf.*, vol. 25, no. 6, pp. 1335–1348, 2014, doi:

10.1007/s10845-013-0733-2.

[101] S. Shafee, B. B. Naik, and K. Sammaiah, “Resistance Spot Weld Quality Characteristics Improvement By Taguchi Method,” in *Materials Today: Proceedings*, 2015, vol. 2, no. 4–5, pp. 2595–2604, doi: 10.1016/j.matpr.2015.07.215.

[102] P. Ravichandran, C. Anbu, B. Meenakshipriya, and S. Sathiyavathi, “Process parameter optimization and performance comparison of AISI 430 and AISI 1018 in resistance spot welding process,” *Mater. Today Proc.*, vol. 33, pp. 3389–3393, 2020, doi: 10.1016/j.matpr.2020.05.197.

[103] D. Zhao, M. Ivanov, Y. Wang, D. Liang, and W. Du, “Multi-objective optimization of the resistance spot welding process using a hybrid approach,” *J. Intell. Manuf.*, 2020, doi: 10.1007/s10845-020-01638-2.

[104] K. Vignesh, A. Elaya Perumal, and P. Velmurugan, “Optimization of resistance spot welding process parameters and microstructural examination for dissimilar welding of AISI 316L austenitic stainless steel and 2205 duplex stainless steel,” *Int. J. Adv. Manuf. Technol.*, vol. 93, no. 1–4, pp. 455–465, 2017, doi: 10.1007/s00170-017-0089-4.

[105] A. K. Biradar and B. M. Dabade, “Optimization of resistance spot welding process parameters in dissimilar joint of MS and ASS 304 sheets,” *Mater. Today Proc.*, vol. 26, pp. 1284–1288, 2019, doi: 10.1016/j.matpr.2020.02.256.

[106] A. E. Hernández, L. O. Villarinho, V. A. Ferraresi, M. S. Orozco, A. S. Roca, and H. C. Fals, “Optimization of resistance spot welding process parameters of dissimilar DP600/AISI304 joints using the infrared thermal image processing,” *Int. J. Adv. Manuf. Technol.*, vol. 108, no. 1–2, pp. 211–221, 2020, doi: 10.1007/s00170-020-05374-y.

[107] T. Khaled, “Preheating , Interpass and Post-Weld Heat Treatment Requirements for Welding Low Alloy Steels,” vol. 6, no. October, pp. 1–14, 2014.

[108] H. Cable and R. S. Funderburk, “Technology Transfer: The Basics,” *Weld. Innov.*, vol. XIV, no. 2, pp. 16–17, 1997.

[109] J. T. Connor, T. G. Digges, S. J. Rosenberg, and G. W. Geil, “Heat Treatment and Properties of Iron and Steel Approved for Public Release,” pp. 1–46, 1966.

[110] D. N. Hawkins, “Heat treatment of steels,” *Steel Times*, vol. 217, no. 5, pp. 284–285, 1989, doi: 10.1201/9781439895238-10.

[111] T. Gela, “Mechanical Design Haandbook,” in *Mechanical Design Handbook*, Hoboken: New Jersey: McGraw-Hill, 2006, pp. 1–48.

[112] S. Kozuh, M. Gojic, and Kose, “Mechanical properties and microstructure of austenitic stainless steel after welding and post-weld heat treatment,” *Kov. Mater.*, vol. 47, no. 4, pp. 253–262, 2009.

[113] J. Lippold and D. Kotecki, *Welding metallurgy and weldability of stainless steels.* Hoboken: New Jersey, 2005.

[114] C. C. Tseng, Y. Shen, S. W. Thompson, M. C. Mataya, and G. Krauss, “Fracture and the formation of sigma phase, M23C6, and austenite from delta-ferrite in an AlSl 304L stainless steel,” *Metall. Mater. Trans. A*, vol. 25, no. 6, pp. 1147–1158, 1994, doi: 10.1007/BF02652290.

[115] I. Hamada and K. Yamauchi, “Sensitization behavior of type 308 stainless steel weld metals after postweld heat treatment and low-temperature aging and its relation to microstructure,” *Metall. Mater. Trans. A Phys. Metall. Mater. Sci.*, vol. 33, no. 6, pp. 1743–1754, 2002, doi: 10.1007/s11661-002-0183-5.

[116] H. Sahlaoui and H. Sidhom, “Experimental investigation and analytical prediction of σ-phase precipitation in AISI 316L austenitic stainless steel,” *Metall. Mater. Trans. A Phys. Metall. Mater. Sci.*, vol. 44, no. 7, pp. 3077–3083, 2013, doi: 10.1007/s11661-013-1647-5.

[117] H. Sahlaoui, H. Sidhom, and J. Philibert, “Prediction of chromium depleted-zone evolution during aging of Ni-Cr-Fe alloys,” *Acta Mater.*, vol. 50, no. 6, pp. 1383–1392, 2002, doi: 10.1016/S1359-6454(01)00444-X.

[118] M. V. Deo, P. Michaleris, and J. Sun, “Prediction of buckling distortion of welded structures,” *Sci. Technol. Weld. Join.*, vol. 8, no. 1, pp. 55–61, 2003, doi: 10.1179/13621710322500900.

[119] M. V. Deo and P. Michaleris, “Mitigation of welding induced buckling distortion using transient thermal tensioning,” *Sci. Technol. Weld. Join.*, vol. 8, no. 1, pp. 49–54, 2003, doi: 10.1179/136217103225008919.

[120] X. Yuan, L. Chen, Y. Zhao, H. Di, and F. Zhu, “Influence of annealing temperature on mechanical properties and microstructures of a high manganese austenitic steel,” *J. Mater. Process. Technol.*, vol. 217, pp. 278–285, 2015, doi:

10.1016/j.jmatprotec.2014.11.027.

[121] K. A. Venkata, S. Kumar, H. C. Dey, D. J. Smith, P. J. Bouchard, and C. E. Truman, "Study on the effect of post weld heat treatment parameters on the relaxation of welding residual stresses in electron beam welded P91 steel plates," *Procedia Eng.*, vol. 86, no. Grade 91, pp. 223–233, 2014, doi: 10.1016/j.proeng.2014.11.032.

[122] C. J. Rosen, A. Gumenyuk, H. Zhao, and U. Dilthey, "Influence of local heat treatment on residual stresses in electron beam welding," *Sci. Technol. Weld. Join.*, vol. 12, no. 7, pp. 614–619, 2007, doi: 10.1179/174329307X227247.

[123] W. T. Jia, J. P. Zhao, and J. Cao, "The Mitigation of Weld Residual Stress on 304L Stainless Steel by Post Weld Cool Treatment Process," *Appl. Mech. Mater.*, vol. 853, pp. 209–215, 2016, doi: 10.4028/www.scientific.net/amm.853.209.

[124] J. Xin, C. Fang, Y. Song, J. Wei, S. Xu, and J. Wu, "Effect of post weld heat treatment on the microstructure and mechanical properties of ITER-grade 316LN austenitic stainless steel weldments," *Cryogenics (Guildf).*, 2017, doi: 10.1016/j.cryogenics.2017.02.001.

[125] E. M. Oluwatobi, "Effect of Pre and Post-Heattreament on the Heat-Affected-Zone (HAZ) of Austenitic Stainless -Steel," 2017.

[126] H. R. Zareie Rajani, H. Torkamani, M. Sharbati, and S. Raygan, "Corrosion resistance improvement in Gas Tungsten Arc Welded 316L stainless steel joints through controlled preheat treatment," *Mater. Des.*, 2012, doi: 10.1016/j.matdes.2011.07.071.

[127] T. Saeid, A. Abdollah-zadeh, T. Shibayanagi, K. Ikeuchi, and H. Assadi, "On the formation of grain structure during friction stir welding of duplex stainless steel," *Mater. Sci. Eng. A*, vol. 527, no. 24–25, pp. 6484–6488, 2010, doi: 10.1016/j.msea.2010.07.011.

[128] T. Kuroda, K. Ikeuchi, and H. Ikeda, "Flash butt resistance welding for duplex stainless steels," *Vacuum*, vol. 80, no. 11–12, pp. 1331–1335, 2006, doi: 10.1016/j.vacuum.2006.01.068.

[129] S. G. Wang, G. P. Dong, and Q. H. Ma, "Welding of duplex stainless steel composite plate: Influence on microstructural development," *Mater. Manuf. Process.*, vol. 24, no. 12, pp. 1383–1388, 2009, doi: 10.1080/10426910902997456.

[130] J. Luo, Y. Dong, L. Li, and X. Wang, "Microstructure of 2205 duplex stainless steel

joint in submerged arc welding by post weld heat treatment," *J. Manuf. Process.*, vol. 16, no. 1, pp. 144–148, 2014, doi: 10.1016/j.jmapro.2013.06.013.

[131] X. Sun, E. V. Stephens, and M. A. Khaleel, "Effects of fusion zone size and failure mode on peak load and energy absorption of advanced high strength steel spot welds under lap shear loading conditions," *Eng. Fail. Anal.*, vol. 15, no. 4, pp. 356–367, 2008, doi: 10.1016/j.engfailanal.2007.01.018.

[132] A. H. I. Mourad, A. Khourshid, and T. Sharef, "Gas tungsten arc and laser beam welding processes effects on duplex stainless steel 2205 properties," *Mater. Sci. Eng. A*, vol. 549, pp. 105–113, 2012, doi: 10.1016/j.msea.2012.04.012.

[133] H. Sarlak, M. Atapour, and M. Esmailzadeh, *Corrosion behavior of friction stir welded lean duplex stainless steel*, vol. 66, no. PA. Elsevier Ltd, 2015.

[134] R. Badji, M. Bouabdallah, B. Bacroix, C. Kahloun, K. Bettahar, and N. Kherrouba, "Effect of solution treatment temperature on the precipitation kinetic of σ-phase in 2205 duplex stainless steel welds," *Mater. Sci. Eng. A*, vol. 496, no. 1–2, pp. 447–454, 2008, doi: 10.1016/j.msea.2008.06.024.

[135] K. D. Ramkumar *et al.*, "Metallurgical and mechanical characterization of electron beam welded super-duplex stainless steel UNS 32750," *J. Manuf. Process.*, vol. 16, no. 4, pp. 527–534, 2014, doi: 10.1016/j.jmapro.2014.07.011.

[136] Y. Yang, B. Yan, J. Li, and J. Wang, "The effect of large heat input on the microstructure and corrosion behaviour of simulated heat affected zone in 2205 duplex stainless steel," *Corros. Sci.*, vol. 53, no. 11, pp. 3756–3763, 2011, doi: 10.1016/j.corsci.2011.07.022.

[137] H. Sieurin and R. Sandström, "Austenite reformation in the heat-affected zone of duplex stainless steel 2205," *Mater. Sci. Eng. A*, vol. 418, no. 1–2, pp. 250–256, 2006, doi: 10.1016/j.msea.2005.11.025.

[138] J. Verma and R. V. Taiwade, "Effect of welding processes and conditions on the microstructure, mechanical properties and corrosion resistance of duplex stainless steel weldments—A review," *J. Manuf. Process.*, vol. 25, pp. 134–152, 2017, doi: 10.1016/j.jmapro.2016.11.003.

[139] F. Nikoosohbat, S. Kheirandish, M. Goodarzi, and M. Pouranvari, "Effect of Tempering on the microstructure and mechanical roperties of Resistance spot welded DP980 Dual Phase steel.," *Mater. Technol.*, vol. 49, no. 1, pp. 133–138, 2015, doi:

10.1016/j.msea.2014.11.005.

[140] H. Tan *et al.*, “Influence of welding thermal cycles on microstructure and pitting corrosion resistance of 2304 duplex stainless steels,” *Corros. Sci.*, vol. 55, pp. 368–377, 2012, doi: 10.1016/j.corsci.2011.10.039.

[141] Y. Yang *et al.*, “Effect of a brief post-weld heat treatment on the microstructure evolution and pitting corrosion of laser beam welded UNS S31803 duplex stainless steel,” *Corros. Sci.*, vol. 65, pp. 472–480, 2012, doi: 10.1016/j.corsci.2012.08.054.

[142] R. A. Perren *et al.*, “Corrosion resistance of super duplex stainless steels in chloride ion containing environments: Investigations by means of a new microelectrochemical method. I. Precipitation-free states,” *Corros. Sci.*, vol. 43, no. 4, pp. 707–726, 2001, doi: 10.1016/S0010-938X(00)00087-1.

[143] F. Malek Ghaini, M. J. Hamedi, M. J. Torkamany, and J. Sabbaghzadeh, “Weld metal microstructural characteristics in pulsed Nd: YAG laser welding,” *Scr. Mater.*, vol. 56, no. 11, pp. 955–958, 2007, doi: 10.1016/j.scriptamat.2007.02.019.

[144] S. Saravanan, K. Raghukandan, and N. Sivagurumanikandan, “Pulsed Nd: YAG laser welding and subsequent post-weld heat treatment on super duplex stainless steel,” *J. Manuf. Process.*, vol. 25, pp. 284–289, 2017, doi: 10.1016/j.jmapro.2016.12.015.

[145] A. Pramanik, G. Littlefair, and A. K. Basak, “Weldability of duplex stainless steel,” *Mater. Manuf. Process.*, vol. 30, no. 9, pp. 1053–1068, 2015, doi: 10.1080/10426914.2015.1019126.

[146] S. Saravanan, K. Raghukandan, and N. Sivagurumanikandan, “Studies on metallurgical and mechanical properties of laser welded dissimilar grade steels,” *J. Brazilian Soc. Mech. Sci. Eng.*, 2017, doi: 10.1007/s40430-016-0658-8.

[147] H. Liu and X. Jin, “Electrochemical corrosion behavior of the laser continuous heat treatment welded joints of 2205 duplex stainless steel,” *J. Wuhan Univ. Technol. Mater. Sci. Ed.*, vol. 26, no. 6, pp. 1140–1147, 2011, doi: 10.1007/s11595-011-0378-y.

[148] H. H. Kellogg, “Anode Effect in Aqueous Electrolysis,” *J. Electrochem. Soc.*, vol. 97, no. 4, p. 133, 1950, doi: 10.1149/1.2777980.

[149] J. Liang, K. Y. Wang, S. M. Guo, and M. A. Wahab, “Influence of electrolytic plasma process on corrosion property of peened 304 austenitic stainless steel,” *Mater. Lett.*, vol. 65, no. 3, pp. 510–513, 2011, doi: 10.1016/j.matlet.2010.10.089.

[150] R. Selvabharathi and R. Muralikannan, “Influence of shot peening and plasma ion nitriding on tensile strength of 2205 duplex stainless steel using A-PAW,” *Mater. Sci. Eng. A*, vol. 709, no. August 2017, pp. 232–240, 2018, doi: 10.1016/j.msea.2017.10.068.

[151] E. Richter, R. Günzel, S. Parasacandola, T. Telbizova, O. Kruse, and W. Möller, “Nitriding of stainless steel and aluminium alloys by plasma immersion ion implantation,” *Surf. Coatings Technol.*, vol. 128–129, pp. 21–27, 2000, doi: 10.1016/S0257-8972(00)00638-1.

[152] L. Schäfer, “Influence of delta ferrite and dendritic carbides on the impact and tensile properties of a martensitic chromium steel,” *J. Nucl. Mater.*, vol. 258–263, no. PART 2 B, pp. 1336–1339, 1998, doi: 10.1016/S0022-3115(98)00200-1.

[153] K. Anderko, L. Schäfer, and E. Materna-Morris, “Effect of the δ-ferrite phase on the impact properties of martensitic chromium steels,” *J. Nucl. Mater.*, vol. 179–181, no. PART 1, pp. 492–495, 1991, doi: 10.1016/0022-3115(91)90132-Q.

[154] S. H. Baghjari and S. A. A. Akbari Mousavi, “Effects of pulsed Nd: YAG laser welding parameters and subsequent post-weld heat treatment on microstructure and hardness of AISI 420 stainless steel,” *Mater. Des.*, vol. 43, pp. 1–9, 2013, doi: 10.1016/j.matdes.2012.06.027.

[155] P. Bilmes, C. Llorente, and J. Pérez Ipiña, “Toughness and microstructure of 13Cr4NiMo high-strength steel welds,” *J. Mater. Eng. Perform.*, vol. 9, no. 6, pp. 609–615, 2000, doi: 10.1361/105994900770345458.

[156] B. Kurt, N. Orhan, I. Somunkiran, and M. Kaya, “The effect of austenitic interface layer on microstructure of AISI 420 martensitic stainless steel joined by keyhole PTA welding process,” *Mater. Des.*, vol. 30, no. 3, pp. 661–664, 2009, doi: 10.1016/j.matdes.2008.05.027.

[157] C. R. Das *et al.*, “Mechanical properties of 9Cr-1W reduced activation ferritic martensitic steel weldment prepared by electron beam welding process,” *Fusion Eng. Des.*, vol. 89, no. 11, pp. 2672–2678, 2014, doi: 10.1016/j.fusengdes.2014.07.001.

[158] M. Taneike, K. Sawada, and F. Abe, “Effect of carbon concentration on precipitation behavior of M23C6 carbides and MX carbonitrides in martensitic 9Cr steel during heat treatment,” *Metall. Mater. Trans. A Phys. Metall. Mater. Sci.*, vol. 35 A, no. 4, pp. 1255–1262, 2004, doi: 10.1007/s11661-004-0299-x.

[159] J. R. Berretta, W. de Rossi, M. David Martins das Neves, I. Alves de Almeida, and N. Dias Vieira Junior, “Pulsed Nd:YAG laser welding of AISI 304 to AISI 420 stainless steels,” *Opt. Lasers Eng.*, vol. 45, no. 9, pp. 960–966, 2007, doi: 10.1016/j.optlaseng.2007.02.001.

[160] M. M. A. Khan, L. Romoli, M. Fiaschi, F. Sarri, and G. Dini, “Experimental investigation on laser beam welding of martensitic stainless steels in a constrained overlap joint configuration,” *J. Mater. Process. Technol.*, vol. 210, no. 10, pp. 1340–1353, 2010, doi: 10.1016/j.jmatprotec.2010.03.024.

[161] M. M. A. Khan, L. Romoli, R. Ishak, M. Fiaschi, G. Dini, and M. De Sanctis, “Experimental investigation on seam geometry, microstructure evolution and microhardness profile of laser welded martensitic stainless steels,” *Opt. Laser Technol.*, vol. 44, no. 5, pp. 1611–1619, 2012, doi: 10.1016/j.optlastec.2011.11.035.

[162] S. Zappa, H. Svoboda, and E. Surian, “Effect of Post-weld Heat Treatment on the Mechanical Properties of Supermartensitic Stainless Steel Deposit,” *J. Mater. Eng. Perform.*, vol. 26, no. 2, pp. 514–521, 2017, doi: 10.1007/s11665-016-2467-8.

[163] V. L. Manugula, K. V Rajulapati, G. M. Reddy, and K. B. S. Rao, “Role of evolving microstructure on the mechanical properties of electron beam welded ferritic-martensitic steel in the as-welded and post weld heat-treated states,” *Mater. Sci. Eng. A*, vol. 698, pp. 36–45, 2017, doi: 10.1016/j.msea.2017.05.036.

[164] X. Li *et al.*, “Effect of post weld heat treatment on the microstructure and properties of Laser-TIG hybrid welded joints for CLAM steel,” *Fusion Eng. Des.*, pp. 175–181, 2018, doi: 10.1016/j.fusengdes.2018.02.034.

[165] S. Sundaresan, M. Manirajan, and B. Nageswara Rao, “On the fracture toughness evaluation in weldments of a maraging steel rocket motor case,” *Mater. Des.*, vol. 31, no. 10, pp. 4921–4926, 2010, doi: 10.1016/j.matdes.2010.05.022.

[166] G. M. Reddy, V. V. Rao, and A. V. S. Raju, “The effect of post-weld heat treatments on the microstructure and mechanical properties of maraging steel laser weldments,” *Proc. Inst. Mech. Eng. Part L J. Mater. Des. Appl.*, vol. 223, no. 4, pp. 149–159, 2009, doi: 10.1243/14644207JMDA258.

[167] J. An *et al.*, “Improvement of mechanical properties of stainless maraging steel laser weldments by post-weld ageing treatments,” *Mater. Des.*, vol. 40, pp. 276–284, 2012, doi: 10.1016/j.matdes.2012.03.020.

[168] P. Venkata Ramana, G. Madhusudhan Reddy, T. Mohandas, and A. V. S. S. K. S. Gupta, “Microstructure and residual stress distribution of similar and dissimilar electron beam welds - Maraging steel to medium alloy medium carbon steel,” *Mater. Des.*, vol. 31, no. 2, pp. 749–760, 2010, doi: 10.1016/j.matdes.2009.08.007.

[169] M. Jahazi and B. Egbali, “The influence of hot rolling parameters on the micro structure and mechanical properties of an ultra-high strength steel,” *J. Mater. Process. Technol.*, vol. 103, no. 2, pp. 276–279, 2000, doi: 10.1016/S0924-0136(00)00474-X.

[170] K. Prasad Rao, G. D. Janaki Ram, and B. E. Stucker, “Improvement in corrosion resistance of friction stir welded aluminum alloys with micro arc oxidation coatings,” *Scr. Mater.*, vol. 58, no. 11, pp. 998–1001, 2008, doi: 10.1016/j.scriptamat.2008.01.033.

[171] A. Abdullah, M. Malaki, and A. Eskandari, “Strength enhancement of the welded structures by ultrasonic peening,” *Mater. Des.*, vol. 38, pp. 7–18, 2012, doi: 10.1016/j.matdes.2012.01.040.

[172] S. R. Ahmed, L. A. Agarwal, and B. S. S. Daniel, “Effect of Different Post Weld Heat Treatments on the Mechanical properties of Cr-Mo Boiler Steel Welded with SMAW Process,” in *Materials Today: Proceedings*, 2015, doi: 10.1016/j.matpr.2015.07.002.

[173] H. C. Dey, S. K. Albert, A. K. Bhaduri, G. G. Roy, R. Balakrishnan, and S. Panneerselvi, “Effect of post-weld heat treatment (PWHT) time and multiple PWHT on mechanical properties of multi-pass TIG weld joints of modified 9Cr-1Mo steel,” *Weld. World*, 2014, doi: 10.1007/s40194-014-0124-0.

[174] G. Taniguchi and K. Yamashita, “Effects of Post Weld Heat Treatment (PWHT) Temperature on Mechanical Properties of Weld Metals for High-Cr,” *Kobelco Technol. Rev.*, vol. 32, pp. 33–39, 2013.

[175] Y. K. Sawada and M. Nakamura, “Lapped friction stir welding between ductile cast irons and stainless steels,” *Weld. Int.*, vol. 27, no. 2, pp. 121–128, 2013, doi: 10.1080/09507116.2011.606150.

[176] B. Sadeghi, H. Sharifi, M. Rafiei, and M. Tayebi, “Effects of post weld heat treatment on residual stress and mechanical properties of GTAW: The case of joining A537CL1 pressure vessel steel and A321 austenitic stainless steel,” *Eng. Fail. Anal.*, vol. 94, no. August, pp. 396–406, 2018, doi: 10.1016/j.engfailanal.2018.08.007.

[177] H. Ma, G. Qin, P. Geng, F. Li, X. Meng, and B. Fu, “Effect of post-weld heat treatment

on friction welded joint of carbon steel to stainless steel," *J. Mater. Process. Technol.*, 2016, doi: 10.1016/j.jmatprotec.2015.08.004.

[178] S. Kolukisa, "The effect of the welding temperature on the weldability in diffusion welding of martensitic (AISI 420) stainless steel with ductile (spheroidal graphite-nodular) cast iron," *J. Mater. Process. Technol.*, vol. 186, no. 1–3, pp. 33–36, 2007, doi: 10.1016/j.jmatprotec.2006.11.148.

[179] P. Marashi, M. Pouranvari, S. Amirabdollahian, A. Abedi, and M. Goodarzi, "Microstructure and failure behavior of dissimilar resistance spot welds between low carbon galvanized and austenitic stainless steels," *Mater. Sci. Eng. A*, vol. 480, no. 1–2, pp. 175–180, 2008, doi: 10.1016/j.msea.2007.07.007.

[180] M. R. Nekouie Esfahani, J. Coupland, and S. Marimuthu, "Microstructural and mechanical characterisation of laser-welded high-carbon and stainless steel," *Int. J. Adv. Manuf. Technol.*, vol. 80, no. 5–8, pp. 1449–1456, 2015, doi: 10.1007/s00170-015-7111-5.

[181] S. Kim, S. Lee, K. Han, S. Hong, and C. Lee, "Cracking behavior in a dissimilar weld between high silicon nodular cast iron and ferritic stainless steel," *Met. Mater. Int.*, vol. 16, no. 3, pp. 483–488, 2010, doi: 10.1007/s12540-010-0621-7.

[182] I. Riposan, M. Chisamera, S. Stan, and D. White, "Chilling properties of Ba/Ca/Sr inoculated grey cast irons," *Int. J. Cast Met. Res.*, vol. 20, no. 2, pp. 90–97, 2007, doi: 10.1179/136404607X239726.

[183] E. Fraś and H. F. López, "A theoretical analysis of the chilling susceptibility of hypoeutectic FeC alloys," *Acta Metall. Mater.*, vol. 41, no. 12, pp. 3575–3583, 1993, doi: 10.1016/0956-7151(93)90238-N.

[184] M. O. H. Amuda and S. Mridha, "Grain refinement in ferritic stainless steel welds: The journey so far," *Adv. Mater. Res.*, vol. 83–86, pp. 1165–1172, 2010, doi: 10.4028/www.scientific.net/AMR.83-86.1165.

[185] F. F. Curiel, R. García, V. H. López, and J. González-Sánchez, "Effect of magnetic field applied during gas metal arc welding on the resistance to localised corrosion of the heat affected zone in AISI 304 stainless steel," *Corros. Sci.*, vol. 53, no. 7, pp. 2393–2399, 2011, doi: 10.1016/j.corsci.2011.03.022.

[186] E. Taban, E. Kaluc, and A. Dhooge, "Hybrid (plasma + gas tungsten arc) weldability of

modified 12% Cr ferritic stainless steel," *Mater. Des.*, vol. 30, no. 10, pp. 4236–4242, 2009, doi: 10.1016/j.matdes.2009.04.031.

[187] M. Vach *et al.*, "Evolution of secondary phases in austenitic stainless steels during long-term exposures at 600, 650 and 800 °C," *Mater. Charact.*, vol. 59, no. 12, pp. 1792–1798, 2008, doi: 10.1016/j.matchar.2008.04.009.

[188] M. Dadfar, M. H. Fathi, F. Karimzadeh, M. R. Dadfar, and A. Saatchi, "Effect of TIG welding on corrosion behavior of 316L stainless steel," *Mater. Lett.*, vol. 61, no. 11–12, pp. 2343–2346, 2007, doi: 10.1016/j.matlet.2006.09.008.

[189] S. Kumar and A. S. Shahi, "Effect of heat input on the microstructure and mechanical properties of gas tungsten arc welded AISI 304 stainless steel joints," *Mater. Des.*, vol. 32, no. 6, pp. 3617–3623, 2011, doi: 10.1016/j.matdes.2011.02.017.

[190] P. Sathiya, S. Aravindan, and A. N. Haq, "Some experimental investigations on friction welded stainless steel joints," *Mater. Des.*, vol. 29, no. 6, pp. 1099–1109, 2008, doi: 10.1016/j.matdes.2007.06.006.

[191] S. Ghorbani, R. Ghasemi, R. Ebrahimi-Kahrizsangi, and A. Hojjati-Najafabadi, "Effect of post weld heat treatment (PWHT) on the microstructure, mechanical properties, and corrosion resistance of dissimilar stainless steels," *Mater. Sci. Eng. A*, vol. 688, pp. 470–479, 2017, doi: 10.1016/j.msea.2017.02.020.

[192] J. Zhang, B. Huang, Q. Wu, C. Li, and Q. Huang, "Effect of post-weld heat treatment on the mechanical properties of CLAM/316L dissimilar joint," *Fusion Eng. Des.*, 2015, doi: 10.1016/j.fusengdes.2015.06.194.

[193] S. S. M. Prabu *et al.*, "Shape memory effect, temperature distribution and mechanical properties of friction stir welded nitinol," *J. Alloys Compd.*, vol. 776, pp. 334–345, 2019, doi: 10.1016/j.jallcom.2018.10.200.

[194] J. P. Oliveira, J. F. Duarte, P. Inácio, N. Schell, R. M. Miranda, and T. G. Santos, "Production of Al/NiTi composites by friction stir welding assisted by electrical current," *Mater. Des.*, vol. 113, pp. 311–318, 2017, doi: 10.1016/j.matdes.2016.10.038.

[195] V. V. Stolyarov, "Deformability and nanostructuring of TiNi shape-memory alloys during electroplastic rolling," *Mater. Sci. Eng. A*, vol. 503, no. 1–2, pp. 18–20, 2009, doi: 10.1016/j.msea.2008.01.094.

[196] S. K. Sadrnezhaad, N. H. Nemati, and R. Bagheri, "Improved adhesion of NiTi wire to

silicone matrix for smart composite medical applications," *Mater. Des.*, vol. 30, no. 9, pp. 3667–3672, 2009, doi: 10.1016/j.matdes.2009.02.016.

[197] L. Sun *et al.*, "Stimulus-responsive shape memory materials: A review," *Mater. Des.*, vol. 33, no. 1, pp. 577–640, 2012, doi: 10.1016/j.matdes.2011.04.065.

[198] Q. Li and Y. Zhu, "Impact butt welding of NiTi and stainless steel- An examination of impact speed effect," *J. Mater. Process. Technol.*, vol. 255, no. August 2017, pp. 434–442, 2018, doi: 10.1016/j.jmatprotec.2017.12.046.

[199] M. Greger, L. Kander, V. Snasel, and M. Cerny, "Microstructure evolution of pure titanium during ECAP," *Mater. Des.*, vol. 18, no. July 2015, pp. 1–8, 2011.

[200] P. Novák, L. Mejzlíková, A. Michalcová, J. Čapek, P. Beran, and D. Vojtěch, "Effect of SHS conditions on microstructure of NiTi shape memory alloy," *Intermetallics*, vol. 42, pp. 85–91, 2013, doi: 10.1016/j.intermet.2013.05.015.

[201] H. Li, D. Sun, X. Cai, P. Dong, and X. Gu, "Laser welding of TiNi shape memory alloy and stainless steel using Co filler metal," *Opt. Laser Technol.*, vol. 45, no. 1, pp. 453–460, 2013, doi: 10.1016/j.optlastec.2012.06.010.

[202] M. Mehrpouya, A. Gisario, and M. Elahinia, "Laser welding of NiTi shape memory alloy: A review," *J. Manuf. Process.*, vol. 31, pp. 162–186, 2018, doi: 10.1016/j.jmapro.2017.11.011.

[203] Y. Chen, S. Sun, T. Zhang, X. Zhou, and S. Li, "Effects of post-weld heat treatment on the microstructure and mechanical properties of laser-welded NiTi/304SS joint with Ni filler," *Mater. Sci. Eng. A*, 2020, doi: 10.1016/j.msea.2019.138545.

[204] G. R. Mirshekari, A. Saatchi, A. Kermanpur, and S. K. Sadrnezhaad, "Effect of Post Weld Heat Treatment on Mechanical and Corrosion Behaviors of NiTi and Stainless Steel Laser-Welded Wires," *J. Mater. Eng. Perform.*, 2016, doi: 10.1007/s11665-016-2034-3.

[205] J. R. Groza, M. Eslamloo-Grami, and R. Bandy, "The effect of thermo-mechanical treatment on The pitting corrosion of reinforcing carbon steel bars," *Mater. Corros.*, vol. 44, no. 9, pp. 359–366, 1993, doi: 10.1002/maco.19930440902.

[206] K. Y. Chiu, F. T. Cheng, and H. C. Man, "Corrosion behavior of AISI 316L stainless steel surface-modified with NiTi," *Surf. Coatings Technol.*, vol. 200, no. 20–21, pp. 6054–6061, 2006, doi: 10.1016/j.surfcoat.2005.09.009.

[207] S. A. A. Akbarimousavi and M. GohariKia, “Investigations on the mechanical properties and microstructure of dissimilar cp-titanium and AISI 316L austenitic stainless steel continuous friction welds,” *Mater. Des.*, vol. 32, no. 5, pp. 3066–3075, 2011, doi: 10.1016/j.matdes.2010.12.057.

[208] A. Fuji, K. Ameyama, and T. H. North, “Improved mechanical properties in dissimilar Ti-AISI 304L joints,” *J. Mater. Sci.*, 1996, doi: 10.1007/BF00367903.

[209] A. Fuji, T. H. North, K. Ameyama, and M. Futamata, “Improving tensile strength and bend ductility of titanium/AlSI 304L stainless steel friction welds,” *Mater. Sci. Technol. (United Kingdom)*, vol. 8, no. 3, pp. 219–235, 1992, doi: 10.1179/mst.1992.8.3.219.

[210] D. G. Barceloux, “Copper,” *Clin. Toxicol.*, vol. 37, no. 2, pp. 217–230, 1999.

[211] M. Merola, F. Escourbiac, R. Raffray, P. Chappuis, T. Hirai, and A. Martin, “Overview and status of ITER internal components,” *Fusion Eng. Des.*, vol. 89, no. 7–8, pp. 890–895, 2014, doi: 10.1016/j.fusengdes.2014.01.055.

[212] M. N. Mohammed, M. Z. Omar, M. S. Salleh, K. S. Alhawari, and P. Kapranos, “Semisolid Metal Processing Techniques for Nondendritic Feedstock Production,” *Sci. World J.*, pp. 7–9, 2013, doi: http://dx.doi.org/10.1155/2013/752175.

[213] J. Yu, G. Wang, and Y. Rong, “Experimental Study on the Surface Integrity and Chip Formation in the Micro Cutting Process,” *Procedia Manuf.*, vol. 1, pp. 655–662, 2015, doi: 10.1016/j.promfg.2015.09.063.

[214] C. Dharmendra, K. P. Rao, J. Wilden, and S. Reich, “Study on laser welding-brazing of zinc coated steel to aluminum alloy with a zinc based filler,” *Mater. Sci. Eng. A*, vol. 528, no. 3, pp. 1497–1503, 2011, doi: 10.1016/j.msea.2010.10.050.

[215] J. L. Song, S. B. Lin, C. L. Yang, and C. L. Fan, “Effects of Si additions on intermetallic compound layer of aluminum-steel TIG welding-brazing joint,” *J. Alloys Compd.*, vol. 488, no. 1, pp. 217–222, 2009, doi: 10.1016/j.jallcom.2009.08.084.

[216] T. Tanaka, T. Morishige, and T. Hirata, “Comprehensive analysis of joint strength for dissimilar friction stir welds of mild steel to aluminum alloys,” *Scr. Mater.*, vol. 61, no. 7, pp. 756–759, 2009, doi: 10.1016/j.scriptamat.2009.06.022.

[217] W. B. Lee, M. Schmuecker, U. A. Mercardo, G. Biallas, and S. B. Jung, “Interfacial reaction in steel-aluminum joints made by friction stir welding,” *Scr. Mater.*, vol. 55, no. 4, pp. 355–358, 2006, doi: 10.1016/j.scriptamat.2006.04.028.

[218] H. Uzun, C. Dalle Donne, A. Argagnotto, T. Ghidini, and C. Gambaro, "Friction stir welding of dissimilar Al 6013-T4 To X5CrNi18-10 stainless steel," *Mater. Des.*, vol. 26, no. 1, pp. 41–46, 2005, doi: 10.1016/j.matdes.2004.04.002.

[219] Y. V. Budkin, "Welding joints in dissimilar metals," *Weld. Int.*, vol. 25, no. 7, pp. 523–525, 2011, doi: 10.1080/09507116.2011.554254.

[220] M. Weigl and M. Schmidt, "Influence of the feed rate and the lateral beam displacement on the joining quality of laser-welded copper-stainless steel connections," *Phys. Procedia*, vol. 5, no. PART 2, pp. 53–59, 2010, doi: 10.1016/j.phpro.2010.08.029.

[221] H. Bang, H. Bang, H. Kim, J. Kim, I. Oh, and C. Ro, "A Study on the weldability and mechanical characteristics of dissimilar materials butt joints by laser assisted friction stir welding.," vol. 28, no. 6, pp. 70–75, 2010.

[222] G. R. Joshi and V. J. Badheka, "Microstructures and Properties of Copper to Stainless Steel Joints by Hybrid FSW," *Metallogr. Microstruct. Anal.*, vol. 6, no. 6, pp. 470–480, 2017, doi: 10.1007/s13632-017-0398-x.

[223] M. A. Mofid, A. Abdollah-zadeh, and F. Malek Ghaini, "The effect of water cooling during dissimilar friction stir welding of Al alloy to Mg alloy," *Mater. Des.*, vol. 36, pp. 161–167, 2012, doi: 10.1016/j.matdes.2011.11.004.

[224] J. Zhang, Y. Shen, X. Yao, H. Xu, and B. Li, "Investigation on dissimilar underwater friction stir lap welding of 6061-T6 aluminum alloy to pure copper," *Mater. Des.*, vol. 64, pp. 74–80, 2014, doi: 10.1016/j.matdes.2014.07.036.

[225] H. S. Bang, H. S. Bang, G. H. Jeon, I. H. Oh, and C. S. Ro, "Gas tungsten arc welding assisted hybrid friction stir welding of dissimilar materials Al6061-T6 aluminum alloy and STS304 stainless steel," *Mater. Des.*, vol. 37, pp. 48–55, 2012, doi: 10.1016/j.matdes.2011.12.018.

[226] H. Dong, C. Liao, L. Yang, and C. Dong, "Effects of post-weld heat treatment on dissimilar metal joint between aluminum alloy and stainless steel," *Mater. Sci. Eng. A*, vol. 550, pp. 423–428, 2012, doi: 10.1016/j.msea.2012.04.110.

[227] A. I. Khuri and S. Mukhopadhyay, "Response surface methodology," *Wiley Interdiscip. Rev. Comput. Stat.*, vol. 2, no. 2, pp. 128–149, 2010, doi: 10.1002/wics.73.

[228] A. Y. Aydar, "Utilization of Response Surface Methodology in Optimization of Extraction of Plant Materials," *Stat. Approaches With Emphas. Des. Exp. Appl. to Chem.*

Process., 2018, doi: 10.5772/intechopen.73690.

[229] V. Raymind H. Myers(virginia plytechnic University, Blacksburg, A. . Douglas C. Montgomery(Arizona state university, department of industrial engineering, Tempe, and N. Christine M. Anderson-cook(Los-Alamos national LAb, Los-Alamos, *RESPONSE SUFACE METHODOLOGY: process and product optimization using designed Experiments*, 4th edition. 2010.

[230] A. Morshedi and M. Akbarian, "Application Of Response Surface Methodology: Design Of Experiments And Optimization: A Mini Review," *Indian J. Fundam. Appl. Life Sci.*, vol. 4, no. 2002, pp. 2231–6345, 2014.

[231] G. W. Oehlert, *Design and Analysis of Experiments: Response Surface Design*. New York: W.H. Freeman and Company, 2000.

[232] M. A. Bezerra, R. E. Santelli, E. P. Oliveira, L. S. Villar, and L. A. Escaleira, "Response surface methodology (RSM) as a tool for optimization in analytical chemistry," *Talanta*, vol. 76, no. 5, pp. 965–977, 2008, doi: 10.1016/j.talanta.2008.05.019.

[233] F. H. S.Vieira, *Estastistical Experimental*. Atlas, sao paulo, 1989.

[234] A. K. and S. M, *Response surface methodology In Computational Statistics*, vol. 2, no. 128–149. John Wiley & Sons, Icn, 2010.

[235] K. . W. G.E.P Box, *J.R.Stat.Soc.* 1951.

[236] H. Eisazadeh, M. Hamedi, and A. Halvaee, "New parametric study of nugget size in resistance spot welding process using finite element method," *Mater. Des.*, vol. 31, no. 1, pp. 149–157, 2010, doi: 10.1016/j.matdes.2009.06.042.

[237] H. R. Zareie Rajani, H. Torkamani, M. Sharbati, and S. Raygan, "Corrosion resistance improvement in Gas Tungsten Arc Welded 316L stainless steel joints through controlled preheat treatment," *Mater. Des.*, vol. 34, pp. 51–57, 2012, doi: 10.1016/j.matdes.2011.07.071.

[238] "ASTM E3-95 : Standard Practice for Preparation of Metallographic Specimens," ASTM International, West Conshohocken, 2011.

[239] Massachusetts Institute of Technology, "The Metallographic Examination of Archaeological Artifacts," *Summer Inst. Mater. Sci. Mater. Cult.*, no. June, pp. 1–42, 2003.

[240] A. kaech(University of Zurich), “An Introduction to Electron Microscopy Instrumentation , Imaging and Preparation,” *Cent. Microsc. Image Anal.*, pp. 1–28, 2013.

[241] “ASTM E384-05a. Standard test method for microindentation hardness of materials,” 2005.

[242] N. S. El-Gendy, H. R. Madian, and S. S. A. Amr, “Design and Optimization of a Process for Sugarcane Molasses Fermentation by *Saccharomyces cerevisiae* Using Response Surface Methodology,” *Int. J. Microbiol.*, vol. 2013, no. 0, pp. 1–9, 2013, doi: 10.1155/2013/815631.

[243] D. Kianersi, A. Mostafaei, and A. A. Amadeh, “Resistance spot welding joints of AISI 316L austenitic stainless steel sheets: Phase transformations, mechanical properties and microstructure characterizations,” *Mater. Des.*, vol. 61, pp. 251–263, 2014, doi: 10.1016/j.matdes.2014.04.075.

[244] S. A. David, “Ferrite Morphology and Variations in Ferrite Content in Austenitic Stainless Steel Welds.,” *Weld. J. (Miami, Fla)*, vol. 60, no. 4, pp. 63–71, 1981.

[245] H. Okamoto and T. B. Massalski., *ASM Handbook: Binary Alloy Phase Diagrams*, 2nd ed., vol. 1. 1990.

LIST OF PUBLICATIONS

M. Muhammed, M. Mustapha, T. L. Ginta, A. M. Ali, F. Mustapha, and C. C. Hampo, "Statistical Review of Microstructure-Property Correlation of Stainless Steel : Implication for Pre and Post-weld Treatment," *MDPI Process.*, vol. 8, no. 7, pp. 1–32, 2020.

Figure 3.5: Computer numerically controlled metal yag laser cutting machine

Figure 3.6: Daiden resistance spot welding machine.

Figure 3.9: Bench Oven

Figure 3.10: Carbolite heat treatment furnace

Figure 3.11 Electrical Discharge Machine (EDM) wirecut.

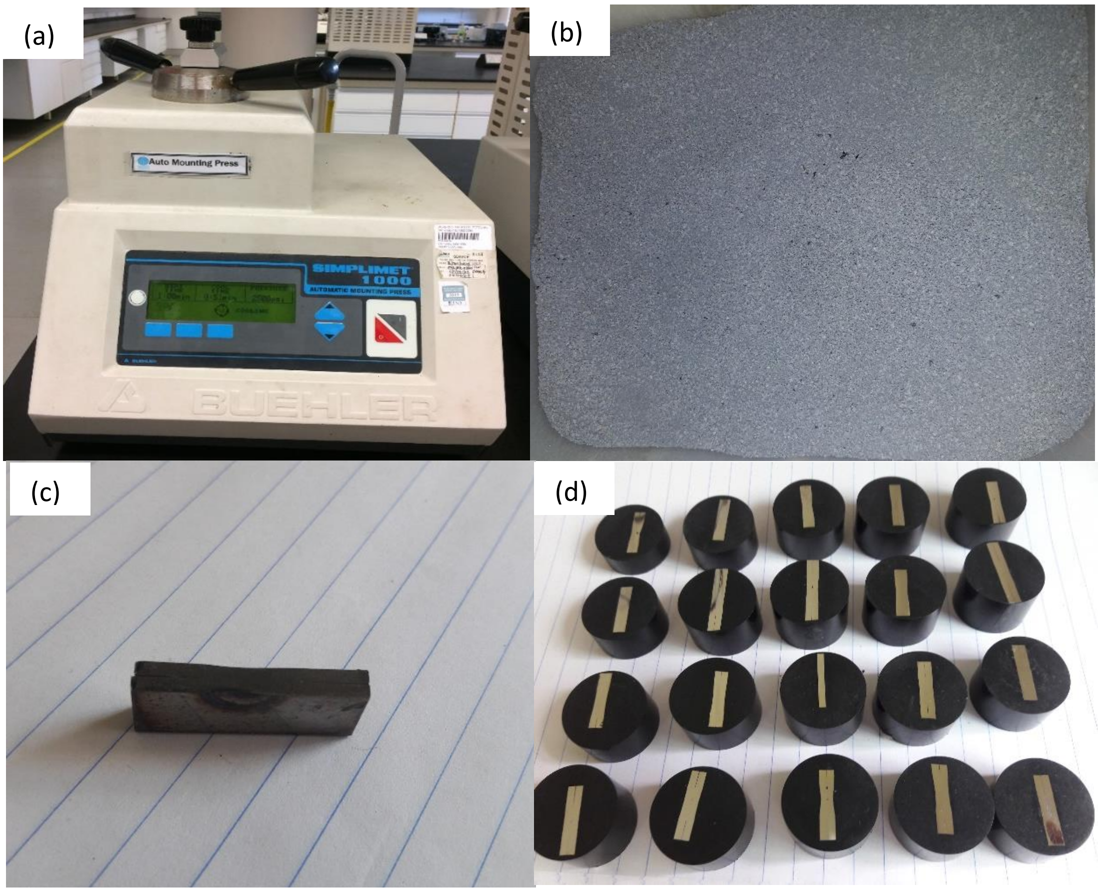

Figure 3.123: (a) Automatic mounting press (b) Phenolic resin (c) unmounted sample (d) mounted samples.

Figure 3.13: Buehler metaserv 250 twin-grinder-polisher.

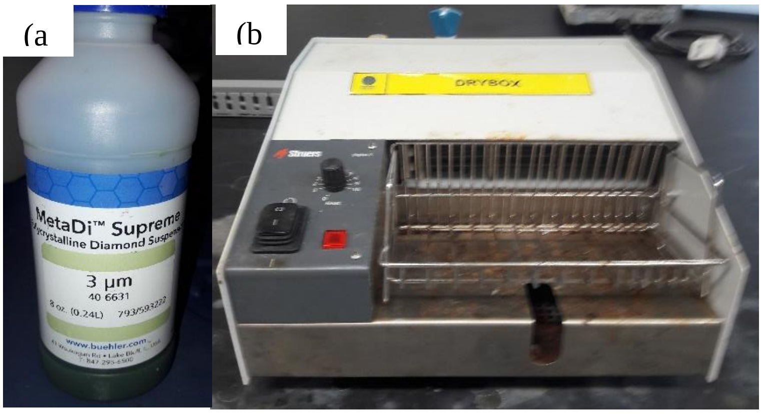

Figure 3.14: (a) MetaDi supreme polycrystalline diamond suspension (b) Drybox

Figure 3.15: Metallurgical microscope

Figure 3.16: FESEM microscope (Zeiss SUPRA 55VP)

Figure 3.17: Vickers microhardness tester.